

UNIVERSITAT POLITÈCNICA DE VALÈNCIA
DOCTORAL SCHOOL

Doctoral Program in Transportation Infrastructure and Territory



**UNIVERSITAT
POLITÈCNICA
DE VALÈNCIA**

**Developing a comprehensive methodology to
improve geometric design and safety in
micromobility infrastructure**

DOCTORAL THESIS

Presented by:

MORTEZA HOSSEIN SABBAGHIAN

Supervised by:

Prof. Dr. ALFREDO GARCÍA GARCÍA

Prof. Dr. DAVID LLOPIS CASTELLÓ

October 2024

Abstract

Micromobility refers to compact, low-mass, low-speed devices for short-distance urban travel, either personal or shared. They are being integrated into busy streets as part of a shift from auto-centric to slower, more pedestrian-friendly city designs. However, the integration has created safety risks and discomfort for both micromobility users and motor traffic due to large differences in speed and mass. To address this, urban designers implement measures such as protected lanes, lanes with differential heights, and buffered lanes to create space between bike lanes and roads on busier streets. Through this dedicated infrastructure, tangent-to-curve transitions or isolated curves are the most critical segments of bike lane when considering safety measures. Their design can significantly influence user behavior, often leading to conflicts with other bike lane users, pedestrians, and frequent fall incidents. Unfortunately, many of these incidents on a bike lane go underreported, but the risk persists in serious scenarios. The primary aim of this thesis is to identify potential conflict situations by introducing a novel safety indicator, the "Effective Fitted Radius", and a dynamic tracking methodology to assess the safety of micromobility users (cyclists and e-scooters) on isolated bike lane curves. This methodology comprises six key components: (i) site selection, (ii) geometric data collection, (iii) video recording, (iv) speed and position extraction, (v) visualization, and (vi) analysis. Naturalistic video data from 900 bike lane users at nine curve sites with varied geometry were collected to examine their spatio-temporal movement patterns. For this purpose, each curve was divided into three sections -Point of Curvature (PC), Midpoint (MP), and Point of Tangency (PT)-, and four areas of interest were defined to capture lateral position and speed. Subsequently, the outcomes were visualized using Python to analyze fitted trajectories, lane violation heat maps, and speed patterns. The Effective Fitted Radius was then computed from fitted circular curves, and one-way Analysis of Variance (ANOVA) was conducted to compare mean values. The resulting raincloud plots revealed significant variations in Effective Fitted Radius between right-turn and left-turn movements, particularly in smaller curve radii. Users, irrespective of their type, tended to cut the curve and generate smaller Effective Fitted Radius values during left-turns. Lateral displacement heat maps further confirmed that left-turn users often violated dedicated lanes, posing collision risks. In larger curve radii (22 and 78 meters), right-turn users maintain similar patterns observed in smaller radii, while left-turn users follow the curve geometry, reducing lane violations. For e-scooters, Effective Fitted Radius values cluster more closely around the actual radius in smaller radii. Speed analysis underscored potential conflicts and reduced handling capabilities for users breaching lane boundaries. In conclusion, the Effective Fitted Radius emerges as a valuable indicator for assessing and identifying risky behavioral patterns among micromobility users, many of which could escalate the risk of head-on, crossing, and side-angled conflicts between users. This thesis advances the understanding and methodology of micromobility infrastructure design by introducing the Effective Fitted Radius (EFR) as a novel movement-based surrogate measure of safety, offering a detailed spatial risk analysis and addressing critical limitations in current motion data extraction and trajectory analysis methods in high resolution.

Resumen

La micromovilidad se refiere a dispositivos compactos, de baja masa y baja velocidad para viajes urbanos de corta distancia, ya sean personales o compartidos. Se están integrando en calles concurridas como parte de una transición de diseños urbanos centrados en automóviles a diseños más lentos y amigables para peatones. Sin embargo, esta integración ha creado riesgos de seguridad e incomodidades tanto para los usuarios de micromovilidad como para el tráfico motorizado debido a las grandes diferencias en velocidad y masa. Para abordar esto, los diseñadores urbanos implementan medidas como carriles protegidos, carriles con alturas diferentes y carriles con separación para crear espacio entre los carriles para bicicletas y las calzadas en recta más transitadas. A través de esta infraestructura dedicada, las transiciones de recta a curva o curvas aisladas son los segmentos más críticos de los carriles para bicicletas al considerar medidas de seguridad. Su diseño puede influir significativamente en el comportamiento de los usuarios, a menudo provocando conflictos con otros usuarios del carril para bicicletas, peatones e incidentes de caídas frecuentes. Desafortunadamente, muchos de estos incidentes en un carril para bicicletas no se informan, pero el riesgo persiste en escenarios graves. El objetivo principal de esta tesis es identificar situaciones potenciales de conflicto mediante la introducción de un nuevo indicador de seguridad, el "Radio Ajustado Efectivo", y una metodología de seguimiento dinámico para evaluar la seguridad de los usuarios de micromovilidad (ciclistas y patinetes) en curvas aisladas de carriles para bicicletas. Esta metodología comprende seis componentes clave: (i) selección de la localización, (ii) recopilación de datos geométricos, (iii) grabación de video, (iv) extracción de trayectorias y velocidad, (v) visualización y (vi) análisis. Se recopiló datos de video naturalistas de 900 usuarios de carriles para bicicletas en nueve localizaciones de curvas con geometría variada para examinar sus patrones de movimiento espaciotemporales. Para este propósito, cada curva se dividió en tres secciones: Punto de Curvatura (PC), Punto Medio (PM) y Punto de Tangencia (PT), y se definieron cuatro áreas de interés para capturar la posición lateral y la velocidad. Posteriormente, los resultados se visualizaron usando Python para analizar trayectorias ajustadas, mapas de calor de violación de carriles y patrones de velocidad. Luego se calculó el Radio Ajustado Efectivo a partir de curvas circulares ajustadas y se realizó un Análisis de Varianza (ANOVA) unidireccional para comparar los valores medios. Los gráficos resultantes revelaron variaciones significativas en el Radio Ajustado Efectivo entre movimientos de giro a la derecha y a la izquierda, particularmente en radios de curvas más pequeños. Los usuarios, independientemente de su tipo, tendieron a cortar la curva y generar valores de Radio Ajustado Efectivo más pequeños durante los giros a la izquierda. Los mapas de calor de desplazamiento lateral confirmaron además que los usuarios que giraban a la izquierda a menudo violaban los carriles dedicados, aumentando el riesgo de colisiones. En radios de curvas más grandes (22 y 78 metros), los usuarios que giraban a la derecha mantuvieron patrones similares observados en radios más pequeños, mientras que los usuarios que giraban a la izquierda seguían la geometría de la curva, reduciendo las violaciones de carril. Para los patinetes, los valores del Radio Ajustado Efectivo se agrupan más cerca del radio real en radios más pequeños. El análisis de velocidad subrayó posibles conflictos y capacidades de manejo reducidas para los usuarios que infringían los límites de los carriles. En conclusión, el Radio Ajustado Efectivo surge como un valioso indicador para evaluar e identificar patrones de comportamiento arriesgado entre los usuarios de micromovilidad, muchos de los cuales podrían aumentar el riesgo de conflictos frontales, de cruce y de ángulo lateral

entre usuarios. Esta tesis avanza en la comprensión y metodología del diseño de infraestructuras de micromovilidad mediante la introducción del Radio Ajustado Efectivo (EFR) como una nueva medida indirecta de seguridad basada en el movimiento, ofreciendo un análisis detallado del riesgo espacial y abordando limitaciones críticas en los métodos actuales de extracción de datos de movimiento y análisis de trayectorias en alta resolución.

Resum

La micromobilitat es referix a dispositius compactes, de baixa massa i baixa velocitat per a viatges urbans de curta distància, ja siguin personals o compartits. S'estan integrant en carrers concorreguts com a part d'una transició de dissenys urbans centrats en automòbils a dissenys més lents i amigables per a vianants. No obstant això, esta integració ha creat riscos de seguretat i incomoditats tant per als usuaris de micromobilitat com per al trànsit motoritzat a causa de les grans diferències en velocitat i massa. Per a abordar això, els dissenyadors urbans implementen mesures com a carrils protegits, carrils amb altures diferents i carrils amb separació per a crear espai entre els carrils bici i les calçades en recta més transitades. A través d'esta infraestructura dedicada, les transicions de recta a corba o corbes aïllades són els segments més crítics dels carrils bici en considerar mesures de seguretat. El seu disseny pot influir significativament en el comportament dels usuaris, sovint provocant conflictes amb altres usuaris del carril bici, vianants i incidents de caigudes freqüents. Desafortunadament, molts d'estos incidents en un carril bici no s'informen, però el risc persisteix en escenaris greus. L'objectiu principal d'esta tesi és identificar situacions potencials de conflicte mitjançant la introducció d'un nou indicador de seguretat, el "Radi Ajustat Efectiu", i una metodologia de seguiment dinàmic per a avaluar la seguretat dels usuaris de micromobilitat (ciclistes i patinets) en corbes aïllades de carrils bici. Esta metodologia comprén sis components clau: (i) selecció de la localització, (ii) recopilació de dades geomètriques, (iii) gravació de vídeo, (iv) extracció de trajectòries i velocitat, (v) visualització i (vi) anàlisi. Es van recopilar dades de vídeo naturalistes de 900 usuaris de carrils bici en nou localitzacions de corbes amb geometria variada per a examinar els seus patrons de moviment espaciotemporals. Per a este propòsit, cada corba es va dividir en tres seccions: Punt de Curvatura (PC), Punt Mitjà (PM) i Punt de Tangència (PT), i es van definir quatre àrees d'interés per a capturar la posició lateral i la velocitat. Posteriorment, els resultats es van visualitzar usant Python per a analitzar trajectòries ajustades, mapes de calor de violació de carrils i patrons de velocitat. Després es va calcular el Radi Ajustat Efectiu a partir de corbes circulars ajustades i es va realitzar una Anàlisi de Variància (ANOVA) unidireccional per a comparar els valors mitjans. Els gràfics resultants van revelar variacions significatives en el Radi Ajustat Efectiu entre moviments de gir a la dreta i a l'esquerra, particularment en radis de corbes més xicotets. Els usuaris, independentment del seu tipus, van tendir a tallar la corba i generar valors de Radi Ajustat Efectiu més xicotets durant els girs a l'esquerra. Els mapes de calor de desplaçament lateral van confirmar a més que els usuaris que giraven a l'esquerra sovint violaven els carrils dedicats, augmentant el risc de col·lisions. En radis de corbes més grans (22 i 78 metres), els usuaris que giraven a la dreta van mantindre patrons similars observats en ràdios més xicotets, mentres que els usuaris que giraven a l'esquerra seguien la geometria de la corba, reduint les violacions de carril. Per als patinets, els valors del Radi Ajustat Efectiu s'agrupen més prop del radi real en ràdios més xicotets. L'anàlisi de velocitat va subratllar possibles conflictes i capacitats de maneig reduïdes per als usuaris que infringien els límits dels carrils. En conclusió, el Radi Ajustat Efectiu sorgix com un valuós indicador per a avaluar i identificar patrons de comportament arriscat entre els usuaris de micromobilitat, molts dels quals podrien augmentar el risc de conflictes frontals, d'encreuament i d'angle lateral entre usuaris. Esta tesi avança en la comprensió i metodologia del disseny d'infraestructures de micromobilitat mitjançant la introducció del Radi Ajustat Efectiu (EFR) com una nova mesura indirecta de seguretat basada en el moviment, oferint una

anàlisi detallada del risc espacial i abordant limitacions crítiques en els mètodes actuals d'extracció de dades de moviment i anàlisi de trajectòries en alta resolució.

Table of Content

Abstract.....	I
Resumen.....	III
Resum.....	V
List of Figures.....	X
List of Tables	XII
Chapter 1 Background	1
Chapter 2 Introduction.....	2
2.1 Overview of the Thesis Structure	3
Chapter 3 Literature Review	5
3.1 Current State of Knowledge of a Safe Bike Lane.....	5
3.1.1 Micromobility Characterization	5
3.2 Literature Review Studies on Micromobility	13
3.2.1 A systematic literature review on safe infrastructure for Micromobility.....	15
3.3 Horizontal Curve Safety on Bike Lanes	21
3.3.1 Design Parameters and Guidelines.....	22
3.3.2 Optimization of Curve Geometry.....	22
3.3.3 Human Factors and Perception	23
3.4 Safety Assessment Methods	23
3.4.1 Interaction-based approach	24
3.4.2 Movement-based approach	24
3.4.3 Safety Assessments through Simulations.....	25
3.4.4 Safety Assessments with Instrumented Devices	25
3.5 Trajectory Analysis Techniques	26
3.5.1 Trajectory Clustering and Classification.....	26
3.5.2 Trajectory Pattern Mining	27
3.6 Conclusions about Current Knowledge	28
Chapter 4 Objectives and Hypotheses	31
Chapter 5 Methodology	33
5.1 Geometric Recreation and Selection of Horizontal Curves.....	33

5.2 Video Data Collection.....	34
5.3 Segmentizing and Regionalizing the Horizontal Curve.....	35
5.4 Track Typology.....	37
5.5 Data Extraction	37
5.5.1 Effective Fitted Radius (EFR).....	38
5.5.2 Speed	38
5.5.3 Track clustering and prediction.....	39
5.6 Data Analysis Techniques.....	40
Chapter 6 Development.....	41
6.1 Selection and Classification of Study Area Curves	41
6.2 Recreation of Selected Curve Geometry in Civil 3D.....	43
6.3 Camera Placement, Recording, and Undistortion.....	44
6.4 Data Collection	46
6.5 Computation of Effective Fitted Radius	48
6.6 Data Analysis	50
Chapter 7 Results.....	52
7.1 Comparison of Effective Fitted Radius and Actual Radius	52
7.2 Displacement Analysis.....	55
7.3 Speed Effect.....	57
7.4 Track Analysis	61
7.4.1 Track Type Classification	61
7.4.2 Track Clustering.....	65
7.4.3 Track Type Prediction.....	65
7.5 Conclusion	70
Chapter 8 Discussion	72
8.1 The challenge of motion data extraction.....	72
8.2 Effective Fitted Radius as Surrogate Measure of Safety	72
8.3 Track classification, clustering and prediction	74
8.4 Comparison with Previous Studies	74
8.5 Limitations of the Study	75
Chapter 9 Conclusions.....	77
Chapter 10 Future Research Direction.....	80
10.1 Incorporation of crash data	80
10.2 Automation of data filtering: image processing with AI	80

10.3 Track type prediction	80
10.4 Using Extreme Value Theory to Model Extreme Conflict Events	81
Acknowledgments	82
References.....	83
Appendix A	96
A.1 Publications in Indexed Journals.....	96
A.2 Participations in International Congresses.....	96
A.3 Participations in National Congresses.....	96
Appendix B	97
Section 6.3.....	97
Section 6.4.....	98
Section 7.2.....	114
Section 7.4.....	118

List of Figures

Figure 1 Classification for MDs, Reprinted with permission from Ref. (Santacreu et al., 2020).....	7
Figure 2 Types of bike lanes: (a) bicycle lane, (b) protected bike lane, (c) sidepath on median,	8
Figure 3 Classification of criteria affecting safe infrastructure for Micromobility.....	13
Figure 4 Categorization of adapted criteria.	16
Figure 5 Criteria clusters for selected studies.....	17
Figure 6 The clusters of the four main pillars.	17
Figure 7 Mode clusters.	18
Figure 8 Geographical clusters.	18
Figure 9 Pie chart of the criteria distribution.....	19
Figure 10 Distribution of modes studies for each area of research.	20
Figure 11 Cartogram of the geographical distribution of literature studies.	21
Figure 12 Overview of the methodology.....	33
Figure 13 Tripod placed at proper distance (a) tripod with camera (b) side view.	35
Figure 14 Bird-eye view settings (a) tripod with camera at zero degree (b) Bird-eye view.	35
Figure 15 Regions of interest for identifying user's position on the curve with users making a right-turn; background image source (NYC DOT Web page, 2024).	36
Figure 16 Six track types for motor vehicle maneuvers on horizontal curves (Spacek, 2005).....	37
Figure 17 Data extraction: (a) curve site camera view and (b) aerial view with the control points.	38
Figure 18 Initial map of identified curve sites in busiest bike lanes in the city of Valencia.....	41
Figure 19 Screenshots of point maps and alignment creation tool in the Civil 3D.....	43
Figure 20 Camera views of curve site under study: (a) SW1 (b) NE3 and (c) SE3.....	45
Figure 21 Python code programmed for automation of EFR computation.	49
Figure 22 Python code programmed for automation of displacement heatmap generation.	50
Figure 23 Progress Flowchart.....	52
Figure 24 Raincloud plots of Effective Fitted Radius in four curve sites: NE3 (b) SW2 (c) SE4 (d) SE3.....	54
Figure 25 Heatmaps illustrating the percentage of user presence at each spatioregions and sections of curve. Example series for two curve sites of NE3 (R=6m) and SE4 (R=22m) divided by user type and movement direction.	56

Figure 26 Box whisker plots of speed data for different radii for curve R1-R4: (a) PC, (b) MP, and (c) PT.....	58
Figure 27 Box whisker plots of speed data for each user type and direction for curve R1-R4: (a) PC, (b) MP, and (c) PT.....	58
Figure 28 Box whisker plots of speed data for different radii for curve R5-R9: (a) PC, (b) MP, and (c) PT.....	58
Figure 29 Box whisker plots of speed data for each user type and direction for curve R5-R9: (a) PC, (b) MP, and (c) PT.....	59
Figure 30 Speed difference bar charts between two segments of curve per user type per turn direction.	60
Figure 31 Track-segment occurrence on curve sites R1 and R2 by user type and direction.....	63
Figure 32 Track-segment occurrence on all nine-curve sites (R1-R9) by user type and direction.....	64
Figure 33 Decision Tree Regression model visualization showing feature splits for predicting variables d-pc, d-mp, and d-pt.....	66
Figure 34 Improved Decision Tree Regression model visualization showing feature splits for predicting variables d-pc, d-mp, and d-pt (see Figure 35 for readability).....	67
Figure 35 Magnified leaves of the improved Decision Tree Regression model in Figure 33.	70

List of Tables

Table 1 Articles that focus on the use criteria affecting safety on MM infrastructure.....	9
Table 2 List of identified curve sites in busiest bike lanes in the city of Valencia.	42
Table 3 Isolated curve sites geometric parameters.....	44
Table 4 Lateral Offset Distances from Center Line for Site NE3 (R = 6m) by User Type and Direction.	46
Table 5 Operating Speed Data per Section for Site NE3 (R = 6m) by User Type and Direction.	47
Table 6 Computed EFRs for NE3 (R = 6m) curve site per user and turn direction.	51
Table 7 ANOVA with post hoc tests for Effective Fitted Radius per user type per movement direction.	53
Table 8 Non-parametric Kruskal-Wallis test results for five curve sites with dispersed Effective Radius.	54
Table 9 ANOVA with dunn post hoc tests for Effective Fitted Radius per user type per movement direction.	55
Table 10 Descriptive analysis of users speed for each four curve site at three sections (R1-R4).....	57
Table 11 Descriptive analysis of users speed for each four curve site at three sections (R5-R9).....	57
Table 12 Descriptive analysis of users speed for each user type and direction at three sections (R1-R4).....	57
Table 13 Descriptive analysis of users speed for each user type and direction at three sections (R5-R9).....	58
Table 14 Acronyms for classifying maneuvers by track type and lateral segment.	62
Table 15 Summery of the clustering result.....	65
Table 16 Lateral Offset Distances from Center Line for Site R2-R9 by User Type and Direction.	98
Table 17 Operating Speed Data per Section for Site R2-R9 by User Type and Direction.	103
Table 18 Operating Speed Data per Section for Site R1-R9 by User Type and Direction.	108

Chapter 1 Background

This research work is presented as the Doctoral Thesis of the student Morteza Hossein Sabbaghian and is supervised by Doctor of Civil Engineering and University Professor, Prof. Dr. Alfredo García García, and by Doctor with International Distinction and Associate Professor, Prof. Dr. David Llopis Castelló, both from the Universitat Politècnica de València (UPV).

The title of the research is "Developing a comprehensive methodology to improve geometric design and safety in Micromobility infrastructure." This title reflects the main objective of the Doctoral Thesis and makes a significant contribution to the existing literature in the field of bike lane design and bike lane safety evaluation.

This work has been carried out in direct collaboration with the Highway Engineering Research Group (HERG), part of the Transport and Territory Institute of the UPV, to which the doctoral candidate has belonged since January 2021.

The current dissertation is associated with the research project "esMicromobility - Evaluation of Road Safety of Micromobility" with reference PID2019-111744RB-I00, funded by MCIN/AEI/10.13039/501100011033, began in February 2021 and ended in September 2024. Among the work packages into which this project was divided, it is noteworthy that the thesis is closely related to the packages on bike lane design, bike lane safety, scientometric review of the literature, and the establishment of criteria and recommendations.

Chapter 2 Introduction

Despite advancements in enhancing Micromobility safety at intersections and during their interaction with motor vehicles, there remains a clear lack of attention in upgrading the geometric design of bike lanes. This oversight may have contributed to the growing rate of serious injuries and crash fatalities in many leading cycling-friendly countries like the Netherlands, where cyclists accounted for 40% of road death in 2022. Several factors influence bike lane user dynamics and can contribute to conflicts and falls: geometry, proximity to pedestrians, sightlines, barriers, grading, markings, side vegetation, and pavement condition (Hossein Sabbaghian et al., 2023a).

Horizontal curves, a main geometric component of bike lane segments, play a pivotal role in ensuring safe Micromobility. Poor design in these segments can lead to unexpected behavior patterns, and increased conflicts or fall incidents. This risk rises when users are unable or unwilling to adhere to the geometry set by designers. Bike lane horizontal curves are categorized into four types: first curves (not influenced by a preceding curve), isolated curves (preceded and followed by a tangent), reverse curves (followed immediately by a curve in the opposite direction), and consecutive curves (succeeding in the same direction). Calculating the forces experienced by cyclists on curves is crucial for optimizing bike lane designs. This is especially important in challenging situations, such as navigating reverse curves around obstacles like bus stops or consecutive curves around trees, where cyclists may struggle to ride smoothly. Although these are rare examples, sharp isolated curves still exist that cause discomfort and require significant speed reduction to navigate. This can confuse cyclists' perceptions, leading them to make risky decisions instead of reducing their speed and following the intended path.

Extracting microscopic traffic parameters like bike lane user trajectories, speed, lane change, deceleration, and acceleration allows for a comprehensive safety analysis (Jackson et al., 2013). Due to distinct dynamics of micromobility compared to motor vehicles, such as higher steering angles, additional degrees of freedom (like rear-frame roll, yaw, lateral motion, and front-fork steer), and their lightweight nature, these devices can perform a range of maneuvers during curvature (Haasnoot et al., 2023). Recent behavioral studies primarily focus on capturing the naturalistic riding behavior dynamics of road users to predict their future positions or compute surrogate measures of safety (SMoS) (Nabavi Niaki et al., 2019).

Surrogate Measures of Safety (SMoS) are defined as “an indicator derived from the observation and the safety evaluation of non-crash events in traffic with the goal to estimate the expected crash/injury frequency as well as to get a better understanding of the crash mechanisms and contributing factors” (Saunier & Lareshyn, 2021a). In this thesis, a geometric-based SMoS will be developed that can be even used for risk assessment without crash data.

According to the International (2021) Lareshyn et al., 2016), “the validity of SMoS is the degree to which it measures what it is supposed to measure, that is, road safety or, in practical terms the expected frequency of crashes. While the ultimate goal is to have a clear and stable relation to the expected number of crashes expressed in mathematical terms, as of today the documented attempts to establish such relations are few and not always conclusive”. (C. Wang et al., 2021) highlight the importance of Surrogate Safety Measures (SSM) for traffic safety evaluation, particularly when reliable statistical safety models are unavailable. This is often due to complex site characteristics or nontraditional

traffic safety treatments, where historical crash data is insufficient or nonexistent for developing predictive safety models.

This study aims to use user trajectory and speed data on isolated horizontal curves to identify risky patterns and understand user responses to specific designs. This is a preliminary step in safety assessment before linking accident data. The data highlights potentially risky movements, some of which may increase individual fall incidents and conflicts with opposite lane users. This approach facilitates proactive safety improvements and establishes a scalable framework. While crash data can be linked to identified risky patterns, the primary goal is to identify safety risks without relying on historical crash data. By incorporating movement-based measures from user trajectories, this method offers more comprehensive safety and design followability analysis than traditional time-based measures like Time to Collision (TTC) and Post-Encroachment Time (PET). A movement-based approach can assess risky patterns that might have been overlooked because they do not involve interactions with other users, as seen in the increasing incidents of falls, which are often underreported. When combined with interaction-based Surrogate Measures of Safety (SMoS), the proposed framework provides a comprehensive perspective on infrastructure safety. To facilitate this, the study introduces a novel trajectory-based measure called Effective Fitted Radius (EFR), which is defined as the radius of the best-fitted circular arc to a user's trajectory when passing through a curve on a bike lane. EFR can also be utilized for before-after studies on isolated curves of bike lanes to assess the impact of geometric treatments or new designs.

To demonstrate the effectiveness of the proposed measure, a selection of case study curves on bike lanes with diverse geometries are chosen. These curves are used to track Micromobility users and extract their Effective Fitted Radius (EFR) and speed for safety analysis. Furthermore, a comprehensive framework is proposed.

2.1 Overview of the Thesis Structure

This doctoral thesis is organized into ten chapters following the Background (Chapter 1) and Introduction (Chapter 2), along with four appendices.

Chapter 3 presents a review and compilation of existing knowledge on bike lane safety, safe horizontal curve design for bike lanes, and proactive safety assessment methods (naturalistic, semi-naturalistic, simulation-based).

Chapter 4 includes the main research objective and the scientific-technical objectives associated with its achievement. This chapter also outlines the main hypotheses of the study, which will be confirmed or rejected through the development of the doctoral thesis.

Chapter 5 presents the research methodology, while Chapter 6 details its implementation. This leads to Chapter 7, where the speed and spatial data of users are analyzed based on the segmentation introduced to compute Effective Fitted Radius (EFR) out users' trajectories during curve navigation. The observed tracks are then classified to facilitate the development of a predictive model that identify the class and risk involved in each class.

Subsequently, Chapter 8 includes the discussion of the results provided in Chapter 7. It compares the proposed EFR measure with other previously developed Surrogate Measures of Safety (SMoS), concluding with a new SMoS measure that could improve the design of curves on bike lanes according to real data.

Finally, Chapter 9 establishes the main conclusions of the doctoral thesis based on the results achieved and the discussion conducted, and Chapter 10 outlines future research

directions related to the further improvement of EFR by associating the accident data and automation methods existed for motion extraction.

Additionally, four appendices below are included:

- Appendix A: Related publications
- Appendix B: Extended data and result from chapter 6 and 7

Chapter 3 Literature Review

3.1 Current State of Knowledge of a Safe Bike Lane

Micromobility (MM) and e-micromobility (eMM) are rapidly becoming popular as a new sustainable mobility solution. Their objectives are to increase mobility during urban congestion and address certain land use and environmental issues like parking space shortage, carbon emission, and sound pollution. In tourist destinations, they are deemed as a flexible, cheap transport solution for tourists and a way to bypass traffic. In addition, they are being promoted to facilitate modal shift from personal cars to personal lightweight Micromobility Devices (MDs) that are more energy efficient, require less space, and have no or less detrimental impact on the environment. The average inner-city trip range of these vehicles is considered short distance and mostly below 20 km range, wherein 70% of most daily trips in urban areas are taking place (Clewlow, 2018; Gomm & Wengraf, 2013; Kaufman & Buttenwieser, 2018; Tiwari, 2019) . In addition, by completing first and last mile distances, they also contribute to more public transport use (Møller et al., 2020; Shaheen et al., 2020).

The European commission has prioritized bicycle usage promotion in the new Sustainable Urban Mobility Plans (SUMP) (Bührmann et al., 2011; Europeia, 2011; Rupprecht et al., 2019). In the United States, different transportation agencies have started to define specific visions for their bicycle network promotion plan. Massachusetts Department of Transportation, for example, declares “Massachusetts’ integrated and multimodal transportation system will provide a safe and well-connected bicycle network that will increase access for both transportation and recreational purposes. The Plan will advance bicycling statewide as a viable travel option –particularly for short trips of three miles or less– to the broadest base of users and free of geographic inequities” (Schultheiss et al., 2019).

This novel form of mobility has been proven to promote safety and accessibility in cities. In fact, in a dense urban area, the likelihood of a fatal crash occurrence is much higher for cars rather than micro-vehicles. Nevertheless, the new mobility also generates safety risks for its users and pedestrians, most of which are associated with cycleway placemaking and design. The International Traffic Forum (ITF) has published an extensive report about “Safe Micromobility” (Santacreu et al., 2020), where out of 10 safety recommendations, three are related to the infrastructure safety development and the rest can be classified to drivers’ behavior, speed, regulation, user’s training, vehicle design, and shared operation.

This chapter conducts a thorough literature review to pinpoint gaps in research regarding safe Micromobility infrastructure. It aims to uncover design and safety inconsistencies in bike lanes, emphasizing the need for the current thesis. Micromobility devices (MDs) present unique dimensions and operating characteristics compared to traditional adult bicycles, challenging the notion of the "design vehicle." Understanding the needs of MD users is crucial for creating a safe infrastructure. This research supports evidence-based decision-making for both practitioners and researchers. What sets this review apart is its focus on an unexplored topic and the innovative scientometric methods used for visualization and analysis.

3.1.1 Micromobility Characterization

Micromobility classification across the world is not consistent. In many countries, bicycles are considered as the smallest design vehicle and many other MD types like

standing e-scooters, e-skateboards, and self-balancing vehicles are not defined or regulated. In Europe, the L-category vehicles were introduced for powered two, three, and four-wheel vehicles, using six classification criteria of power, power source, speed, length, width, and height. Light two-wheel powered vehicles are categorized as L1e-A powered cycle and L1e-B two-wheel moped. In type A, the net power of the electric bicycle is between 250 watts and 1000 watts, with a maximum speed of 25 km/h. For type B, the net power is up to 4000 watts and the design speed range is between 25 km/h to 45 km/h. Human-powered bicycles, kick e-scooters, skates, pedelecs (up to 250 watts), self-balancing vehicles with no seat, like standing e-scooters, are excluded from L1e category (Ajuntament de València, 2019).

In the United States, e-scooters and e-bikes are distinguished from mopeds by various states to enable their operation on cycleways. However, the only thorough classification found in the literature was published by the Pedestrian and Bicycle Information Centre (PBIC) (NTSB, 2019), where three categories of Electric standing or sitting e-scooters, electric bicycles, and other (i.e., skates, seaways, one-wheel hoverboards) are proposed. For electric bicycle category, three classes of pedelec, throttle assist, and pedelec at higher speed, are defined. In total 8 criteria of device type, brands, weight, occupants, power supply, speed, operating space, and regulation entity were considered.

The International Transport Forum (ITF) (Santacreu et al., 2020) has proposed a classification for Micromobility, based on the operational characteristics of MDs (Figure 1). In this definition, speed, and weight of the MDs, which directly correlate with the kinetic energy of a vehicle and thus determine the risk of fatality or serious injuries, are considered as the two main factors for determining their type. As can be seen in Figure 1, two weight ranges of below 35 kg and between 35 kg to 350 kg, and speed range of up to 25 km/h and between 25 to 45 km/h are introduced that divide MDs to four distinct types: A, B, C, and D.

A Bike Lane is defined by the National Association of City Transportation Officials (NACTO) as a portion of the roadway that has been designated by striping, signage, and pavement markings for the preferential or exclusive use of bicyclists (NACTO, 2014) [14]. Bike lanes enable bicyclists to ride at their preferred speed without interference from prevailing traffic conditions and facilitate predictable behavior and movements between bicyclists and motorists. A bike lane is distinguished from a cycle track in that it has no physical barrier (bollards, medians, raised curbs, etc.) that restricts the encroachment of motorized traffic. Conventional bike lanes run curbside when no parking is present, adjacent to parked cars on the right-hand side of the street or on the left-hand side of the street in specific situations. Bike lanes typically run in the same direction of traffic, though they may be configured in the contra-flow direction on low-traffic corridors necessary for the connectivity of a particular bicycle route (NACTO, 2014).


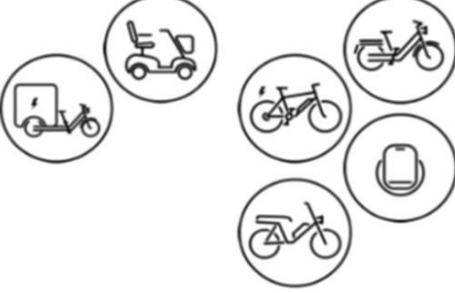
Type A	Type B	Type C	Type D
unpowered or powered up to 25 km/h (16 mph)		powered with top speed between 25-45 km/h (16-28 mph)	
<35 kg (77 lb)	35 – 350 kg (77 – 770 lb)	<35 kg (77 lb)	35 – 350 kg (77 – 770 lb)
			

Figure 1 Classification for MDs, Reprinted with permission from Ref. (Santacreu et al., 2020).

The configuration of a bike lane requires a thorough consideration of existing traffic levels and behaviors, adequate safety buffers to protect bicyclists and other MDs from parked and moving vehicles, and enforcement to prohibit motorized vehicle encroachment and double-parking. Bike Lanes may be distinguished using color, lane markings, signage, and intersection treatments.

This research covers a variety of bikeways that were defined by guidelines and researchers. The ministry of interior in Spain (Sánchez, 2016) has distinguished five types of cycle lanes according to their placement, boundary features, and traffic mixture (Figure 2):

1. Bicycle lane: a bicycle path adjacent to a road, that can be in the same direction of motor vehicle circulation or a two-way lane (Figure 2a).
2. Protected bike track: a bike lane, physically separated from the road and sidewalk with lateral elements (Figure 2b).
3. Sidepath: a bicycle route that is marked on the sidewalk or median island (Figure 2c), that can be with (Figure 2d) or without (Figure 2e) vegetated/physical curb.
4. Bike track: a bike path with an independent layout that is completely segregated from motorized traffic (Figure 2f).
5. Cycle path: dedicated path for both pedestrians and cycles, segregated from traffic (Figure 2g).

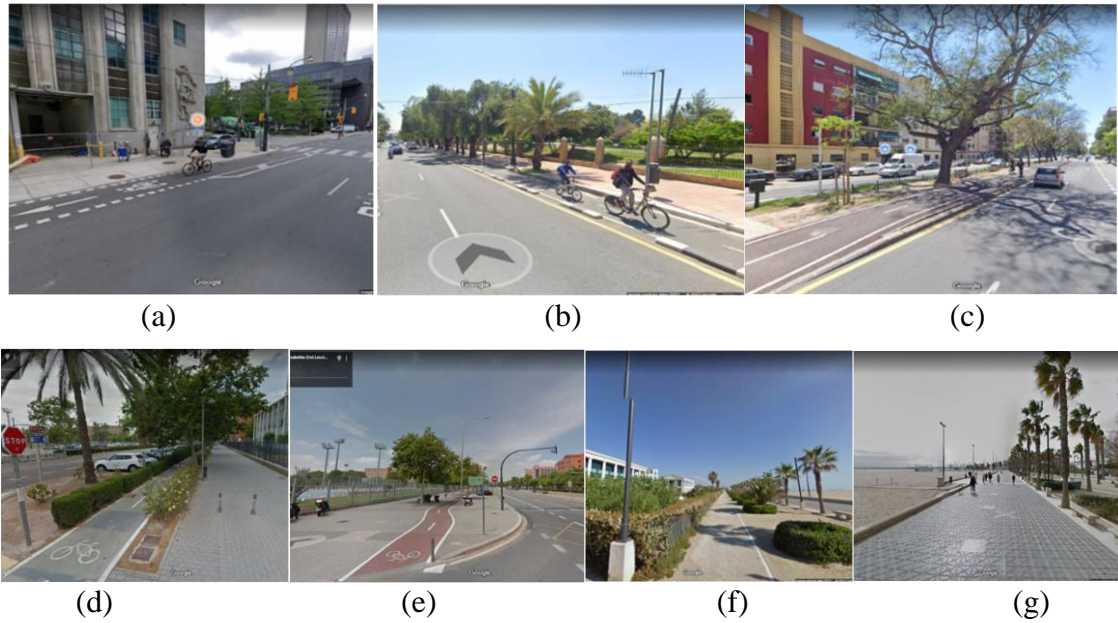


Figure 2 Types of bike lanes: (a) bicycle lane, (b) protected bike lane, (c) sidepath on median, (d) sidepath with vegetated curb, (e) sidepath without curb, (f) bike track, and (g) cycle path (Google Maps, 2024b, 2024a).

Research in the field of micromobility safety has focused on various aspects, including infrastructure, pavement conditions, traffic patterns, and operating conditions. When it comes to geometry, studies have shown that narrow lane widths pose higher risks for micromobility users, as they increase the likelihood of collisions with curbs, other cyclists, and conflicts with cars during overtaking maneuvers (Greibe & Buch, 2016; Park & Abdel-Aty, 2016). Additionally, research has examined the proximity of obstacles to e-scooter riders, highlighting the importance of considering the surrounding environment to ensure user safety (Q. Ma et al., 2021).

Pavement conditions also play a significant role in micromobility safety. Studies have found that the type of pavement surface can affect skid resistance, which is particularly crucial for lightweight devices like e-scooters. For example, painted cobble and smooth painted tile pavements have been found to have lower skid resistance compared to asphalt and concrete surfaces (López-Molina et al., 2022). Monitoring methods using smartphone sensors have been proposed to assess pavement conditions and determine key performance indicators for user comfort and safety (Cafiso et al., 2022). Vibrations experienced by e-scooter riders have also been investigated, with concrete pavements found to impose higher vibrations on riders compared to Hot Mix Asphalt (HMA) (Q. Ma et al., 2021). Other relative studies on vibration are summarized in Table 1.

Table 1 Articles that focus on the use criteria affecting safety on MM infrastructure.

#	(Researcher, Year)	Criteria	Sub-criteria	MD Modes	Sample Size & Location
1	(Wyman, 2022)	operating condition	crash & conflict	bike	300 h of video recording at 5 bike lanes (Portland, USA)
2	(Pérez-Zuriaga et al., 2022)	pavement, geometry	vibration, clearance	e-scooter	850 m of bike lane (Valencia, Spain)
3	(Tian et al., 2022a)	operating condition	crash & conflict	e-scooter	worldwide (social media data)
4	(Prencipe et al., 2022)	operating condition	intersection, long.control, connectivity	e-scooter	336 buffers (Bari, Italy)
5	(Dozza et al., 2023)	operating condition	longitudinal control	e-scooter, segway, e-bike, bike	34 participants (Chalmers, Sweden)
6	(Folco et al., 2023)	traffic, operating condition	route planning, crash & conflict	bike, e-scooter	314 crashes in 2019, 40,694 trips (Turin, Italy)
7	(Clewlow et al., 2022)	traffic, operating condition	route planning, crash & conflict	e-scooter	22,022 crash data from 2014–2021 (4 cities, USA)
8	(Anke et al., 2023)	traffic, operating condition	route planning, connectivity	e-scooter	six sites/738 recording (Dresden & Berlin, Germany)
9	(Gehrke et al., 2022)	traffic, operating condition	route planning, crash & conflict	e-scooter	eight months (Brookline, Massachusetts, USA)
10	(Cafiso et al., 2022)	pavement	distress	bike, e-scooter	979 tests (Italy)
11	(F. Chang et al., 2022)	operating condition	crash & conflict	e-bike	2222 crash records from 2014 to 2016 (Hunan, China)
12	(Pérez-Zuriaga et al., 2022)	geometry	clearance	bike, e-scooter	80 km bicycle tracks/25 h video (Valencia, Spain)
13	(Q. Ma et al., 2021)	pavement, geometry	vibration, clearance	e-scooter	One road segment—vehicle lane & sidewalk (Norfolk, VA)
14	(Zuniga-Garcia et al., 2021)	traffic	route planning	e-scooter	80,000 trips/11 million location points (Austin, TX)
15	(Hosseinzadeh et al., 2021)	traffic	route planning	e-scooter	494,008 trips/159 route planning analysis zone (Louisville, KY)
16	(Hawa et al., 2021)	traffic	route planning	e-scooter	1671 geographic grid cells of 0.19 km ² (Washington, DC)
17	(Q. Ma et al., 2021)	operating condition	longitudinal control	e-scooter	NA
18	(Kamel & Sayed, 2021)	operating condition	crash & conflict	bike	NA
19	(Tan & Tamminga, 2021)	operating condition	crash & conflict	multiple	1 case study (Washington, DC, USA)
20	(Tomiyama & Moriishi, 2020)	pavement	vibration, skidding	e-scooter	10 different surfaces—grading & roughness (Saitama, Japan)
21	(Carrignon, 2020)	pavement	skidding, distress	e-scooter	Synthesis of literature (France & UK)
22	(Gössling, 2020)	operating condition	crash & conflict, longitudinal control	e-scooter	173 news items (10 cities *)
23	(S. He & Shin, 2020)	traffic	route planning	e-scooter	2,430,806 trips (Austin, TX)
24	(Zou et al., 2020)	traffic	route planning	e-scooter	138,362 trips (Washington, DC)
25	(Almannaa et al., 2021)	operating condition	longitudinal control	e-scooter	15,400 E-scooters (Austin, TX)
26	(Caspi et al., 2020)	traffic	route planning	e-scooter	11,358 trips per day (Austin, TX)
27	(Jiao & Bai, 2020)	traffic	route planning	e-scooter	158,208 trips per month (Austin, TX)

#	(Researcher,Year)	Criteria	Sub-criteria	MD Modes	Sample Size & Location
28	(Yang et al., 2020)	operating condition	crash & conflict	e-scooter	169 news on E-scooter-involved crashes
29	(Bai & Jiao, 2020)	traffic	route planning	e-scooter	661,367 & 225,543 trips/month (Austin TX, Minneapolis MN)
30	(Lazarus et al., 2020)	traffic	route planning	bike, e-bike (shared)	124,980 trips per month (San Francisco, CA)
31	(Politis et al., 2021)	operating condition	crash & conflict	bike	2 one-way & 1 two-way bike lane (Karditsa, Greece)
32	(K. Wang & Chen, 2020)	traffic	route planning	bike (shared)	430,560 trips in September 2016 (New York, DC)
33	(Hu et al., 2020)	operating condition	crash & conflict, longitudinal control	e-bike	219 accidents—2014 to 2016 (6 cities, China)
34	(Xing et al., 2020)	traffic	route planning	bike (shared)	1,023,603 trips in August 2016 -Mobike (Shanghai, China)
35	(Austin Public Health, 2019)	operating condition	crash & conflict	e-scooter	271 E-scooter-related injuries (Austin, TX)
36	(McKenzie, 2019)	traffic	route planning, composition	bike, e-scooter	1,414,055 bike & 937,590 e-scooter trips (Washington, DC)
37	(Voinov et al., 2019)	operating condition	crash & conflict	e-scooter	10,811 e-scooter owners (Enschede Netherlands)
38	(A. Y. Chang et al., 2019)	traffic, operating condition	route planning, longitudinal control	multiple	Synthesis of literature (Washington, DC)
39	(Du et al., 2019)	traffic	route planning	bike	830,000 trips in September 2016 (Shanghai, China)
40	(Y. He et al., 2019)	traffic	route planning	e-bike (shared)	7921 trips in 107 days-20 July to 3 Nov. 2017 (Park City, UT)
41	(Y. Guo et al., 2019)	operating condition	crash & conflict	e-bike, e-scooter	310 e-bike collision records (Ningbo, China)
42	(Y. Zhang et al., 2019)	traffic	route planning	bike (shared)	Approximately 48,000 trips per day (Shanghai, China)
43	(C. Xu & Yu, 2019)	operating condition	crash & conflict	e-bike	1091 crashes records from 2015 to 2016 (Hangzhou, China)
44	(Smith & Schwieterman, 2018)	traffic	route planning	e-scooter	10,000 trips per study area (Chicago, IL)
45	(T. Wang et al., 2018)	operating condition	crash & conflict	e-bike	4000 crash records from 2008 to 2014 (Guilin, China)
46	(X. Zhang et al., 2018)	operating condition	crash & conflict	e-bike	3200 e-bike owner participants (Jiangsu Province, China)
47	(Y. Zhang et al., 2018)	traffic	route planning	bike (shared)	12,915 trips per day (Zhongshan, China)
48	(Yuan et al., 2017)	operating condition	crash & conflict	e-bike	150 serious crash samples from 2009 to 2015 (Beijing, China)
49	(Greibe & Buch, 2016)	geometry	alignment features	bike	8 one-way cycle tracks (Copenhagen, Denmark)
50	(Park & Abdel-Aty, 2016)	geometry	alignment features	bike	6420 urban roadway segments with 2514.518 miles (FL)
51	(J. Xu, Shang, Qi, et al., 2016)	operating condition	crash & conflict	ESS, bike	Synthesis of literature (Beijing, China)
52	(J. Xu, Shang, Yu, et al., 2016a)	operating condition	crash & conflict, longitudinal control	self-balancing ESS **	Accident simulation in MADYMO software (v.2010)
53	(Bordagaray et al., 2016)	operating condition	route planning, composition	bike	24,664 trips in July & August 2011 (Santander, Spain)
54	(Greibe & Buch, 2016)	operating condition	longitudinal control, lateral control	bike	Video observation of 8925 cyclists (Copenhagen, Denmark)
55	(Zuniga-Garcia et al., 2021)	operating condition	crash and conflict	bike	2928 motor vehicles pass (Valencia, Spain)

#	(Researcher,Year)	Criteria	Sub-criteria	MD Modes	Sample Size & Location
56	(Corcoran et al., 2014)	operating condition	route planning	bike (shared)	448 trips per day (Brisbane, Australia)
57	(Ohri, 2013)	pavement	skidding	e-scooter	4 different surfaces (Toronto, ON)
58	(Blackman & Haworth, 2013)	operating condition	crash & conflict	e-scooter, moped	5 years crash data (Queensland, Australia)
59	(Montella et al., 2012)	operating condition	crash & conflict	mopeds, motorcycles	254,575 PTW involved crashes from 2006 to 2008 (Italy)
60	(Dondi et al., 2011)	geometry, pavement	alignment, clearance, skidding, distress	bike	1500 m bike lane (Rimini, Italy)

* Brisbane (Australia), Christchurch (New Zealand), Copenhagen (Denmark), Dallas & Los Angeles (USA), Malaga (Spain), Paris (France), Stockholm (Sweden), Vienna (Austria), Zurich (Switzerland) ** Electric Self-balancing E-scooters.

Traffic patterns and distribution of micromobility users have been extensively studied. These studies that are listed in Table 1 have explored the usage distribution of e-scooters on sidewalks, bike lanes, and roadways, providing valuable data for the development of effective surrogate safety measures. Factors such as comfort and convenience have been found to influence e-scooter riders' behavior, including instances of sidewalk riding violations. Correlations between trip generation, crash frequency, and the promotion of shared micromobility services through safer infrastructure have also been identified.

Operating conditions, including network characteristics and interactions between different micromobility users, have been investigated. Accordingly, Street network characteristics correlate with road safety outcomes, emphasizing the importance of considering the design of the network (Marshall & Garrick, 2011). Studies have examined conflicts between different modes, such as cyclists and e-scooter riders, and highlighted the impact of bike lane positioning on conflict frequency (Fonseca-Cabrera et al., 2021a). Risk factors for e-scooter-related crashes (injury and non-injuries) have been developed (Tian et al., 2022b). Additionally, Acceleration and deceleration performance between cyclist, e-scooter, and Segway riders are different (Dozza et al., 2022).

While there is a growing body of research in the field of micromobility safety, there are some limitations. Reliable crash data for e-e-scooters from traffic management agencies are lacking, with most studies relying on data provided by shared micromobility companies. However, studies on bikes and mopeds have shown satisfactory accessibility to reliable crash data. Simulation studies have also been conducted to explore the risks associated with electric self-balancing e-scooters (ESS) and their impact on head injury intensity (J. Xu, Shang, Yu, et al., 2016b). All studies that are classified under operating conditions are included in Table 1.

In conclusion, research in micromobility safety has provided valuable insights into the impact of infrastructure design, pavement conditions, traffic patterns, and operating conditions on user safety. These findings can help inform the development of safer micromobility networks and improve the design and maintenance of infrastructure to ensure the well-being of micromobility users. However, there is a need for more comprehensive and reliable crash data to further enhance our understanding of micromobility safety and develop effective safety measures.

Assuming the homogeneity of fundamental aspects of infrastructures used for motor vehicles and those of the micromobility users, the criteria affecting users' safety on bikeways were adapted from ASSHTO Green Book 2011 (AASHTO, 2011). The relative diagram is demonstrated in Figure 3. This diagram will be the base for further literature synthesis and analysis. These adapted criteria are useful to better filter relative studies to the topic of this research, and to avoid missing any research that may lack sufficient relative keywords to be selected through the scientometric review.

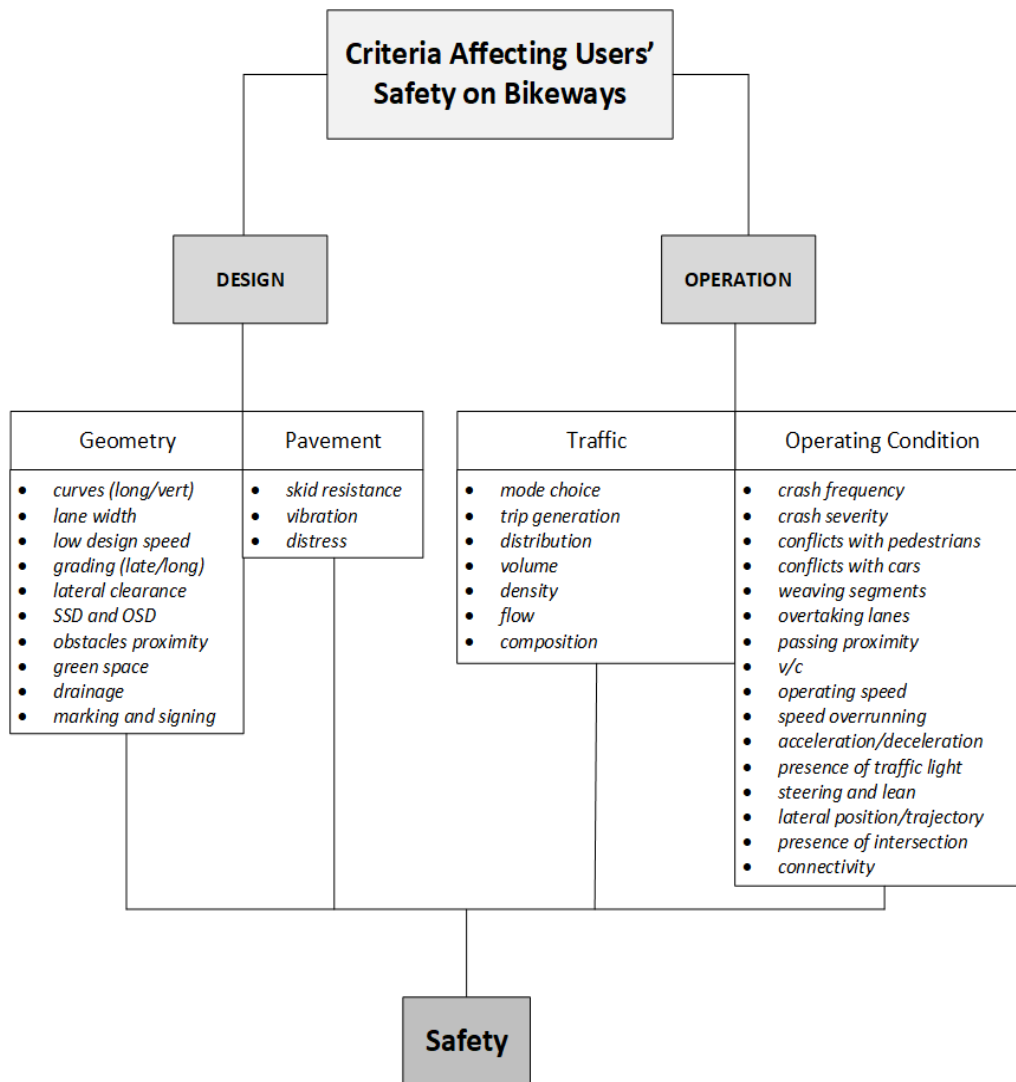


Figure 3 Classification of criteria affecting safe infrastructure for Micromobility.

3.2 Literature Review Studies on Micromobility

Previous review studies on micromobility have successfully identified gaps and directed subsequent research efforts. The main focus was on the integration of micromobility with the public transport, sustainability, users' behavior, and usage pattern. For instance, Oeschger et al. (Oeschger et al., 2020) conducted a systematic literature review on micromobility and public transportation integration in 2020. The gaps identified in that study, such as spatiotemporal analysis of e-scooters and transit systems, sustainable parking for micromobility, and mode shift potential, later became focal points for researchers (Deveci et al., 2023; Nigro et al., 2022; Yan et al., 2021).

Two bibliographic analysis studies focused on the impact of micromobility on sustainability of transportation in cities. The study conducted by Abduljabbar et al. (Abduljabbar et al., 2021) visualized the transforming landscape of micromobility research, whereas Sengul & Mostofi (Şengül & Mostofi, 2021) used the PRISMA method (Preferred Reporting Items for Systematic Reviews) to compare literature worldwide in terms of their findings about the future role of micromobility in urban transportation. In neither of the two studies was a gap analysis involved. Lia and Correia (Liao & Correia,

2022) performed a similar study that contained all shared e-mobility modes: electric car sharing, e-bike sharing, and e-scooter sharing. The results presented a comprehensive review of their usage pattern, demand estimation, and potential impacts on the transportation system.

Elmashhara et al. (Elmashhara et al., 2022) conducted a SLR study to find the factors driving behavior of micromobility users. The study found 25 driving factors and offered directions for future studies. The factors were grouped into three categories: (i) temporal, spatial, and weather-related factors; (ii) system-related factors, and (iii) user-related factors. Kathis (2022) conducted a comprehensive literature review on conflicts between cyclists, pedestrians, motorists, heavy-duty vehicles, and buses in urban areas. The study found that researchers were more focused on dangerous interactions that are classified on top of the Hyden's Safety Pyramids rather than normal encounters (Kathis, 2022). The USA National Academies of Sciences, Engineering, and Medicine (NASEM) has recently published a comprehensive report that reveals the relationship between e-scooter crashes, injuries, and fatalities and contributing factors: behavioral and environmental. In this study, the emerging behavioral safety issues of e-scooter users are discussed. Moreover, a summary of all safety solutions attempted by cities are presented, providing real case studies (Sandt et al., 2022).

A comprehensive scientometric review on powered micromobility was conducted by O'Hern and Estgfaeller (O'Hern & Estgfaeller, 2020). The study reviewed 474 publications from 1991 to 2020 in a wide range of topics including user behavior, vehicle technology, planning, policy, health, and safety for powered micromobility. The result shows e-bikes user behavior studies were ranked first with 55 related studies, while keywords like safety, road safety, accident, and crashes were in the bottom of the ranking (9th and 10th).

However, to the knowledge of the authors, no studies have yet found to have synthesized the literature for identification of the research gaps on the micromobility infrastructure. A systematic and compressive review on a new trending topic like micromobility can in fact provide a comprehensive understanding of the current state of knowledge on the topic. The scientometric analysis tools integrated within journals search platforms can only provide limited insights about their own publication. Therefore, such review studies where relevant studies are carefully selected, evaluated and synthesized are contributing extensively to the advancements of the topic in the right direction. Moreover, the scientometric tool used in this study (VOSviewer version 1.6.20) allows unique visualization and analysis of the existing literature, identifying gaps and potential areas for future research. This approach goes beyond traditional literature review methods and provides a data-driven perspective to uncover patterns, trends, and relationships within the literature.

The identification, classification, and cluster analysis (Section 3) of criteria that impact micromobility safety can lead to a clear insight on areas that micromobility researchers can direct their studies to have the most impact on this field. Although there are aspects of infrastructure for motor vehicle and micromobility that are similar, however, they are never identical. The main motivation and potential future impact of this research could be directing studies on micromobility pavement (skid resistance, vibration, distress), and micromobility naturalistic traffic behavior (longitudinal control, lateral control, impact of geometry or alignment). These important areas, if elaborated, can have significant impact on cost-beneficial safety improvements.

This research is in fact useful for evidence-based decision-making of both practitioners and researchers. The principal aspect that distinguishes this review from similar studies are the focus of the literature review on a topic that is unique and not covered at this level to this date, and as well the novel scientometric methods used for visualization and analysis.

3.2.1 A systematic literature review on safe infrastructure for Micromobility

The objective of this study is to develop a literature map that helps identify gaps in the literature focused on planning, designing, and safety assessment of micromobility infrastructure. The result of this study is intended to allow micromobility designers and operators better understand the safety criteria and considerations for each recent modes of micro-vehicles and their mixed use on cycle paths, providing best practices for improving safety on this infrastructure.

The scope of this literature review includes the keywords and criteria related to safety on bikeways that correlate with their geometry, pavement, traffic, and operational condition. The following pillars and sub-pillars are covered in the literature analysis:

- Geometry: curves (horizontal/vertical), lane width, low design speed, grading (lateral/longitudinal), lateral clearance, Stopping Sight Distance (SSD) and Overtaking Sight Distance (OSD), obstacle proximity, green space, drainage, and marking and signing.
- Pavement: skid resistance, vibration, distress.
- Traffic: mode choice, trip generation, distribution, volume, density, flow, and composition.
- Operating condition: crash frequency, crash severity, conflicts with pedestrians, conflicts with cars, weaving segments, overtaking lanes, passing proximity, v/c, operating speed, speed overrunning, acceleration/deceleration, presence of traffic light, steering and lean, lateral position/trajectory, presence of intersection, and connectivity.

To effectively collect and synthesize relative literature, a systematic literature review method was used, that had been adapted in similar studies from Thomas and Harden (Thomas & Harden, 2008) method. The method has four steps: (i) designing the research process; (ii) conducting the research; (iii) analyzing and extracting information; and (iv) reviewing the findings.

In the first step, the research database, terms, and criteria were determined. This was performed by reviewing recent publications and relative guidelines. Common academic search portals were used that include Science-Direct/Scopus, Taylor & Francis online, OneSearch, and other sources such as Google Scholar, TRID, Web of Science, JSTOR, and SAGE. After the initial review of terms, the criteria that could impact on user's safety on bikeways were classified (Figure 4) and were used as the base for the next step. The criteria were grouped into two main pillars of design and operation and four subcategories of geometry, pavement, traffic, and operating condition.

Secondly, the literature data collection was conducted on selected portals online, and then stored in a classified manner based on associated terms and criteria. Next, the classified literature was visualized in the form of tables, literature map, and cartogram. This was to identify gaps that existed in the literature in terms of defined criteria, location, and Micromobility modes.

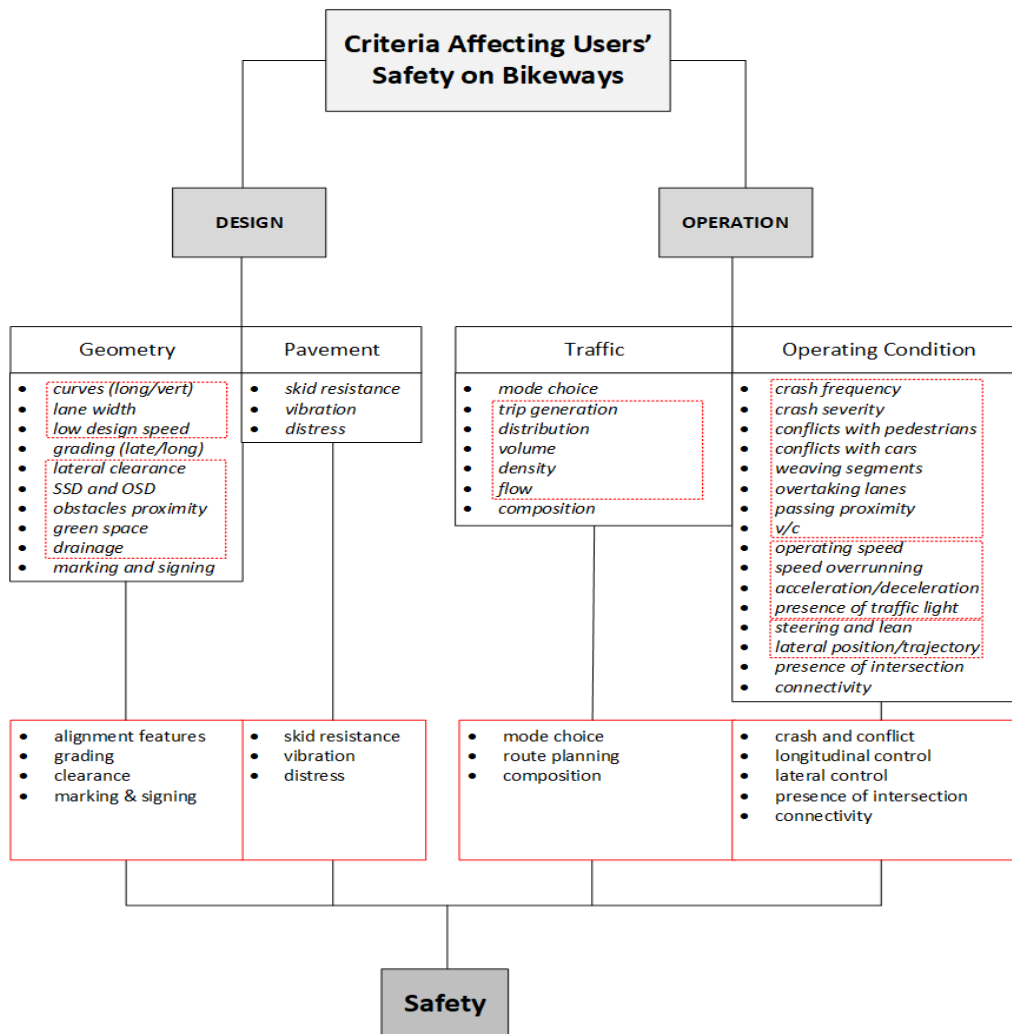


Figure 4 Categorization of adapted criteria.

The associated subcategories and criteria for the selected articles were clustered with VOSviewer. Accordingly, from the four main pillars, and their subset 12 criteria, two maps were developed that shows their cluster and interconnection. The visualized map (Figure 5) clearly shows three main cluster groups. Primarily, “route planning” and “crash and conflict” are both equally the largest cluster, that are interconnected and have links to two and one other criteria, respectively. The second cluster is “longitudinal control” with a major link to crash and conflict, and other links to route planning, lateral control, connectivity, and intersection. In the third cluster “skidding” and “clearance” are positioned with three other keywords of alignment features, distress, and vibration centered around them.

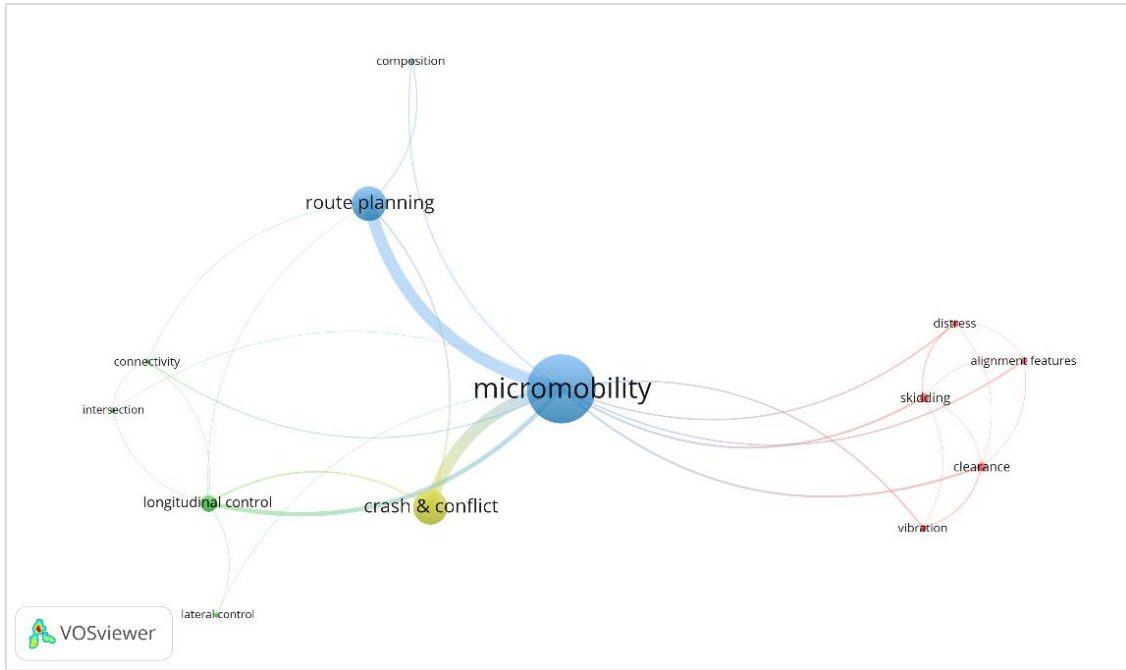


Figure 5 Criteria clusters for selected studies.

For having a clearer scientometric view of the safety for micromobility infrastructure, another map was developed using only the major four pillars of the adopted map. This map (Figure 6) illustrates how geometry and pavement are overlooked in the literature for improving safety of micromobility users.

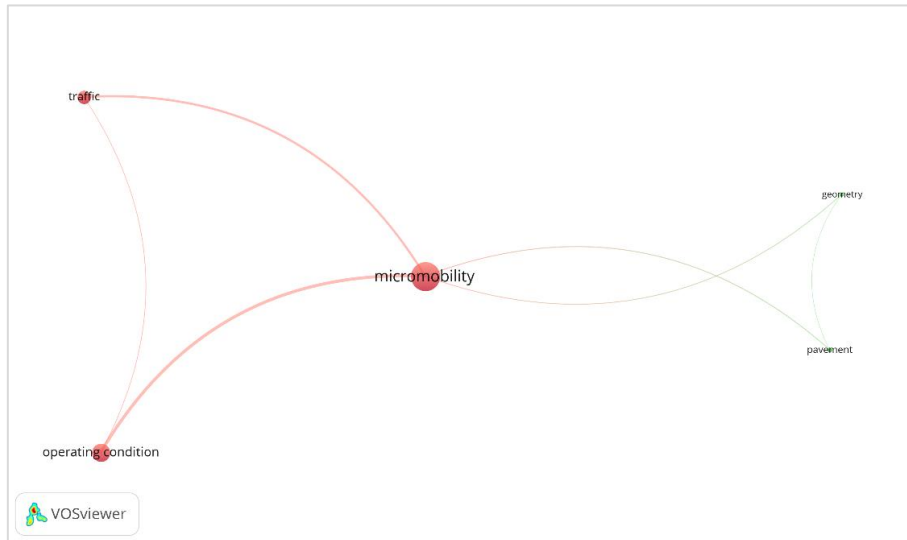


Figure 6 The clusters of the four main pillars.

In terms of modes, the cluster analysis map (Figure 7) shows that e-scooters have been the center of attention in the selected studies, with links to four other modes of bike, e-bike, moped, and segway. Next are bikes surrounded by four modes of e-scooter, e-bike, segway, and ESS. E-bike is the third cluster, with three links to bike, e-scooter, and segway. The map clearly shows that there are limited studies that include multiple modes, ESS, segway, and moped.

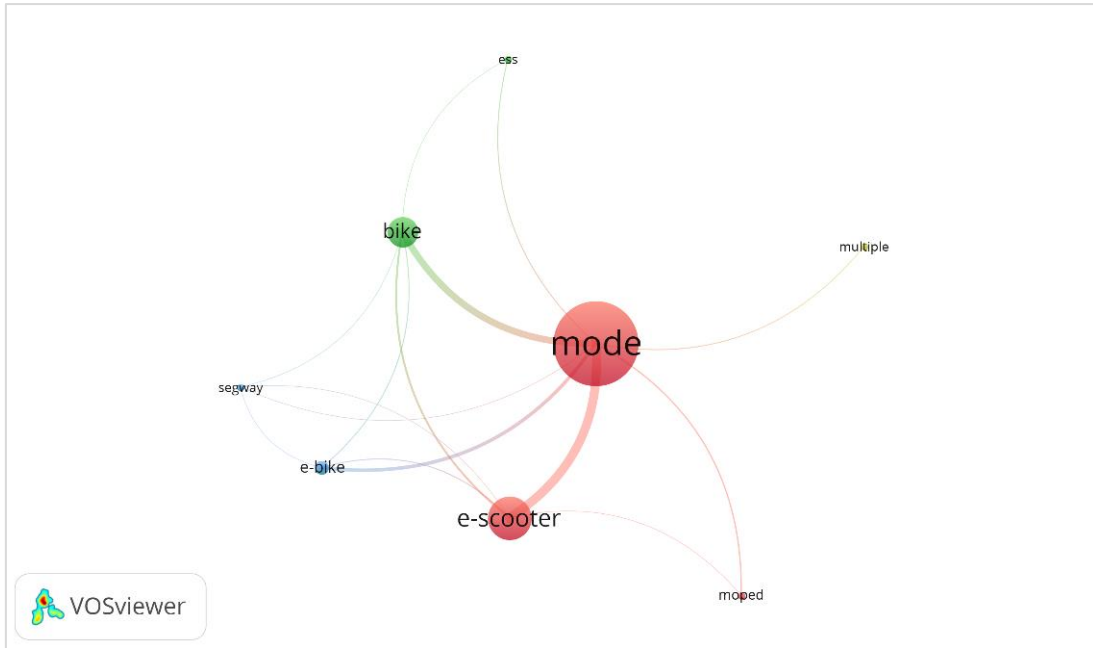


Figure 7 Mode clusters.

Geographically, the literature can be divided into three major clusters, as are illustrated in Figure 8. USA and China contain the largest clusters, with USA being the largest. Nine European countries were also involved in the sampled cities for micromobility studies linked to safety, that are usually interconnected and have links to some other countries like Australia, New Zealand, and UK. In Europe, Spain and Italy have the largest share. The map also shows that relative studies that include a wide variety of geographical locations are rare.

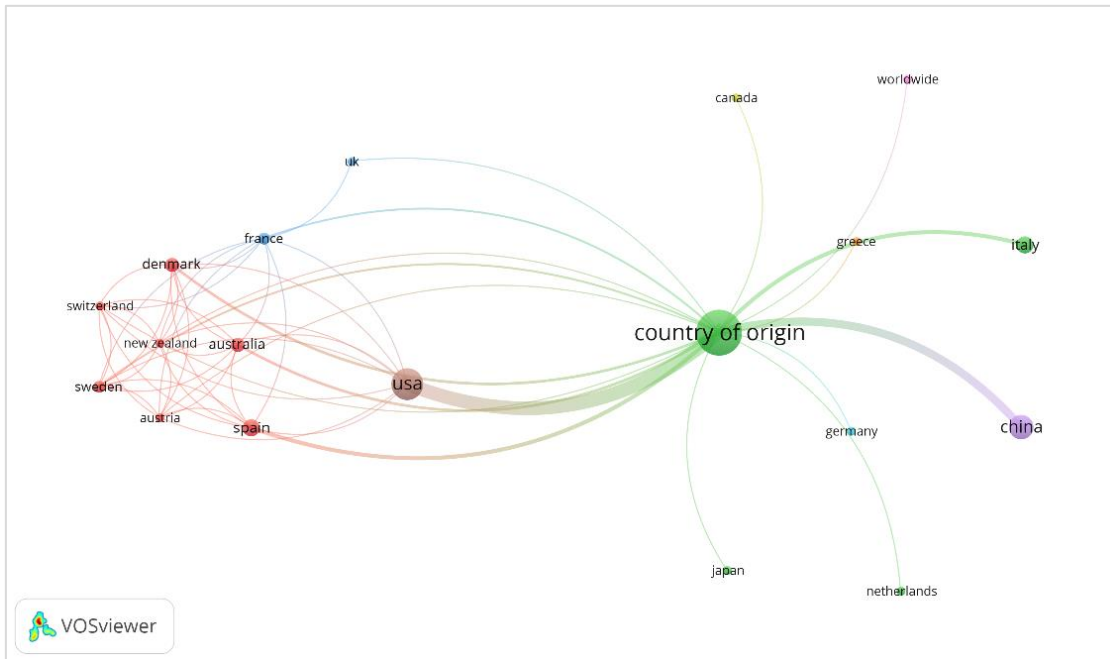


Figure 8 Geographical clusters.

A pie chart (Figure 9) is developed from the cluster analysis on table 1. In this way, most studies related to safe infrastructure for micromobility are focused on two criteria of “crash and conflict” and “route planning”. For each of these criteria, 24 relative academic research were found, that together accounts for 60% of all the existing literature. After that, longitudinal control was studied the most, with nine related research (approximately 11%). 30% of the rest is shared between nine other criteria (see Figure 9).

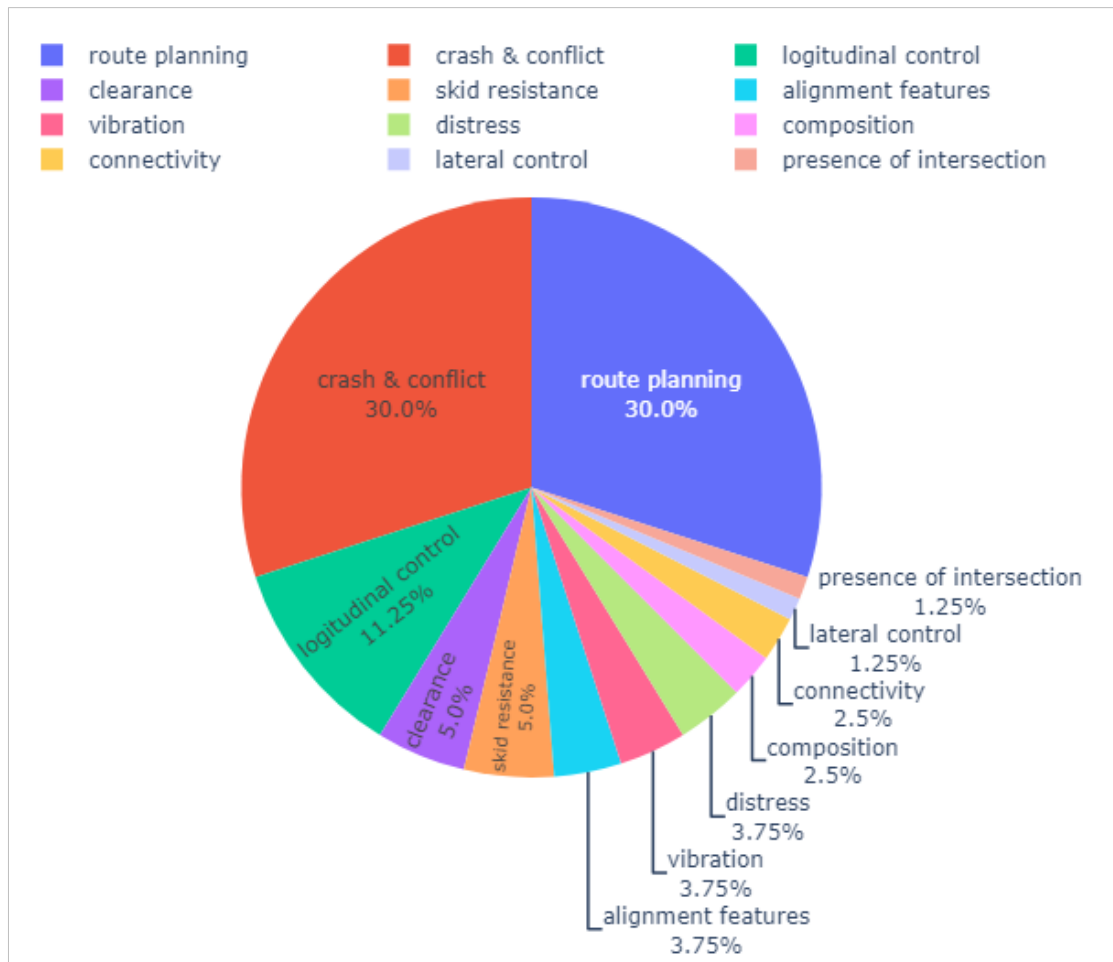


Figure 9 Pie chart of the criteria distribution.

The observed cluster of academic research on only two factors impacting safety for micromobility can suggest that regardless of the growing research interest on safety for micromobility, the research trend may be misdirected and clustered on areas that amount for only 13% of the real demands. Consequently, major areas of research such as geometry and pavement still lack attention, and so potential safety concerns in those areas have remained unanswered. For example, concerning geometry, there are no studies yet conducted on two aspects of “grading” and “marking and signing”, even though they both are key elements of safety development for the MM users.

Some other important criteria like lateral control, presence of intersection, connectivity, and composition have seen limited attention, with one or two dedicated research work to each. It is believed that to eliminate all the existing safety concerns and increase public acceptance for micromobility, that could increase ridership, the future research should be directed towards the understudied identified in this research.

Existing studies lack multi modes in their analysis. Consequently, in some areas, the results offered may not be extendable to other modes because of the major physical and maneuvering differences, and thus remain unverified for the use of city planners.

A categorized bar chart (Figure 10) was developed to clearly illustrate the studied mode of micromobility for each area of the research on safe infrastructure. The horizontal axle is divided for each area and shows six different micromobility mode for each criterion, and the vertical axle shows the number of studies existed for each mode. Accordingly, in most criteria groups, there are only one or two modes included in the studies.

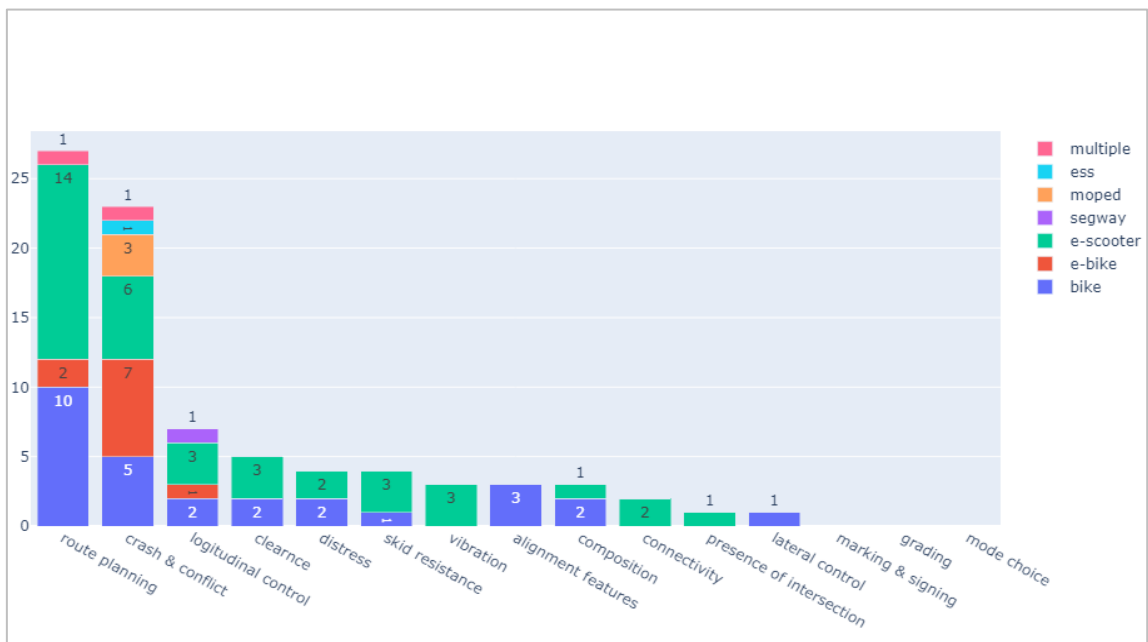


Figure 10 Distribution of modes studies for each area of research.

There are only three areas where the studies have covered more than two modes of micromobility. In the area of crash and conflict, five modes of bike, e-bike, e-scooter, electric self-balancing e-scooter (ESS), and moped were studied. The two areas of longitudinal control and route planning contained four and three modes, respectively.

Overall, Figures 9 and 10 clearly show traffic and operation are the areas where most research on micromobility are centered over the past decades, whereas for the two major areas of geometry and pavement, few studies were observed in comparison despite their essential role in safety. Therefore, they are suggested to be the focus of future studies related to safety for micromobility users. Specifically, three areas of marking and signing, grading, mode choice that are missing from the literature.

Tableau (version 2022.3) was used to create a cartogram of the studies (Figure 11). The findings demonstrate that US cities were among the largest sampled locations. China was next with 12 studies that was almost half of the samples in USA. After that, Spain, and Italy each have 5 studies sampled their cities, more than France and Denmark with only 3 studies. However, overall, the nine European countries have a large of the literature, with 23 studies that is the same as USA share.

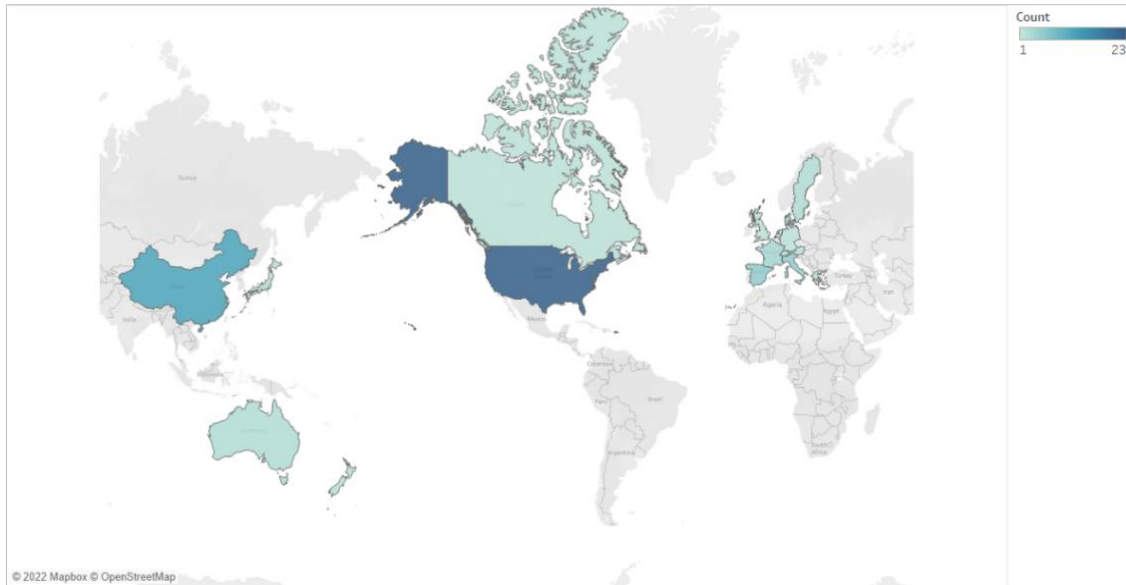


Figure 11 Cartogram of the geographical distribution of literature studies.

The Cartogram clearly shows that the studies are only centered in developed nations, and so many developing countries that have initiated the use of micromobility are still missing from the literature.

The results revealed that three areas of marking and signing, grading, mode choice are overlooked in the literature that focus on addressing safety on micromobility infrastructure. There are also nine other areas identified as understudied. They include vibration, distress, skidding, alignment features, clearance, lateral control, connectivity, traffic composition, and presence of intersection. Due to major differences between motor vehicles and micro devices in terms of the dimensions, weight and driving characteristics, future studies that focus on these identified areas can be effective in improving the infrastructure and operation of micromobility.

Geographically, most relative studies have been conducted for cities in US and China, and between the recent years of 2020 to 2022. E-scooter was the most studied mode (over 40%) for the topic of this research, and then bike, and e-bike had the rest of the attentions. Some rare studies were also found to include other modes like mopeds, and ESS. This shows that there is still a lack of information about the operational characteristics and safety requirements of some recently developed micro devices that need to be addressed in the future. Especially, for the recently trending self-balancing devices that have specific steering, and physical characteristics.

Finally, from the four pillars adapted for this study, the most share of the literature was allocated to the two pillars of traffic and operating condition, suggesting lack of attention to pavement and geometry studies for the safety of micromobility users that needs to be addressed in future studies related to this topic.

3.3 Horizontal Curve Safety on Bike Lanes

Horizontal curves in road and bike lane design are essential for ensuring smooth transitions between straight sections. There are several types of horizontal curves, each with specific characteristics and applications. The most common type in bike lane is the simple circular curve that has a constant radius that provides a smooth and continuous

change in direction. It is specified by parameters such as the degree of curve, radius, and length. Another type is the compound curve, which consists of two or more simple curves with different radii joined together to accommodate complex alignments, often used in mountainous terrains or constrained spaces. Reverse curves are composed of two simple curves in opposite directions, separated by a short tangent, useful in switchbacks and areas with limited space. Transition or spiral curves are used to gradually change the curvature from a straight path to a circular curve, improving driver comfort and safety by reducing sudden changes in lateral acceleration. Specifications for these curves include the length of the spiral, radius, and the rate of change of the radius. Each type of curve is designed to meet specific needs, ensuring safe and efficient vehicle movement along the road (AASHTO, 2010; Groot, 2007).

The review of literature on horizontal curve safety on bike lanes is organized into three subsections to examine previous research efforts comprehensively. Firstly, it analyzes studies concerning the safety implications of bike lane geometry, aiming to understand how bike lane design influences safety outcomes. Following this, the review discusses the dynamic tracking approach, which is the primary methodology employed in the current research. This section aims to elucidate the methodology used for dynamic tracking and its relevance to the study's objectives. Finally, the review explores semi-naturalistic and simulation-based research, investigating studies that have utilized these methodologies to explore topics relevant to the overarching research goals.

3.3.1 Design Parameters and Guidelines

The Dutch design manual for bicycle traffic (CROW) outlines five key parameters for designing horizontal curves on bike lanes: route type (basic network/connection or main cycle route), design speed (12 km/h, 20 km/h, 30 km/h), minimum associated radius (5m, 10m, 20m), minimum sight distance in motion (distance covering in 4-5 seconds), and stopping sight distance (40 meters at 30 km/h; 21 meters at 20 km/h). Additionally, it mandates an operational width for cyclists of 750 mm, with a 250 mm safety distance (clearance) for passing or overtaking cyclists. The safety distance is set for the conditions in which cyclists are forced to ride slower than 15 km/h due to factors like swaying motion, crosswinds, and so may have a lateral deviation of 200mm under normal conditions (Groot, 2007).

3.3.2 Optimization of Curve Geometry

Reviewing the literature reveals a significant emphasis on optimizing the geometry of horizontal curves for road safety, yet bike lanes, with distinct optimization needs, receive considerably less attention (Hosseini Sabbaghian et al., 2023b). Determining an optimal radius of curvature and widening value requires consideration of imposed forces and human factors specific to all micromobility users. They are making riding decisions based on experienced forces and perceptions of the path ahead (Ul-Abdin et al., 2020).

Calculating experienced forces by cyclists during curvature is an initial step in optimization of curves. Ul-Abdin et al. (2018) developed an optimized bike lane design system using theoretical trigonometric derivations. They calculated the optimal radius of curvature, accounting for centrifugal, centripetal, and gyroscopic forces on users, while considering variations in the radius of curvature depending on the location of the center of gravity: whether it is on the cyclists themselves, on the bicycle, or on the connection point between cyclists and the road surface (Ul-Abdin et al., 2020). Nee et al. (2022) constructed a mathematical model of road cycling on various routes, employing the Frenet-Serret frame. Their analysis revealed that braking is needed to minimize

centripetal acceleration occurred prior to the point of maximum curvature. This can facilitate acceleration through pedaling out of a bend (Nee & Herterich, 2022). Other related studies have concentrated on velodrome and track cycling, providing predictive models to assess applied power of cyclists on a velodrome, and centripetal forces stemming from tire scrubbing effects and the tipping motion of a cyclist maneuvering through a corner of a velodrome (Bos et al., 2024; Lukes et al., 2012).

3.3.3 Human Factors and Perception

The second parameter explored in literature to assess safety on horizontal curves is human factors, particularly anticipation and infrastructure predictability, and their impact on users' behavior and crash risks. A recent study on curves safety in roadways by Afghari et al. (2023) unveiled that users' anticipation of infrastructure (predictability) is a crucial latent variable to be integrated into crash risk modeling. They formulated an econometric model that incorporates the predictability of drivers as they navigate through different curves (Afghari et al., 2023). Other studies have primarily utilized simulators to examine the effects of various modifications on curves. For instance, a study by Meuleners (2023) investigating the widening of an on-road bike lane using this approach found that increasing the bike lane width on curved sections of mid-block roads could significantly benefit cyclists, potentially reducing bike lane excursions by up to 68% (Meuleners et al., 2023). Ma and Luo (2016) conducted a microsimulation study on cyclist acceleration behavior on bike lane, utilizing naturalistic GPS data collected from commuter cyclists recruited for the study (X. Ma & Luo, 2016). Overall, the review on horizontal curves suggests that the perceptual impact of design has not been thoroughly investigated. This aspect holds significant importance in determining design values optimized for the safety of micromobility users, as they are more likely to adhere to designs that align with their perceptions and behaviors.

3.4 Safety Assessment Methods

Proactive safety assessment monitors real road user movements to preemptively identify potential safety hazards arising from factors like infrastructure, human behavior, vehicles, traffic, and the environment, all without dependence on accident records (Llopis Castelló, 2018).

To fulfill this purpose, Surrogate Measures of Safety (SMoS) were introduced in 1977 to serve as proactive safety indicators derived from non-collision events, which occur more frequently than accidents (Amundsen, 1977). The measures are derived from observing mobility users' motion and mainly evaluate their interactions in potential conflict scenarios. For instance, Time to Collision (TTC) estimates the remaining time before a potential collision if trajectories continue unchanged. Meanwhile, Post-Encroachment Time (PET) measures how long it takes for a road user to regain a safe distance after a near-miss event. This approach is known as a more effective and ethical approach for safety assessment without the need to rely on historical accident data.

SMoS are commonly classified based on their application (direction, operational attributes), usefulness scope, and time nature of the data (Mullakkal-Babu et al., 2020). Regarding their application scope, SMoS are categorized by interaction dimensions, including longitudinal interaction, lateral interaction, and two-dimensional interaction. Common longitudinal SMoS indicators include TTC (Time to Collision), GT (Gap Time), DRAC (Deceleration Rate to Avoid Collision) or DST (Deceleration to Safety Time), and PICUD (Potential Indicator of Collision with Urgent Deceleration). Lateral SMoS like

PET (Post-Encroachment Time) are used to predict risks in lane change controllers, intersections, and lateral maneuvers. Some SMOs have applications in both longitudinal and lateral driving scenarios, such as Time to Accident (TA), Conflicting Speed (CS), and Single-step Probabilistic Driving Risk Field. In terms of operational attributes, SMOs are divided into four groups: time-based (e.g. TTC and GT), distance-based (e.g. PICUD), deceleration-based (e.g. DRAC), and others (Lu et al., 2021). Additionally, SMO indicators can be either continuous (TTC, DST, GT) or discrete (TA, CS, PET) in terms of time (Kathuria & Vedagiri, 2020).

A significant limitation of metrics like TTC and PET is their assumption that users would maintain constant speed and direction in conflicting situations, which is not realistic. To address this, probabilistic Surrogate Measures of Safety (SMoS) were introduced in 2008 (Saunier & Sayed, 2008). These models consider the dynamic motion changes in near-miss events, offering a more realistic safety assessment. Yet, recent improvements include analyzing commuters' complete trajectory footprints, leading to higher accuracy at micro resolution. (Nabavi Niaki et al., 2019).

3.4.1 Interaction-based approach

Studies that used interaction-based safety analysis mostly developed algorithms to evaluate micromobility near misses and crashes, occurring on bike lanes and during interactions with motor vehicles. For example, a cross-comparative study (Laureshyn et al., 2017) used video data from three intersections in Norway, employing the Swedish Traffic Conflict Technique (Swedish TCT), Dutch Conflict Technique (DOCTOR), and Probabilistic Surrogate Measures of Safety (PSMoS) to assess surrogate safety measures by analyzing car-cyclist conflicts and potential collision points. While conflict techniques aligned well in identifying conflicts, PSMoS detected more safety-relevant interactions, suggesting promise for future road safety analysis with a need for further refinement, particularly in cyclist-involved scenarios amidst decreasing accident rates and stagnant data quality.

Another study (Reijne et al., 2022) examines AV-cyclist interaction during cyclist-initiated emergency braking to avoid other vehicles, and evaluates the risk of cyclist falls. The study tests Threat Assessment Algorithms (TAA) accuracy in Automated Vehicles (AVs) using Time-to-Collision (TTC) and Headway (H).

3.4.2 Movement-based approach

The movement-based safety analysis enables the identification of unsafe maneuvers and assesses traffic response to designated designs. With the advancement in Artificial Intelligence (AI) and Computer Vision (CV), researchers assessing the safety of micromobility are increasingly utilizing these technologies to automate the tracking of users' and extract their microscopic operational parameters. These studies primarily focus on riders' motion, speed, and trajectories, aiming to proactively assess risky movements and mitigate crash risks for micromobility users.

Nabavi Niaki et al. (2019) utilized the "Traffic Intelligence" open-source tool (Jackson et al., 2013) to identify the most hazardous maneuvers, particularly when cyclists follow discontinuous facilities. The tool extracted user types and trajectories to analyze these movements (Nabavi Niaki et al., 2019). Gildea et al. (2023) proposed an advanced cyclist tracking algorithm utilizing CV to assess single bicycle crashes (SBC) or fall incidents from bikes. The study involves three main components: object detection to determine the

position and orientation of the bicycle, semantic segmentation of the bicycle and rider, and human pose estimation to analyze the rider's posture and lean angle (SWOV, 2023).

3.4.3 Safety Assessments through Simulations

Since naturalistic data might not include all the scenarios influenced by infrastructure, human behavior, vehicles, traffic, and environmental conditions, some studies use equipped vehicles with sensors, cameras, or simulation packages and virtual reality to evaluate bike lane safety in different situations, avoiding dependence on limited or sometime inaccessible real-world data. A recent simulation-based study assessed the human factor to test various on-road cycling lane layouts, and found that colored cycle lanes enhance safety on left alignment curves, while uncolored lanes are safer for straight and right curve alignments (Almallah et al., 2024). Another study examined human perception and used a bicycle simulator in a virtual environment to see how safe people felt in different setups. They found that protected bike lanes were seen as the safest type of bike lane (X. Guo et al., 2023).

In terms of the traffic factor or user interaction, most studies have examined cyclists-cars interactions, rather than cyclists-cyclists or cyclists-e-scooters. This might be because such conflicts can result in more serious injuries. For example, Rampf et al (2023) used Simulation of Urban Mobility (SUMO) software to model the interaction between automated vehicles and cyclists. They concluded that their model could sometimes perform better than existing car-following and lane-changing models (Rampf et al., 2023).

The infrastructure factor was also studied using a bicycle simulator. For example, Meuleners et al. (2023) examined how the presence or absence of sharrows at a roundabout and widening an on-road bike lane (1.2 meters or 1.8 meters) affected a curved mid-block section of the road (see section 2.2.3). The findings showed that widening the bike lane to 1.8 meters led to a notable 68% decrease in bike lane excursions on the curved mid-block section of the road. Moreover, the study found that the presence of sharrows did not significantly impact the distance from the left curb when entering a single lane roundabout (Meuleners et al., 2023).

3.4.4 Safety Assessments with Instrumented Devices

Experimental studies using instrumented micromobility devices are increasing. This method is useful in better understanding of the motion and interaction between users. Fonseca-Cabrera et al. (2021) examined perceived risk during meeting maneuvers between e-scooters and cyclists (Fonseca-Cabrera et al., 2021b). Lopez et al. (2020) assessed objective and subjective risk of overtaking maneuvers of motorized vehicles to cyclists' groups riding instrumented bicycles. They found high speed, low lateral clearance (1.5 meters), and rear position to higher risk (López et al., 2020). Shoman et al. (2023) analyzed data from instrumented city bicycles to investigate the behavior of public users. They collected information on bicyclist demographics, users' perceptions, and cyclists' dynamics (speed, pedaling power, and cadence rate) to observe user reactions to various features of the road surface and geometric design, as well as interactions with other road users such as pedestrians. This study also introduced multicriteria behavioral risk indicators (BRIs), which encompass risk factors associated with users' perceptions in various weather, road, and traffic conditions, interactions with other road users, and responses to infrastructure deficiencies. The indicator primarily relies on users' speed and surveys regarding their perceptions and experiences on bike lanes rather than analyzing trajectories directly. (Shoman et al., 2023).

Johansson et al. (2023) examined how infrastructure affects cyclists and developed a method to gather data for studying cyclist-infrastructure interaction in microscopic traffic simulations. They utilized electric and conventional bicycles equipped with instruments to track movement through curves, uphill sections, and intersections. They also surveyed cyclists to better understand human behavior (Johansson, 2023).

3.5 Trajectory Analysis Techniques

Understanding user behavior in micromobility and enhancing microsimulation models requires sophisticated analysis of movement patterns. Trajectory clustering and classification techniques are crucial in this regard. Methods such as the k-means algorithm and model-based clustering with the expectation-maximization (EM) algorithm and Bayesian Information Criterion (BIC) enable detailed categorization of user maneuvers. Following clustering, classification techniques like the K-nearest neighbors method further refine the data. Advanced models, including Locally Weighted Regression (LWR), Multivariate Adaptive Regression Splines (MARS), and Gaussian Processes (GP), offer improved accuracy in analyzing user interactions. This section will discuss these methods in detail, highlighting their applications and benefits in trajectory analysis.

3.5.1 Trajectory Clustering and Classification

To gain deeper insights into user behavior across different interactions and enhance microsimulation models, researchers employed clustering methods to categorize user maneuvers. The k-means algorithm, introduced in 1967 (MacQueen, 1967) and further developed in 1979 by (Hartigan & Wong, 1979), is a popular clustering method. It aims to minimize the distance between each data point and the centroid of its assigned cluster for a specified number of clusters, denoted as 'k'. This is achieved by iteratively assigning each point to the nearest centroid and updating the centroid to the mean of its cluster. The algorithm optimizes the following objective function:

$$\min_{(\mu_1, \dots, \mu_k)} \sum_{h=1}^k \sum_{x \in X_h} \|x - \mu_h\|^2 \quad (1)$$

The goal is to establish a hypothesis, $h_1 = \{\mu_1, \dots, \mu_k\}$, consisting of means from k different normal distributions. Initially, a random hypothesis is set for initialization. Each instance is represented as $h_{xi}, z_{i1}, z_{i2}, \dots, z_{iki}$, where x_i is the observed variable, and z_{ij} is 1 if it stems from the j th normal distribution, and 0 otherwise. Through iterative estimations of z_{ij} 's expected values, a maximum-likelihood hypothesis is pursued. Subsequently, a new hypothesis, h_2 , is calculated using these expected values. This new hypothesis replaces the previous one, and iterations continue until convergence to a final hypothesis.

Following the k-means algorithm, in 2002, model-based clustering and classification emerged. This approach integrates hierarchical clustering, the expectation-maximization (EM) algorithm for mixture models, and Bayesian Information Criterion (BIC). The EM algorithm involves two key steps:

1. The E-step computes z_{ik} , which reflects the likelihood of observation i belonging to cluster k based on current parameter estimates.
2. The M-step calculates maximum-likelihood parameter estimates using the computed z matrix.

Each cluster is described by a Gaussian model $\phi_k(x|\mu_k, \Sigma_k)$, where x represents the data, μ_k signifies cluster means, and Σ_k denotes covariances. The maximum-likelihood

values for the Gaussian mixture model are determined by Equation (2), (Fraley & Raftery, 2003) with τ_k representing mixing proportions.

$$f(z) = \arg \min_{y \in \mathcal{Y}} d(z, y) \quad (2)$$

After clustering, the clusters will be classified using the K-nearest neighbors method (Mitchell et al., 1990).

Overall, various flexible fitting models have been developed that are superior fit over conventional models that are restricted by their theory-based functional forms. However, these models are less easy to interpret. In short, these models are:

- 1) LWR: Locally Weighted Regression (Cleveland, 1979).
- 2) MARS: Multivariate Adaptive Regression Splines (Friedman, 1991).
- 3) SVM: Kernel Support Vector Machines (Cortes & Vapnik, 1995).
- 4) BRNN: Bayesian Regularized Neural Networks (Foresee & Hagan, 1997).
- 5) GP: Gaussian Processes (Quinonero-Candela & Rasmussen, 2005).

(Shen et al., 2023)

In a recent study, Mohammed et al. (2019) applied the GP method to analyze cyclist behavior. They introduced a clustering approach based on a multivariate finite mixture model to categorize cyclist maneuvers during following and overtaking interactions. The maneuvers were grouped into initiation, merging, and post-overtaking states. The interaction data collected were include longitudinal distance, lateral distance, and speed difference using computer vision and video data (Mohammed et al., 2019).

3.5.2 Trajectory Pattern Mining

With advancements in global positioning systems (GPS), more trajectory data is now available for mobility analysis, which has spurred increased research in data mining techniques and computer science. Challenges such as low frequency of positioning data, high power consumption, and personal privacy concerns are discussed in the literature. According to Shen et al. (2023), current applications of large-scale trajectory data include traffic jam detection, automatic driving, navigation route planning, and mobility modeling (Shen et al., 2023).

The sampling rate in GPS trajectory datasets encompasses two crucial aspects: spatial and temporal. Spatially, it reflects the distribution of users across observed areas, while temporally, it concerns the time interval of the collected GPS data. Enhancing the quality of an existing trajectory dataset can be accomplished through various methods. One such approach is trajectory completion, employing heuristic search algorithms or intricate probability models (Chen et al., 2011) to depict the transition pattern between locations. Additionally, addressing issues such as the low sample rate and prolonged time intervals between location records is vital, as these factors contribute to an accumulated deviation within trajectories, resulting in significant aggregation errors. Researchers are actively working to tackle these challenges, aiming to refine trajectory datasets for more precise analysis and diverse applications across multiple fields.

For generation of trajectory data with a high sample rate, researchers have directed their efforts towards extracting features from a restricted pool of existing high-quality trajectory data. Deep learning methodologies, including Recurrent Neural Networks (RNNs) and Generative Adversarial Networks (GANs) (Goodfellow et al., 2014), have

been leveraged to construct sequential mobility prediction models like the Markov Chain (Li & Zhang, 2009). Additionally, some studies have incorporated random mobility models alongside realistic road topologies. Despite these advancements, many generated trajectories in these studies are deemed unrealistic (Shen et al., 2023), thereby potentially impacting the outcomes of data mining research conducted using such trajectories.

To overcome this limitation, super-resolution techniques (Farsiu et al., 2004), commonly used in computer vision studies, are employed to enhance the clarity and sharpness of low-resolution images. In simpler terms, trajectory data, which tracks the movement of objects or individuals over time using a series of points, often lacks detail, with points recorded at intervals such as every 10 minutes instead of every 3 minutes. However, by applying super-resolution methods, researchers can enhance the granularity of this data, enabling more frequent point capture.

When examining trajectory generation models, researchers adopt diverse metrics to assess performance at both micro and macro levels. At the microscale, the comparison between truth and predicted trajectories is crucial. This evaluation hinges on metrics like normalized Dynamic Time Warping (nDTW) (Keogh & Ratanamahatana, 2005) and Average Displacement Error (ADE) (Sadeghian et al., 2018). DTW, renowned for its robustness in measuring time series distances (Hall & Albers, 2023), accommodates matches between similar shapes, even if their temporal alignment differs. Meanwhile, ADE measures the Euclidean distance between predicted and actual trajectories, providing valuable insights into model accuracy.

Expanding the scope to the macrolevel involves assessing the spatial distribution of trajectories across the entire study area. Here, the goal is to identify similarities between the overall distributions of predicted trajectories and ground truth data. Researchers employ three operations—addition, shifting, and deletion—to align predicted mobility patterns with true ones. They utilize various indicators to evaluate the similarity between two sets of mobility data. Manhattan distance (MD) compares overall differences between corresponding elements of the matrices, while Normalized Manhattan distance (NMD) scales differences for comparison irrespective of matrix size. Shift proportion (SP) determines the ratio of shifts required for alignment. Normalized mass angle (NMA) gauges directional agreement using eigenvectors, and Normalized structural angle (NSA) assesses structural alignment employing singular value vectors (Yao et al., 2021).

3.6 Conclusions about Current Knowledge

The main limitations or gaps in current knowledge identified as a result of the state-of-the-art analysis are presented below, categorized into the following fields: bike lane safety, horizontal curve design, safety assessment measures, and trajectory generation.

Regarding bike lane safety, the scientometric analysis in section 3.1 shows that there is very limited research on how alignment features of bike lanes (both tangents and various curves) influence user maneuvering. Most studies on bike lane safety focus on intersections and interactions between cyclists and motor vehicles, analyzing crash data and conflicts. Other research gaps include the effects of bike lane width, lane widening, clearance, speed control, and signage for bike lane. Additionally, pavement-related factors such as skidding, distress, and vibration, which can affect safety and comfort, are understudied. Overall, there is much less focus in the literature on the geometry and pavement of bike lanes than on traffic and operation.

For horizontal curve design, the most explicit resource found was the Dutch design manual for bicycle traffic (Groot, 2007). It outlines five key parameters for designing horizontal curves on bike lanes: route type, design speed, minimum associated radius, minimum sight distance in motion, and stopping sight distance. Thresholds for these metrics are provided in the guideline. However, there is little compatibility and homogeneity between existing bike lanes in many European countries and these standard metrics.

Another issue that some relative studies have highlighted is the incompatibility between the design speed of curves and the actual speed at which users travel. Literature suggests that users often exceed the design speed, and there is no enforcement. These facts indicate a need for more post-implementation studies on user maneuvering behavior to determine whether they follow the design and to identify major safety risks.

In terms of safety assessment, as detailed in section 3.4, many of the developed measures used to assess conflicts between micromobility users are derived from traditional Surrogate Measures of Safety (SMoSs) such as Time to Collision (TTC) and Post-Encroachment Time (PET). These measures typically estimate time in a conflict scenario to gauge the likelihood of a crash given constant speed and direction of users. However, research on motor vehicle conflicts has shown that such assumptions can lead to inaccurate and biased results. Furthermore, there is still considerable controversy among researchers regarding the acceptable time thresholds on these measures to differentiate between safe and unsafe scenarios.

In the realm of micromobility, where users have greater maneuverability due to their light weight and increased degrees of freedom, reliance on traditional measures can introduce even more errors. Even utilizing more advanced versions like probabilistic SMoSs still necessitates access to extensive historical crash data, which is often lacking for bike lanes, leading many studies to focus on intersections, where they could use crash data to analyze car-cyclist conflicts. Consequently, most of these studies often exclude single-user falls that can result in serious injuries, as data on such incidents is frequently unavailable for bike lanes. Moreover, there is also a lack of naturalistic studies on bike lanes that analyze users' maneuvering under free-flow conditions without solely focusing on their interactions. Therefore, what is lacking is a metric that can assess the safety risks associated with various behavioral patterns of vulnerable bike users in relation to geometry and can serve as a preliminary safety assessment when historical crash data is absent. Of course, when crash data exist and are available, the same measure can become more powerful in identifying black spots on bike lanes.

Trajectory data is crucial for the current study, yet generating accurate trajectories has posed challenges in previous research due to the complexity of the process. While GPS positioning has been the primary method for tracking road users, the number of bikes or e-scooters equipped with GPS remains limited. Additionally, challenges persist with the accuracy and frequency of GPS positioning.

In conclusion, current research reveals several gaps in trajectory data retrieval and processing. Although video-based methods and computer vision tools are used to address challenges in obtaining user trajectory data, there is still a need for improved GPS positioning techniques to enhance accuracy. Super-resolution methods aim to reduce the time interval between data points, but their effectiveness remains under evaluation. Additionally, the segmentation of bike lanes, which could help assess the spatial risk of maneuvers at higher resolutions, is not explored in the literature. Furthermore, there is a

need for better algorithms or a simplified process to manage the computational complexity of generating accurate trajectories from video data and ensuring their practical application.

Chapter 4 Objectives and Hypotheses

The primary objective of this research is to develop a comprehensive methodology for evaluating horizontal curve design on bike lanes by introducing a novel trajectory-based metric named the Effective Fitted Radius (EFR). The EFR is defined as the radius of a fitted trajectory passing through three fixed points with equal distances between them on a bike lane. The EFR allows for comparison with the actual radius of the curve through descriptive and statistical variance analysis across different turn directions and user types. The operating speed of users is the second microscopic metric to be analyzed alongside the EFR, offering complementary insight into user behavior during curve navigation.

For this study, the analysis is limited to users passing through the curve in free-flow conditions (lane violation events). The aim is to assess individual risky maneuvering and speeding to determine if geometry influences specific patterns. It is important to note that interactions between users are not within the scope of this research, as the focus is on non-conflict events.

To achieve this objective, the following scientific and technical objectives are proposed:

- O1. Identify key factors influencing cyclist safety on horizontal curves.
- O2. Evaluate trajectory analysis methods and data collection techniques.
- O3. Synthesize findings to identify if there is a robust methodological framework for segmenting bike lanes and computing cyclist trajectories through point positioning and micro-spatial analysis.
- O4. Segmentation of bike lane on horizontal curve to facilitate computation of trajectories through point positioning and further micro-spatial analysis.
- O5. Selection of horizontal curve sites on bike lanes in the city of Valencia based on factors such as average daily traffic, geographical distribution, and diversity in curvature degrees and radius, including flat and sharp curves with varying degrees of sharpness.
- O6. Collection of video recordings on selected sites using a small camera with wide lens and a portable tripod of at least 6 meters height. The tripod is preferably placed inside the curve or parallel to one of the tangents, at a distance that ensures coverage of the entire curve site without attracting the attention (gaze) of the majority of users, thereby minimizing any potential impact on their maneuvering.
- O7. Initial verification of users not being influenced by the presence of the camera is achieved by monitoring the head and gaze of passing users at the beginning of the recording.
- O8. Preprocessing the recorded videos: labeling, trimming, undistortion, storing in a cloud-based platform.
- O9. Selecting an accurate computer vision algorithm or software package available for motion analysis of recordings that includes detection and tracking of objects.
- O10. Calibrating the 3D coordinates of the videos by defining a calibrated coordinate grid to establish consistent observational distance references, such as central markings. Some computer vision (CV) tools achieve this using a perspective calibration grid that compares it with a pre-estimated ground reference.
- O11. Defining spatiotemporal parameters that need to be extracted from the video recordings for calculating the desired microscopic metrics (speed and trajectory). This depends on the features and capabilities of the chosen computer vision (CV) tool.

- O12. Extraction and computation of the desired microscopic metrics using combined methods: the CV tool and an suitable libraries in Python such as NumPy, Pandas, and SciPy.
- O13. Analysis of the computed EFRs and speeds using descriptive and statistical analysis of variances (parametric or non-parametric).
- O14. Proposing of a complete framework for using EFR in the safety assessment of horizontal curves on existing bike lane for free-flow analysis and highlighting the potentials in interaction-based studies with historical accident data in the future.

Next, the research hypotheses are presented. These have been divided into two groups: initial hypotheses, which serve as the basis upon which the research will be grounded but are considered sufficiently validated by previous research, and hypotheses that will be tested with the development of this doctoral thesis.

As initial hypotheses, the following should be highlighted:

- H1. The motion on a bike lane include trajectory footprints, speed, acceleration, deceleration, lean, lane changing, and overtaking of micromobility devices.
- H2. A bike lane infrastructure comprises three main components: bike lane alignment, side bike lane, and pavement condition.
- H3. Observing cyclists in free-flow conditions is essential to assess how bike lane geometry impacts user behavior, eliminating the influence of user interactions.
- H4. The motions of bike lane users are not randomly distributed; various factors contribute to their variations and risk level. Among these factors, human factors (perception and error) and bike lane infrastructure play a significant role in most risky motions.
- H5. There is a relationship between human factors and bike lane infrastructure. For instance, a change in the geometric design of a horizontal curve can significantly influence riders' motion behavior.
- H6. The motion of bike lane users can be detected, tracked, and measured as various metrics through video motion analysis using computer vision.

On the other hand, the hypotheses to be tested are:

- H1. Bikes and e-scooters may exhibit different motion patterns on bike lane due to variations in size, steering angle, and handling characteristics.
- H2. The direction of turn on curves can influence the trajectory and speed patterns of users.
- H3. Lateral segmentation on bike lanes facilitates the identification of unsafe regions and potential causes, allowing for a micro-resolution safety assessment.
- H4. Horizontal curves with a radius below certain limits and high curvature may not only fail to encourage users to adhere to the design, but they can also provoke more violations, risky patterns, and speeding.
- H5. The highest frequency of minimum speed occurs at Mid-Point (MP) of curve.
- H6. Similar to motor vehicles, micromobility users navigating isolated horizontal curves generate specific trajectory patterns that can be clustered and classified.
- H7. The geometry of the curve may be one of the top three predictors of a user's trajectory on a horizontal curve.

Chapter 5 Methodology

This doctoral thesis introduces a novel safety assessment metric, referred to as Effective Fitted Radius (EFR), aimed at enhancing the safety of horizontal curves on bike lanes during the design and improvement phase. To validate this metric, a comprehensive sample of isolated horizontal curves in Valencia (Spain) needs to be selected. These curves must encompass a diverse range of radii and degrees of curvature to effectively test the performance of EFR across various geometric configurations and evaluate its effectiveness in understanding the impact of geometry on user behavior.

In the review of previous studies (section 2), the trajectory and operating speed of real bike lane users, including cyclists and e-scooterists, emerged as the most utilized parameters in the movement-based safety assessments for micromobility. To collect these motion data naturalistically, several hours of video footage of real bike lane users at enough sample of curve sites needs to be recorded.

As the first step, a small wide-lens camera and a six-meter tripod are used to record video footage of real bike lane users at a sufficient number of curve sites. Next, the collected videos are analyzed with the software tool "Kinovea version 2023.1" to retrieve the required motion data, categorized by user type (cyclists and e-scooterists) and direction of movement (left-turn or right-turn). Finally, a new segmentation method specific to bike lanes is proposed, followed by the computation of EFR using the Powell optimization method in SciPy. The extracted EFR data undergoes preprocessing and is divided for comparative qualitative and quantitative statistical analysis to identify risky maneuvers, segments and track types. Below, each step of the method is explained details in the diagram (Figure 12).

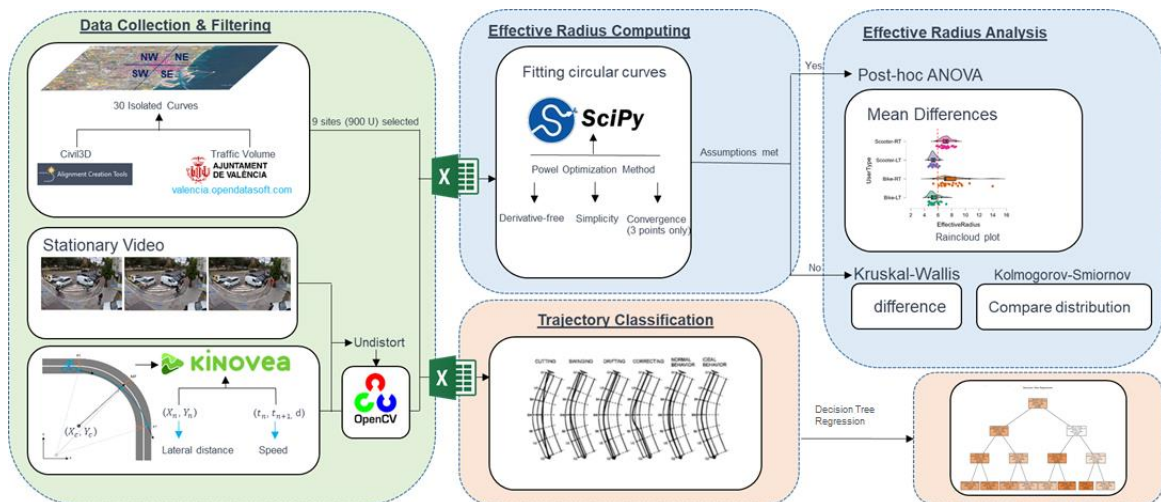


Figure 12 Overview of the methodology.

5.1 Geometric Recreation and Selection of Horizontal Curves

To accurately recreate the geometry of horizontal curve sites within the city of Valencia, several methods can be employed. For this study, the Alignment creation tool in Civil 3D, alongside orthophoto maps, will be utilized. Civil 3D is specifically chosen for its advanced capabilities in detailed alignment creation, which is crucial for precise geometric replication. This tool allows for meticulous control over curve parameters, ensuring that the recreated geometries closely match real-world conditions. Other

methods of geometric recreation include total station surveys, which provide high accuracy through precise geospatial data collection but are labor-intensive; GPS surveys, which are less labor-intensive but may lack precision in areas with poor satellite reception; and laser scanning (LiDAR), which captures high-resolution 3D data efficiently but requires specialized equipment. Additionally, photogrammetry uses aerial or terrestrial photographs to create detailed spatial data, though it necessitates careful processing, and manual measurement, the least precise method, relies on traditional tools like tapes and measuring wheels, useful in contexts where advanced technologies are unavailable (Mishra et al., 2024).

High-resolution orthophoto maps of Valencia, can be obtained from the PNOA (Plan Nacional de Ortofotografía Aérea) website (CNIG, 2024), and then be integrated into Civil 3D to provide an accurate base for tracing and aligning the geometric features of selected curves. Using Civil 3D's alignment creation tool, detailed curve alignments will be specified by radii, degree of curvature, deflection angle, arc length, and chord length. These geometries are meticulously verified and adjusted against the orthophoto maps to ensure accuracy and reliability. All horizontal curves in this study are simple circular curves with a constant radius, as they are the most commonly observed in the bike lane network (see section 3.2).

To select the case study curves, the traffic conditions of the bike lanes in the city of Valencia were first examined (*Geoportat València | Ajuntament de València*, n.d.). The bike lane segments with the highest Average Daily Traffic (ADT) in the study area were then identified for reducing collection time. From these segments, a representative sample of horizontal curves were selected based on several key conditions. Curve sites were chosen to cover a wide range of radii, from the sharpest curve existed in the city with small radii of 2 meters to flat curves, encompassing various degrees of navigational difficulty. The degree of curvature was another critical factor, with selected sites ranging from 769 degree to 22 degree for the flattest curve with minimal deflection. Moreover, ensuring a representative geographic spread across the city of Valencia was crucial, with curve sites selected from distinct segments of the city – Northwest (NW), Northeast (NE), Southwest (SW), and Southeast (SE) – to allow for the analysis of spatially diverse traffic behaviors and environmental influences.

5.2 Video Data Collection

Collecting naturalistic data requires specific techniques and considerations to avoid users detecting the camera, ensure a proper angle of the camera view, and ensure recordings are saved properly and stored in a secure online platform. For this study, a six-meter tripod and over four Garmin Virb cameras, three for substitute, will be used for each day of data collection. These cameras are equipped with a wide lens and have small sizes (32 mm x 53 mm x 111 mm), which will be beneficial for being hidden. They will provide 1080p HD video recording with a 16-megapixel CMOS image processor. They have Bluetooth capability, allowing connection to a mobile device for live remote monitoring of the recordings when the camera is installed at the top of the tripod.

To keep the camera from the users, the tripod will need to be placed at a minimum lateral distance of 10 meters or more from the outer edge of the horizontal curve at the measurement point (MP). In areas where this distance cannot be met, the tripod can be placed close to one of the tangents, with a minimum lateral offset equal to the width of the bike lane or 2 meters. In all cases, it is necessary to continuously monitor the users' gaze and head movement to ensure they are not aware of being recorded during curve

navigation. Users who notice the camera will be excluded from data extraction. If the number of users detecting the camera increases, the location of the tripod will need to be adjusted.

The most ideal view of the camera will be a bird's-eye view (see Figure 14), but for naturalistic studies, this will not be practical because it would require using drones or placing the tripod very close to the edge of the bike lane. Therefore, for this study, the camera will preferably be installed on top of an extendable six meters tripod at a 90-degree angle from the tripod's vertical axis. In cases where the lateral distance is not sufficient, the camera can be tilted down slightly (up to 45 degree) to capture a full view of the entire horizontal curve. Figure 13 illustrates an example of the tripod with the camera installed at a proper distance from the curve site.

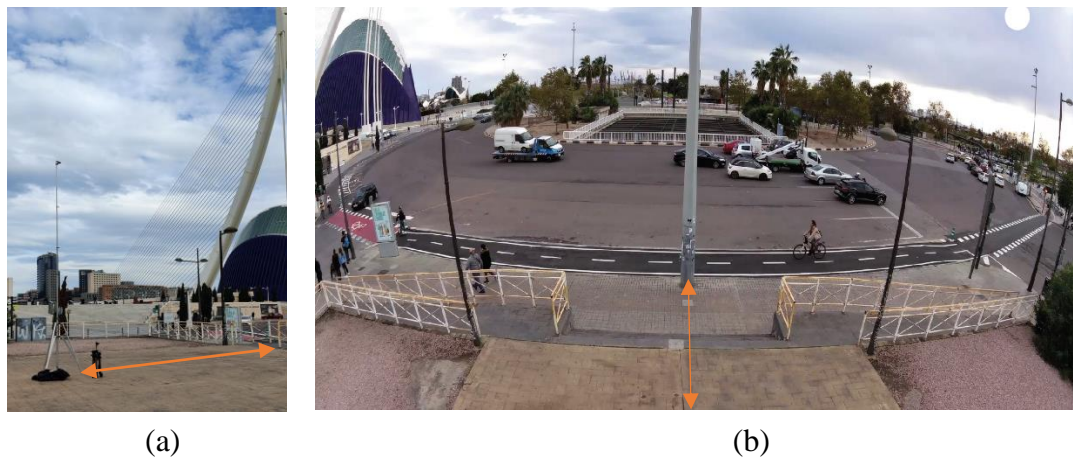


Figure 13 Tripod placed at proper distance (a) tripod with camera (b) side view.

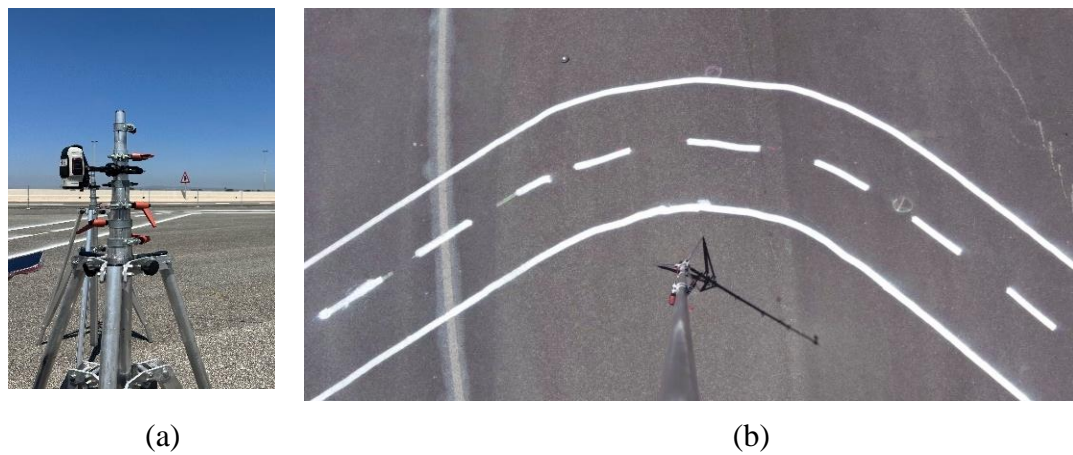


Figure 14 Bird-eye view settings (a) tripod with camera at zero degree (b) Bird-eye view.

5.3 Segmentizing and Regionalizing the Horizontal Curve

The observation area for user trajectory and speed extended beyond the bike lane borders to include adjacent areas, especially where bike lanes were integrated with pedestrian walkways. The typical width of the studied bike lanes in this study is 2 meters with the markings (1.7m without markings). To enable detailed analysis of trajectory data on horizontal curves, regionalization and segmentation were implemented (see Figure 15).

This involved dividing the bike lane into three sections: PC (point of curvature), MP (midpoint), and PT (point of tangency); and four spatial areas as described below:

- 1) Lane (LN): User's wheel is positioned within the lane, spanning from the right edge to 42.5 cm towards the central marking.
- 2) Central Marking (CL): User's wheel is positioned on or within 42.5 cm to the right of the central marking, which accounts for half of the operational width (75 cm) and the marking width (10 cm) combined. This positioning poses a risk of crossing conflicts with opposite users.
- 3) Opposite Lane (OPL): Users breach their lane, causing their wheel to enter the lane for opposite direction travel (in bidirectional bike lanes), leading to head-on and side-angled conflicts.
- 4) Out of Lane (OTL): The area to the right of users' movement direction within the bike lane, where interactions with pedestrians or collisions with fixed objects can occur.

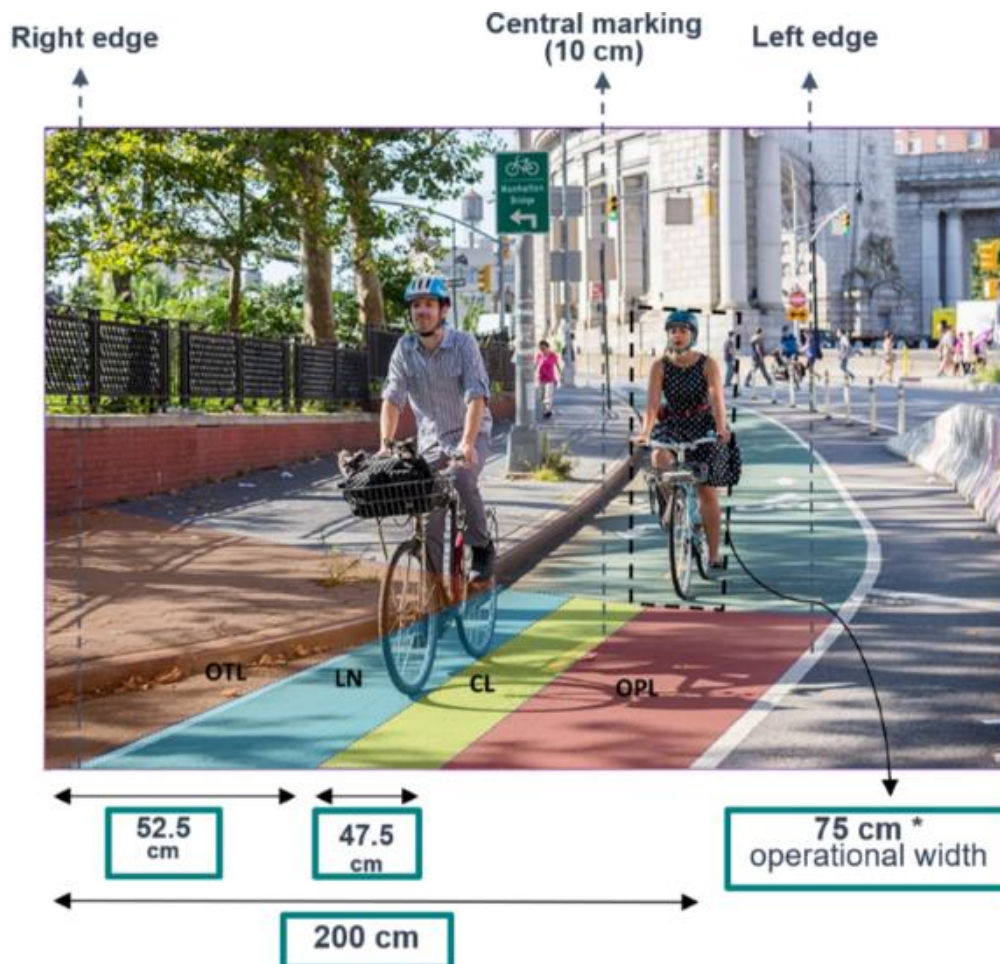


Figure 15 Regions of interest for identifying user's position on the curve with users making a right-turn; background image source (NYC DOT Web page, 2024).

5.4 Track Typology

To effectively classify the maneuvers of bike lane users, six track types previously defined in motor vehicle dynamics research on horizontal curves were adopted (Spacek, 2005). Ideal behavior (ID) represents the optimal track, characterized by a symmetrical path along the center of the dedicated lane in each direction, closely adhering to the idealized design standards. This type means the user have maximum stability and minimal deviation, promoting consistent and predictable movement within a narrow central area. Normal behavior (NR) also indicates a symmetrical track along the center but allows for a broader area of movement, accommodating slight deviations such as minor cutting towards the curve's inside without encroaching on the lane's center line. These two types aim to provide cyclists with a reliable and secure riding path, emphasizing minimal deviation from the initial path.

More complex behaviors include Correcting (CR), Cutting (CT), Swinging (SW), and Drifting (DR). Correcting (CR) involves an S-shaped path, where cyclists initially drift toward the curve's outside before correcting their steering midway through, often due to an underestimation of the curve's length or sharpness. Cutting (CT) involves deliberate, strong cutting to the inside of the curve, a conscious effort to balance centrifugal forces. Swinging (SW) and Drifting (DR) both describe asymmetrical track paths but in opposite manners: Swinging (SW) sees cyclists start on the right side of the lane and drift left toward the curve's end, while Drifting (DR) involves starting on the left and drifting right. These behaviors highlight the diverse ways cyclists navigate curves, influenced by both conscious decisions and unconscious adjustments to the bike lane's geometry.

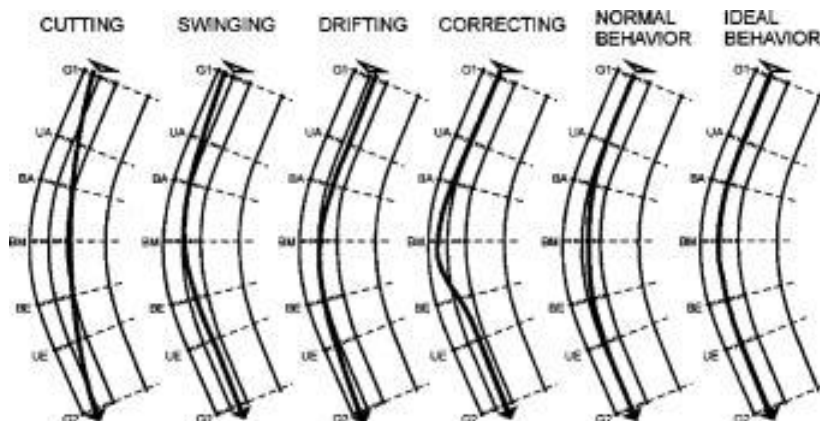


Figure 16 Six track types for motor vehicle maneuvers on horizontal curves (Spacek, 2005).

5.5 Data Extraction

In this section, the methods and procedures for extracting and analyzing the data collected from video recordings of bike lane users will be detailed. Section 5.5.1 will describe the process of determining the Effective Fitted Radius (EFR) using Kinovea motion analysis software and a custom Python script to fit circular arcs and compute geometric properties. Section 5.5.2 will focus on estimating the average speed between sections using timestamps and distances, and performing comparative analysis through descriptive statistics and box-and-whisker plots to visualize speed distributions across different sections, user types, directions, and curve geometries. Finally, Section 5.5.3 will outline

the use of the DBSCAN clustering algorithm to identify patterns in the lateral offsets of users, addressing noise and outliers to uncover meaningful trends in the data.

5.5.1 Effective Fitted Radius (EFR)

The process of capturing data from videos involved extracting users' spatio-temporal data, including wheel position and timestamps for average speed estimation, using Kinovea motion analysis software (version 2023.1) at PC, MP, and PT. This data was then formatted in Excel and utilized by a Python script designed to fit circular arcs. The script calculated various geometric properties of the arc, such as start and end points, midpoint, tangent vector, and normal vector, based on predefined parameters like degree of curvature, radius, and deflection angle. It then iterated through each row of positions (offset distances) from the Excel file, defining the arc's offset at the start, midpoint, and end points.

For each set of offset distances, the script minimized a distance function representing deviation from the circle using the Powell method from the SciPy library to find the optimal center and radius of the fitted circle. The Powell optimization method in SciPy facilitates the generation of the best-fitting circular curve between three points with minimized squared deviation. This method only requires the coordinates of the three points; there is no need for the center of the curve or the radius. Consequently, it enables the computation of the Effective Fitted Radius.

Finally, the original arc, control points, offset points, and the fitted circle were plotted with annotations for geometric parameters, and the radius of the fitted circle was printed for each row of offset distances. Additionally, a second Python script was written to find the best-fitted polynomial curves to plot trajectory heatmaps. Figure 17 (a) depicts a case study of a curve analyzed within the Kinovea software environment and the calibrated perspective grid used for frame calibration before data extraction, whereas Figure 17 (b) presents an aerial view of the curve, displaying control points, the actual trajectory (gray), and the fitted polynomial curve (yellow).

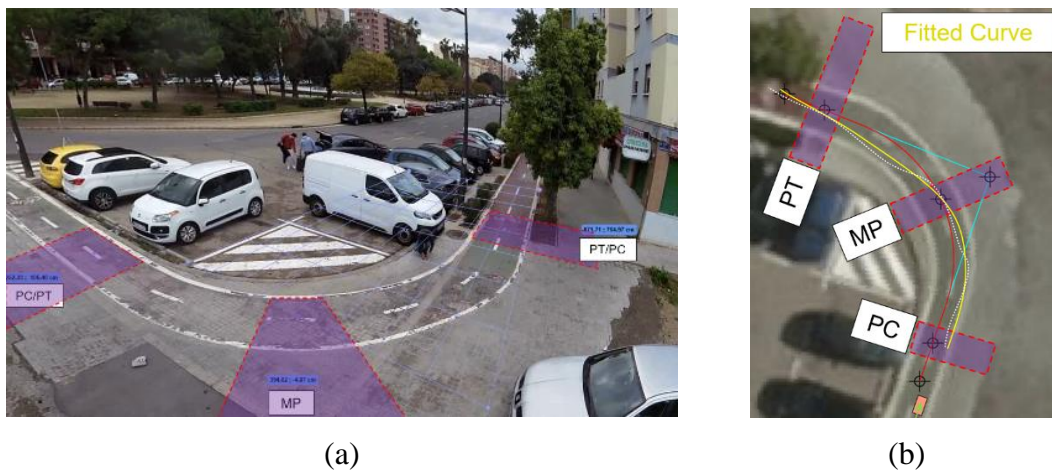


Figure 17 Data extraction: (a) curve site camera view and (b) aerial view with the control points.

5.5.2 Speed

In this method, the average speed between each consecutive section will be estimated based on the timestamps and the distance between them. These timestamps will be

extracted from the Kinovea software while the user navigates through the curve, allowing for precise calculations of instantaneous speed between sections. Then, the tracking feature in Kinovea will be used to also record the spot speed (speed at a specific position) at each section of interest. This velocity will be compared with the average speeds for verification purposes, and if verified will be recorded as the speed of user at that section.

To provide a comprehensive comparative analysis, a descriptive analysis method will be employed, along with box-and-whisker plots. Descriptive analysis will involve summarizing and interpreting the data to highlight patterns and central tendencies, such as mean and median speeds, as well as variability through measures like standard deviation. Box-and-whisker plots will then be used to visually compare the speed distributions between different sections, user types, directions, and curve sites with varying geometries. These plots will illustrate the spread and skewness of the data, highlighting any outliers and differences across the categories, thereby offering deeper insights into the factors influencing cyclist behavior and speed.

5.5.3 Track clustering and prediction

Clustering is the process of dividing a large collection of entities into smaller groups based on their similarity, without predefined classes. On the other hand, classification is the process of grouping entities by similarity into predefined classes (Kononenko & Kukar, 2007), as conducted in the previous subsection. There are several types of clustering techniques, including K-Means Clustering, Hierarchical Clustering, Prototype-based clustering, Density clustering, and Model-based clustering. Clustering techniques can also be classified based on the algorithmic approach used to find clusters in the dataset. The different types of clusters include exclusive or strict partitioning clusters, overlapping clusters, hierarchical clusters, and fuzzy or probabilistic clusters (Kononenko & Kukar, 2007).

In this research, the objective is to identify patterns in the lateral offsets of users across different sections (d-pc, d-mp, d-pt) on a curve. The analysis began with the loading and normalization of the dataset. The DBSCAN (Density-Based Spatial Clustering of Applications with Noise) algorithm was chosen for clustering due to its ability to identify clusters of arbitrary shape and its robustness to noise and outliers.

DBSCAN works by grouping together points that are closely packed together while marking points that lie alone in low-density regions as outliers. This property is particularly useful in the dataset, which might contain outliers due to variations in track conditions or measurement errors. After an initial clustering to identify and remove outliers, the data was reclustered to better capture the true patterns within the data.

DBSCAN was suitable for this research for several reasons. First, it does not require the number of clusters to be specified a priori, which is advantageous when the appropriate number of clusters is unknown. Second, DBSCAN is capable of finding clusters of arbitrary shape, making it flexible enough to handle complex trajectories. Third, it effectively handles noise and outliers, which is critical in this dataset, as evidenced by the identification of outliers in the initial clustering step. This adaptability and robustness make DBSCAN an excellent choice for analyzing the lateral offset data.

After clustering analysis, a decision tree plot will be produced using a Python script through several key steps. First, data from a CSV file will be read into a pandas DataFrame. Categorical variables will be identified and one-hot encoded using

OneHotEncoder within a ColumnTransformer. Next, the dataset will be split into training and testing sets using `train_test_split`. A DecisionTreeRegressor will be initialized and trained on the training data. Predictions will be made on the test set, and root mean squared error (RMSE) will be calculated for each target variable. Finally, the decision tree will be visualized using `plot_tree` from `sklearn.tree`, with the `filled=True` parameter for better clarity and `feature_names` provided to label the nodes appropriately. This comprehensive approach will utilize `matplotlib.pyplot` to display a clear decision tree structure, aiding in understanding the model's decision-making process visually.

To enhance the performance and interpretability of the DecisionTreeRegressor model, hyperparameter tuning will be integrated using GridSearchCV from `sklearn.model`. This will involve systematically exploring a predefined parameter grid (`max_depth`, `min_samples_split`, `min_samples_leaf`) to identify the optimal configuration via cross-validation, evaluating based on negative mean squared error scoring. Once the best parameters and model are determined, predictions will be generated for the test dataset, and root mean squared errors (RMSE) will be computed for each target variable (d-pc, d-mp, d-pt). The top-performing model selected by GridSearchCV will be visualized using `plot_tree`. This visualization will depict the most influential features and their splits, facilitating interpretation of the model's decision-making process. Additionally, the script will save the optimal model using `joblib.dump` and document crucial outcomes—parameters, scores, and RMSE values—in both text and image formats, enabling comprehensive analysis and future reference. These enhancements will collectively ensure a more robust and effective decision tree regression model, elevating its predictive accuracy and explanatory power for diverse applications.

5.6 Data Analysis Techniques

To assess safety using computed EFRs, a combination of quantitative and qualitative methods will be employed. Post-hoc Analysis of Variances (ANOVA) and raincloud plots will be used to analyze the impact of user type and movement direction on risky maneuvers on curves. ANOVA is applied when assumptions of normality and homogeneity were met ($p > 0.05$), and when EFRs had minimal outliers. For datasets with high dispersion, the non-parametric Kruskal-Wallis test is used to identify differences among four independent groups at each site (Left-turn cyclists, Right-turn cyclists, Left-turn e-scooterists, Right-turn e-scooterists). For the statistical analysis the JASP software will be used. JASP (Jeffreys's Amazing Statistics Program) is an open-source statistical analysis software developed by a collaboration of researchers and software developers from the University of Amsterdam, the University of Groningen, and other institutions. It is designed to provide a user-friendly interface for conducting a wide range of statistical analyses, including descriptive statistics, t-tests, ANOVAs, regression analysis, Bayesian inference, and more (*JASP 18.3*, 2024).

To assess differences, median EFRs are calculated and compared instead of mean EFRs, which can be influenced by skewness. Subsequently, the Kolmogorov-Smirnov test can also be conducted on groups showing differences to compare distributions and assess the degree of difference using cumulative distribution functions (CDFs). Additionally, data visualization is carried out using Python to generate heatmaps and trajectory maps of selected sites.

Chapter 6 Development

This chapter outlines the comprehensive development process undertaken for the study, focusing on the methodologies and technical steps used to gather, process, and analyze data on bike lane safety on horizontal curves. It begins with the selection and classification of study area curves, explaining the criteria and process for identifying and categorizing curves within specified districts. The chapter then covers the recreation of selected curve geometry using Civil 3D software, detailing the techniques for accurately modeling these curves. Camera placement, recording, and undistortion are discussed next, including strategic positioning, recording methods, and video correction processes. The extraction of motion outputs from videos is then explained, followed by the computation of the Effective Fitted Radius (EFR) using mathematical and computational approaches. Finally, the chapter presents the data analysis techniques used to interpret the data and draw conclusions about bike lane safety on horizontal curves.

6.1 Selection and Classification of Study Area Curves

A systematic approach was employed to identify relevant curves, ensuring a diverse representation of urban environments. This section provides a detailed account of the methods used for this crucial step. As shown in Figure 18, the identified curves are distributed in three main districts:

- Algiros: Including the avenues of Blasco Ibañez and Tarongers.
- El Plà del Real: Near Turia Park.
- Ciutat Vella: Primarily on the streets of Angel Guimerá and Peris y Valero.

Initially, 50 curves were located in these high-traffic segments. The GPS coordinates (Global Positioning System), curve type, location, segment type, and storage folder of each 50 curves were then documented and listed in Table 2.

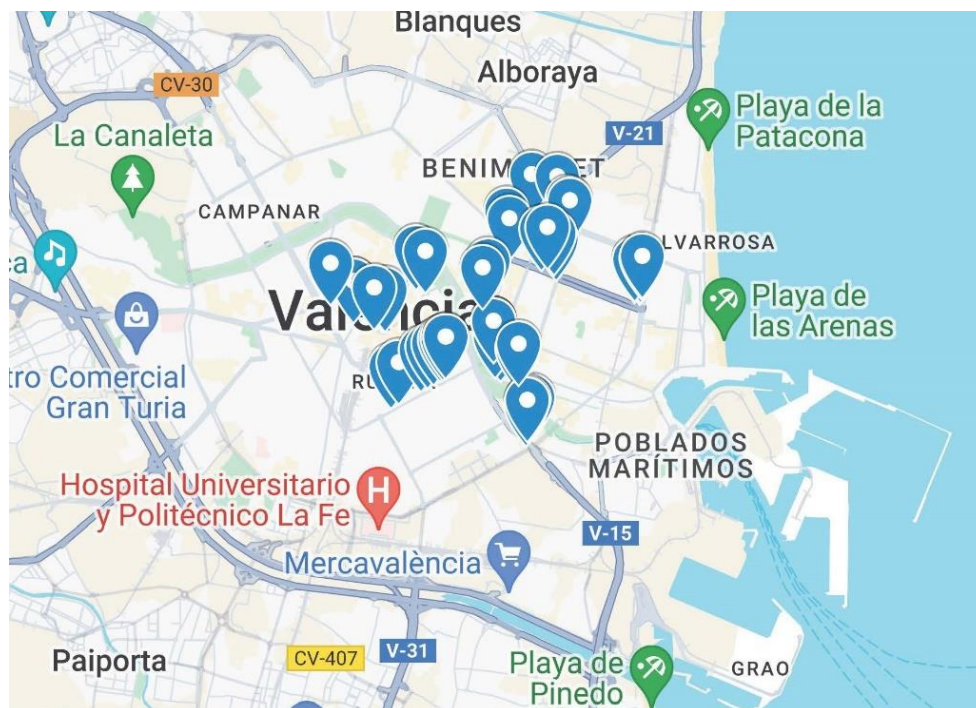


Figure 18 Initial map of identified curve sites in busiest bike lanes in the city of Valencia.

As can be seen in Table 2, 10 out of 50 curves were successive, meaning that several bends occur in a short distance. Therefore, these were excluded from the list for further selection. The remaining horizontal curves, which were isolated, were classified based on whether they are circular (tangent-circular curve-tangent) or tangents with a small bend (tangent-tangent), and on their degree of curvature: flat or sharp (high curvature).

Table 2 List of identified curve sites in busiest bike lanes in the city of Valencia.

#	Label	GPS	Curve Type	Location	Folder	Segment
1	SE1	39.4605159 -0.3540564	circular-flat	Plaça d'Europa	12,14,19	roundabout
2	M1	39.469773 -0.3597295	tangent-flat	Av d'Arago	12.13	midblock
3	NE1	39.4711587 -0.3345507	tangent-flat	Mari Blas de Lezo	12.2	roundabout
4	NE2	39.4709779 -0.3346739	tangent-flat	Mari Blas de Lezo	12.2	roundabout
5	NE3	39.4708101 -0.3357394	circular-sharp	Mari Blas de Lezo	12	roundabout
6	NE4	39.4747042 -0.3495153	tangent-flat	Av Blasco Ibanez	12	midblock
7	SE2	39.453720, -0.352684	circular-flat	Plaça Saller	14	roundabout
8	NE5	39.470606 -0.3347898	tangent-flat	Mari Blas de Lezo	14	roundabout
9	NE6	39.4745263 -0.350406	tangent-flat	Av Blasco Ibanez	14	midblock
10	SE3	39.453861 -0.352518	circular-flat	Plaça Saller	16.18	roundabout
11	SE4	39.460008, -0.354225	circular-flat	Plaça d'Europa	16.4	roundabout
12	SE5	39.460008, -0.354225	circular-flat	Plaça d'Europa	16,19,13	roundabout
13	SW1	39.470317 -0.383590	circular-sharp	Guillem de Camidblockro-Xàtiva	18	midblock
14	SW2	39.471784 -0.368658	circular-sharp	Plaça Porta de la Mar	18	roundabout
15	SE6	39.4633132 -0.3579977	circular-sharp	Escultura Sol de Ripollés	18.8	roundabout
16	SE7	39.4633132 -0.3579977	circular-sharp	Escultura Sol de Ripollés	18.8	roundabout
17	SE8	39.4633132 -0.3579977	circular-sharp	Escultura Sol de Ripollés	18.8	roundabout
18	SE9	39.461417 -0.357701	circular-sharp	Pont del Regne	18, 8	bridge
19	NE7	39.473959 -0.348474	circular-flat	Plaça d'Emilio Attard	18	roundabout
20	SE10	39.453166 -0.352845	circular-sharp	Plaça Saller	16.18	roundabout
21	SE11	39.453166 -0.352845	circular-sharp	Plaça Saller	18	roundabout
22	SE12	39.453997 -0.351845	circular-flat	Plaça Saller	18	roundabout
23	SE13	39.453505 -0.352840	circular-flat	Plaça Saller	18	roundabout
24	NE8	39.4703922 -0.3349863	circular-sharp	Mari Blas de Lezo	19, 4	roundabout
25	M2	39.4706023 -0.35883	tangent-flat	Av d'Arago	2, 4	midblock
26	SW3	39.467372 -0.376738	circular-sharp	Xàtiva	3	midblock
27	SW4	39.472207 -0.370118	circular-flat	Palau de Jumidblockicia	3, 8	midblock
28	SE14	39.4610174 -0.3568832	circular-flat	Pg. de l'Albereda	3	roundabout
29	M3	39.4757801, -0.3554835	circular-sharp	Av d'Arago-Blasco	3	roundabout
30	NE9	39.470618 -0.335771	circular-sharp	Mari Blas de Lezo	3	roundabout
31	NE10	39.473321 -0.348102	tangent-flat	Av Blasco Ibanez	5	roundabout
32	NE11	39.477921 -0.346000	tangent-flat	Ramon Llull	8	midblock
33	NE12	39.478138 -0.346351	circular-sharp	Ramon Llull	8	midblock
34	NE13	39.480826 -0.347920	successive	Tarongers	8	midblock
35	SW5	39.468132 -0.379963	circular-sharp	Xàtiva	7	midblock

36	SW6	39.468132 -0.379963	tangent-flat	Xàtiva	7	midblock
37	SW7	39.467045 -0.374975	circular-flat	Xàtiva	7	midblock
38	M4	39.4767544 -0.3559002	circular-sharp	Av Catalunya-Blasco	8	roundabout
39	M5	39.4811459 -0.3520229	circular-flat	Av Catalunya-Tarongers	8,4	roundabout
40	NE14	39.474315 -0.348030	circular-flat	Plaça d'Emilio Attard	18	roundabout
41	NE15	39.474867 -0.350184	tangent-flat	Av Blasco Ibanez	12	midblock
42	SE15	39.461402 -0.365455	successive	Av. de Peris i Valero	76	midblock
43	SE16	39.461407 -0.365470	successive	Av. de Peris i Valero	77	midblock
44	SE17	39.461176 -0.365927	successive	Av. de Peris i Valero v1	78	midblock
45	SE18	39.461041 -0.366340	successive	Av. de Peris i Valero v1	79	midblock
46	SE19	39.460610 -0.367356	successive	Av. de Peris i Valero v1	80	midblock
47	SE20	39.460177 -0.368338	successive	Av. de Peris i Valero v1	81	midblock
48	SE21	39.459772 -0.369340	successive	Av. de Peris i Valero v1	82	midblock
49	SE22	39.458278 -0.372872	successive	Av. de Peris i Valero v1	84	midblock
50	SE23	39.457765 -0.374075	successive	Av. de Peris i Valero v1	85	midblock

6.2 Recreation of Selected Curve Geometry in Civil 3D

After the high-volume segments and their corresponding isolated curves are identified, the next crucial step involves using an accurate tool and an updated Lidar-based orthophoto map of Valencia to extract the geometric features of these curves. The base map and the points where the curve sites are located, as listed in Table 3, are imported into the Civil 3D software. The alignment creation tool in Civil 3D is then used to recreate the geometrical alignments (tangent-curve-tangent) along the central markings of the bike lanes. Figure 19 provides screenshots of the point maps on the base orthophoto and the alignment creation tool in use.

The radius of the curve sites ranged between 2 to 10 meters, with the addition of two flat curves (with radii of 22 m and 78 m). The degree of curvature ranged from as high as 796 degrees to as low as 22 degrees for the flattest curve site. The selection of curve sites was also based on their spatial distribution and traffic volume. The aim was to choose sample sites with the highest average daily traffic rates (to minimize data collection time) while ensuring representation from various segments of the city of Valencia, divided into Northwest (NW), Northeast (NE), Southwest (SW), and Southeast (SE). These spatial locations were used to label each site accordingly.

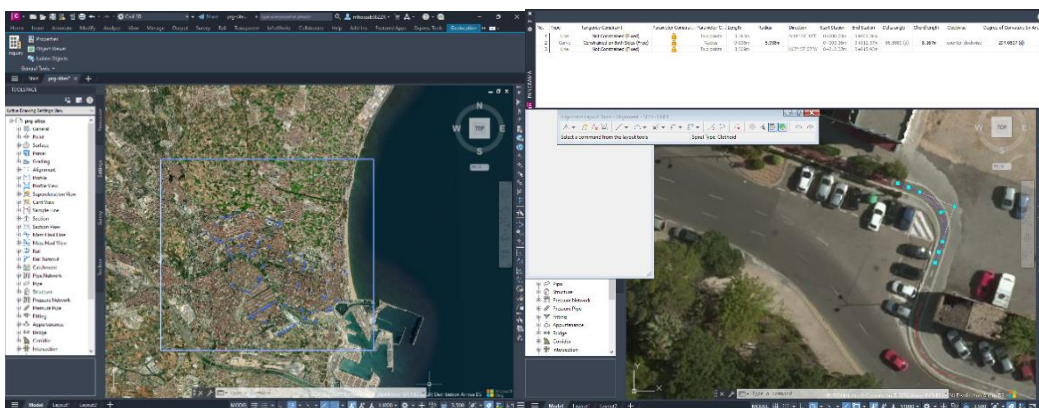


Figure 19 Screenshots of point maps and alignment creation tool in the Civil 3D.

The geometric data extracted from Civil 3D varied widely, yet many curves were quite similar. To filter out a representative group and reduce the data, their geometries were compared. Ultimately, out of 40 curves, nine with different radii, deflection angles, and sharpness (degree of curvature) were selected to be represent sample of various geometrical conditions (Table 3).

Table 3 Isolated curve sites geometric parameters.

#	Site	Type	Length (m)	Radius (m)	Deflection angle (d)	Chord length (m)	Degree of Curvature by Arc (d)
1	NE3	Sidewalk	10	6	89	8.8	278
2	SW2	Protected	12	10	69	11.1	178
3	SE4	Sidewalk	13	22	33	12.7	78
4	SE3	Protected	37	78	27	36.9	22
5	NW1	Sidewalk	4	2	89	3.2	769
6	SW1	Protected	6	5	71	5.9	341
7	SW3	Protected	4	5	46	4	341
8	NE9	Sidewalk	11	7	84	9.8	240
9	NE8	Sidewalk	13	9	85	11.8	200

6.3 Camera Placement, Recording, and Undistortion

After site selection recording videos starts at selected points. The key factors in this process are the camera's location and the discreetness of the recording process to avoid drawing riders' attention. The camera can be positioned parallel to one of the tangents, with a lateral distance of up to 4 meters from the edge of the bike lane, covering the entire curve to the next tangent. Figure 20-a provides a clear illustration of the parallel view before undistortion. It is evident from this image that positioning the camera in this manner is sometimes inevitable for sharp curves, especially in densely built-up areas like this sidewalk. Alternatively, the camera can be placed outside the curve, at a greater distance that can be adjusted on site to cover the entire curve. This placement enhances concealability and is suitable for less sharp, flatter curves (see Figure 20-b and c). In order to ensure users are not noticing the camera and their behavior is not being impacted by the presence of the camera, the recording crew had to monitor the gaze and head movements of the users to make sure that are not aware of the presence of the camera. Since the camera used is relatively small and placed atop a thin tripod at a height of 6 meters, it was observed that when it is positioned out of direct sight of users, the recording process goes unnoticed by anyone.

Before recording starts, another important process is to obtain permission from the city council. In this study, this process was followed based on the instructions of the municipality of Valencia, conducted through their website. Providing information regarding the streets and time of recording for each location is essential for approval. In cases where privacy protection laws apply, it is recommended to use other types of surveillance cameras, such as thermal cameras, that do not reveal the identity of users.

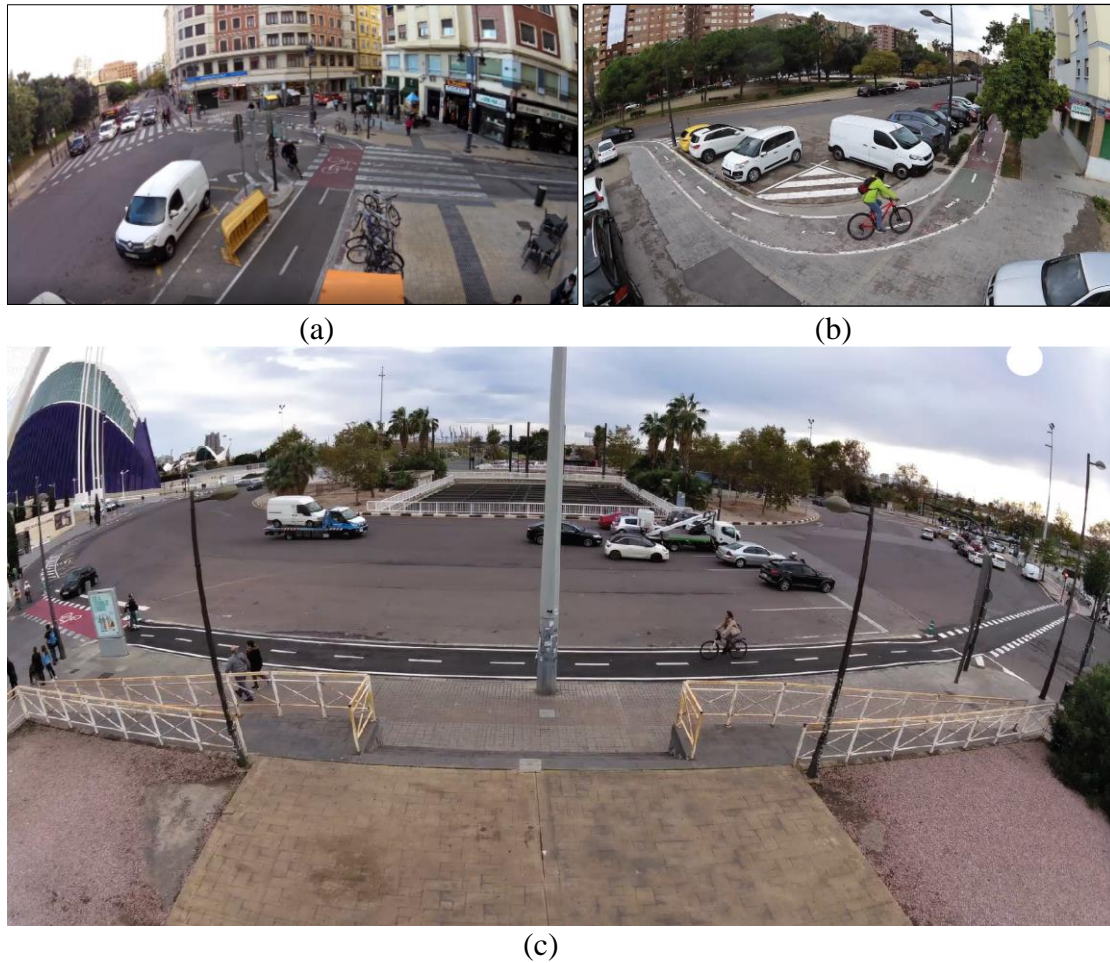


Figure 20 Camera views of curve site under study: (a) SW1 (b) NE3 and (c) SE3.

The selected sites' video data was captured using Garmin Virb Elite cameras, that allow recording 1080p HD video, mounted on six-meter tripods. The data collection was developed from September to November 2023, primarily during morning and evening rush hours (7am-10am and 4pm-7pm). At each site, recordings continued until reaching a minimum of 25 users per direction per user type (100 users in total) under free-flow conditions. This criterion was met by ensuring that the user is alone in its direction/lane or in other words other users (if any) have no influence on the user's speed (Teodorović & Janić, 2017). The minimum threshold of 25 users per user type and direction has been validated in previous research as the minimum requirement for conclusive results in similar behavioral studies (Fonseca Cabrera, 2021).

Moreover, if a traffic light was positioned within a curve, only movements during green lights were considered. To avoid attracting users' attention and ensure users' behavior was not affected by the presence of cameras, tripods were typically placed outside the curve near the intersection point, inconspicuously. The users' gaze was also monitored, and those showing signs of noticing the camera (e.g., turning head, eye movement) were removed from the analysis.

The video data is labeled by position (NE, NW, SE, SW) and numbered (e.g., SW1), then stored in a cloud-based space for analysis. Empty minutes without traffic were removed, and the videos were undistorted so as to then obtain more accurate speed and position data. A script based on OpenCV package in Python was programmed for this last step.

6.4 Data Collection

Before analyzing the recorded videos, it is necessary to remove the distortion caused by the wide-angle lens used in the camera. This preprocessing step is carried out using OpenCV (see appendix C), NumPy, and JASON library in Python. The programmed Python code is designed to undistort the videos captured with a wide-angle lens camera. It begins by loading the video file and camera calibration parameters from a JASON file. Using these parameters, it calculates the optimal new camera matrix to correct for distortion. Then, it iterates through each frame of the video, undistorts it, and writes the undistorted frames to a new video file. This process ensures that the resulting video has minimal distortion, making it suitable for further analysis or viewing. Overall, the script automates the preprocessing step of undistorting video footage, which is essential for obtaining faster and more accurate results in subsequent motion extraction tasks.

The motion analysis tool Kinovea (version 2023.1) (*Kinovea*, n.d.) is utilized to retrieve the necessary motion data, including trajectory and speed. The extraction process begins after calibrating each video to its specific view. This calibration is achieved using a measured reference area or line on the ground, along with the calibration grid feature within the software. Additionally, the calibration is verified using the line distance feature, which serves as control lines. At least three lines are placed at various locations within the video frame, typically along the central marking of the bike lane or spanning the width of the bike lane. Moreover, if a video contains prolonged periods with no users passing through the curve, these empty intervals are trimmed using the software's function to reduce the video file size and expedite the extraction process. This ensures efficiency in data extraction and minimizes unnecessary footage, focusing solely on relevant user movement analysis. To illustrate a sample of the outputs, Table 4 summarizes the position data for site NE3, which will be used for EFR computation in the next subsection. Table 5 lists the operating speeds of users at each defined section (PC, MP, and PT). These speeds are calculated based on the timestamp and distance method explained in the previous chapter. Refer to Appendix B, Tables 14 and 15, for all position and speed data.

Table 4 Lateral Offset Distances from Center Line for Site NE3 (R = 6m) by User Type and Direction.

#	Bike Left-Turn			Bike Right-Turn			E-scooter Left-Turn			E-scooter Right-Turn		
	PC	MP	PT	PC	MP	PT	PC	MP	PT	PC	MP	PT
1	61	42	72	34	50	8	49	-34	0	35	83	17
2	72	-10	26	47	37	-75	22	-48	13	32	44	-24
3	45	14	51	50	89	-16	38	-59	32	19	35	-13
4	16	0	202	35	55	19	10	-24	32	36	33	-16
5	50	24	0	43	30	-21	16	-51	-21	25	31	21
6	138	37	43	32	51	-16	33	-17	12	39	55	33
7	33	-17	39	-25	90	-11	0	-55	16	19	-28	-50
8	62	96	55	0	62	-15	27	-30	11	39	56	0
9	86	68	42	23	-22	0	-14	-17	37	21	14	0
10	0	-58	0	22	58	25	50	0	26	29	48	-54
11	27	17	26	18	78	31	28	-37	20	25	45	-51
12	33	26	0	26	63	-22	54	20	24	19	30	0
13	28	-82	16	25	0	-34	44	-23	0	33	49	-8
14	28	-78	26	36	60	27	33	37	24	22	58	9

15	22	-62	0	32	66	-10	31	-78	-18	37	22	-44
16	112	37	23	25	98	0	50	14	35	27	37	14
17	54	-7	45	13	34	0	27	0	29	34	65	7
18	133	45	32	39	34	0	10	-14	37	18	38	-27
19	44	-24	20	43	63	21	10	0	19	31	29	-5
20	0	-20	22	39	51	0	125	8	-16	23	41	0
21	37	0	-36	30	37	14	49	40	45	38	63	10
22	16	-90	0	32	78	-9	105	0	42	30	46	-18
23	62	68	39	25	20	-50	29	23	32	36	55	-30
24	50	-71	0	19	48	-14	37	18	24	24	42	-3
25	21	-41	0	16	82	0	-50	-30	-5	20	39	-23

Table 5 Operating Speed Data per Section for Site NE3 (R = 6m) by User Type and Direction.

#	Bike Left-Turn			Bike Right-Turn			E-scooter Left-Turn			E-scooter Right-Turn		
	PC	MP	PT	PC	MP	PT	PC	MP	PT	PC	MP	PT
1	29	22	28	17	17	26	29	20	24	13	18	26
2	26	21	25	21	23	32	30	21	23	13	16	25
3	33	22	27	20	18	28	33	24	27	25	13	18
4	23	18	15	11	11	16	31	17	18	22	18	28
5	25	19	18	21	17	22	40	22	23	17	15	23
6	22	16	23	18	17	24	40	24	25	12	9	18
7	22	18	19	23	21	30	40	25	26	26	17	25
8	16	14	15	26	23	31	30	16	23	24	15	19
9	24	17	21	20	19	29	27	19	29	19	10	15
10	30	22	23	19	18	25	23	15	18	31	20	27
11	20	14	16	12	16	26	42	16	32	32	17	25
12	22	18	20	22	16	23	21	15	18	21	10	17
13	22	14	20	20	19	29	34	24	40	14	20	27
14	22	16	15	18	16	17	31	15	25	13	14	24
15	22	18	17	19	18	18	37	25	30	24	15	19
16	16	12	24	21	16	27	30	17	26	23	17	27
17	22	17	21	18	17	21	26	14	16	17	15	24
18	22	18	23	16	12	15	15	9	16	12	10	18
19	24	17	21	21	16	20	41	21	28	26	18	25
20	21	30	20	18	14	19	27	19	25	23	15	21
21	26	17	20	16	15	17	31	17	26	19	11	15
22	32	22	19	17	12	16	20	15	22	31	20	25
23	21	13	17	28	18	28	28	17	26	32	17	27
24	33	24	30	26	15	26	33	17	26	21	12	17
25	18	12	10	27	20	30	21	15	24	32	18	26

6.5 Computation of Effective Fitted Radius

After extracting all motion data, the offset data will be used to generate circular fitting curved trajectories, representing the footprints of users navigating the horizontal curve. From these circular trajectories, the proposed measure of Effective Fitted Radius will be calculated to be later compared with the actual radius of the horizontal curve. This process is automated using a Python code, thoroughly explained in the previous chapter. For future reference, the code is provided below in Figure 21. The code calculates the coordinates of the offset points, which are displaced from the original arc points by the given offset distances (Table 4) in the direction of the normal vector to the arc at those points. In the code, `normal_x` and `normal_y` represent the components of the normal vector, which is perpendicular to the tangent vector of the arc. Each offset point is computed by adding the product of the offset distance and the normal vector to the coordinates of the corresponding arc point (start, mid, end). The minimizing function calculates the sum of squared distances from the offset points to a circle defined by the parameters (`center_x`, `center_y`, `radius`). For each offset point, it computes the distance to the circle as the Euclidean distance from the point to the circle's center minus the circle's radius. The objective function to be minimized is the sum of these squared distances, which represents the total deviation of the offset points from the circle. Fitting a circle to offset points by minimizing the sum of squared distances ensures that the best possible circle is found that minimizes the overall deviation of the points from the circle.

```

In [1]: import numpy as np
import matplotlib.pyplot as plt
from scipy.optimize import minimize
import pandas as pd

# Read the Excel file
df = pd.read_excel("NE3.B.LT.xlsx")

# Given parameters
radius = 6 # meters
length = 10 # meters
delta_angle = np.radians(89) # Convert angle to radians
curvature = np.radians(278) # Convert angle to radians

# Compute the arc center coordinates
center_x = 0
center_y = radius

# Compute the start point coordinates
start_x = radius * np.sin(curvature)
start_y = radius * (1 - np.cos(curvature))

# Compute the end point coordinates
end_x = radius * np.sin(curvature + delta_angle)
end_y = radius * (1 - np.cos(curvature + delta_angle))

# Compute the midpoint coordinates
mid_x = radius * np.sin(curvature + delta_angle/2)
mid_y = radius * (1 - np.cos(curvature + delta_angle/2))

# Compute the tangent vector at the mid-point
tangent_x = end_x - start_x
tangent_y = end_y - start_y
tangent_length = np.sqrt(tangent_x**2 + tangent_y**2)
tangent_x /= tangent_length
tangent_y /= tangent_length

# Compute the normal vector (perpendicular to tangent)
normal_x = -tangent_y
normal_y = tangent_x

# Read offset distances from the Excel file
offset_distances = df[['PC', 'MP', 'PT']] / 100 # Convert centimeters to meters

fitted_radii = [] # Store the computed fitted radii

for index, row in offset_distances.iterrows():
    # Compute the offset distances for each row
    offset_distance_start, offset_distance_mid, offset_distance_end = row

    # Compute the offset points from start, mid, and end points with different distances
    offset_start_x = start_x + offset_distance_start * normal_x
    offset_start_y = start_y + offset_distance_start * normal_y
    offset_end_x = end_x + offset_distance_end * normal_x
    offset_end_y = end_y + offset_distance_end * normal_y
    offset_mid_x = mid_x + offset_distance_mid * normal_x
    offset_mid_y = mid_y + offset_distance_mid * normal_y

    # Function to minimize: Distance from points to the circle
    def distance_to_circle(params):
        center_x, center_y, radius = params
        distances = np.sqrt((offset_start_x - center_x)**2 + (offset_start_y - center_y)**2) - radius
        distances = np.append(distances, np.sqrt((offset_end_x - center_x)**2 + (offset_end_y - center_y)**2) - radius)
        distances = np.append(distances, np.sqrt((offset_mid_x - center_x)**2 + (offset_mid_y - center_y)**2) - radius)
        return np.sum(distances**2)

    # Initial guess for the center and radius
    initial_guess = [0, radius, radius]

    # Minimize the distance function to find the center and radius of the circle
    result = minimize(distance_to_circle, initial_guess, method='Powell')

    # Extract the center and radius from the optimization result
    center_x_fit, center_y_fit, radius_fit = result.x

    # Append the fitted radius to the List
    fitted_radii.append(radius_fit)

# Add the fitted radii to the DataFrame
df['Fitted Radius'] = fitted_radii

# Write the DataFrame to an Excel file
df.to_excel("output.NE3.B.LT.fitted_radii.xlsx", index=False)

```

Figure 21 Python code programmed for automation of EFR computation.

6.6 Data Analysis

After computation of EFRs, all data required for descriptives and statistical analysis are made read. The offset data that in the previous section used for calculation of EFRs will be used again during the statistical analysis for creating displacement heatmaps for each curve site, divided by user type and direction. The heatmaps generation process is also automated using seaborn library in python. The code is provided below in Figure 22.

```
In [1]: import pandas as pd
import seaborn as sns
import matplotlib.pyplot as plt

# Read data from Excel file
df = pd.read_excel('NE3.S.RT.xlsx')

# Define the classification function
def classify_offset(x):
    if 42.5 <= x < 190:
        return 'LN'
    elif -5 <= x < 42.5:
        return 'CL'
    elif x < -5:
        return 'OPL'
    else:
        return 'OTL'

# Apply classification to each value in the dataframe
for col in df.columns:
    df[col+'_class'] = df[col].apply(classify_offset)

# Melt the dataframe for easier plotting
melted_df = df.melt(value_vars=df.columns, var_name='Point', value_name='Classification')

# Reorder the categories for 'Classification'
melted_df['Classification'] = pd.Categorical(melted_df['Classification'], categories=['OPL', 'CL

# Calculate percentages
crosstab_df = pd.crosstab(index=melted_df['Point'], columns=melted_df['Classification'], normaliz

# Create the heatmap with thin white lines between cells
plt.figure(figsize=(12, 8))
heatmap = sns.heatmap(crosstab_df, cmap="coolwarm", annot=True, fmt=".0f", cbar=True, linewidths
plt.xlabel('Spatioregion', fontsize=30) # Increase x-axis label font size
plt.ylabel('Section', fontsize=30) # Increase y-axis label font size
plt.title('NE3.S.RT Heatmap', fontsize=30) # Increase title font size

# Save the plot in high quality to a directory
plt.savefig('NE3.S.RT Heatmap.png', dpi=300)

plt.show()
```

Figure 22 Python code programmed for automation of displacement heatmap generation.

The effective radii of curvature (EFRs) and their associated speeds are meticulously arranged and saved in CSV files to facilitate thorough analysis. These files provide the groundwork for the comprehensive descriptive and statistical evaluations outlined in the forthcoming chapter. As depicted in Table 6, a sample representation showcases the structured formatting of the EFRs data. These meticulously prepared data sets will be imported into JASP. The rest of the computed EFRs are shown in Appendix B (Table 16).

Table 6 Computed EFRs for NE3 (R = 6m) curve site per user and turn direction.

#	Bike		E-scooter	
	Left-Turn	Right-Turn	Left-Turn	Right-Turn
1	5.5	6.9	5	8.2
2	5	8.1	4.9	7.4
3	5.3	9.4	4.6	7
4	4.7	6.9	5.2	6.7
5	6	6.6	5.1	6.2
6	5.1	7.5	5.2	6.6
7	5.1	14	4.9	5.8
8	7.2	9.1	5.1	7.2
9	6.1	5.3	5.4	6.1
10	5	7.1	5.3	8.6
11	5.8	8.1	5	8.4
12	6.3	8.6	5.6	6.7
13	4.6	6.1	5.2	7.2
14	4.6	6.9	6.2	7.5
15	4.8	8.2	4.7	6.8
16	5.4	10.6	5.4	6.5
17	5	6.9	5.4	7.6
18	5.3	6.5	5.3	7.5
19	5	7	5.7	6.5
20	5.4	7	5.3	6.9
21	6	6.4	5.8	7.3
22	4.6	8.9	4.9	7.4
23	6.5	7.1	5.8	8
24	4.7	7.7	5.7	7
25	5.1	9.5	6	7.4

Chapter 7 Results

In this research, the geometry of nine curve sites (Table 3) and the maneuvering behavior of 900 bike lane users navigating them were extracted and evaluated. The results of the extracted data are presented in this section. In general, the effectiveness of Effective Fitted Radius is proven, and impacts on users' behavior were found for assumed parameters such as curve radius, user type, and direction of travel. Both quantitative and qualitative methods are employed for analyzing the extracted microscopic data.

Figure 23 presents the data types (circles) and associated analysis methods (rectangles) used in the research. First, curve geometry and users' EFR data were compared using parametric and non-parametric post hoc Analysis of Variance (ANOVA). Next, lateral user positions on curves were analyzed in Python and visualized with heatmaps showing the percentage of users in each lateral segment by section, user type, and turn direction. Operational speed data were then used for descriptive analysis by section, user type, and turn direction. Finally, trajectory data were analyzed using Density-Based Spatial Clustering of Applications with Noise (DBSCAN) and a decision tree regression model to identify key geometric factors influencing user motion during curve navigation.

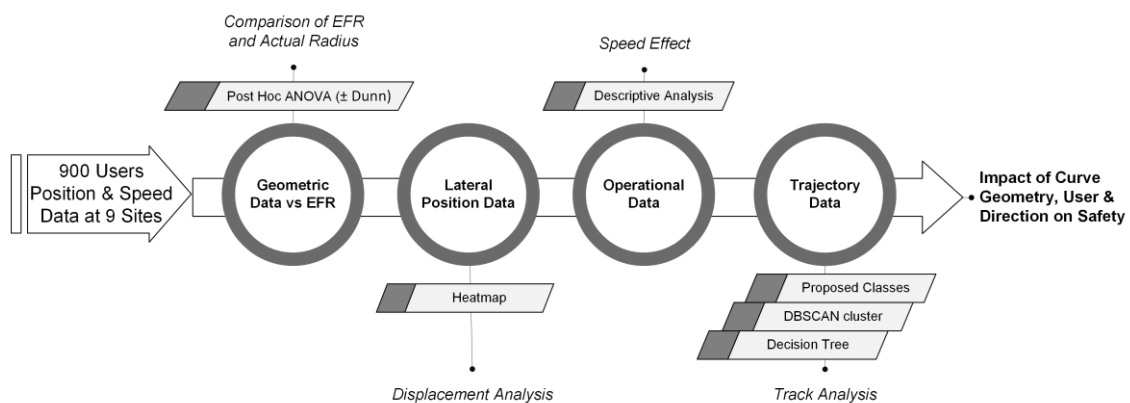


Figure 23 Progress Flowchart.

7.1 Comparison of Effective Fitted Radius and Actual Radius

To conduct a detailed comparison of the risk associated with horizontal curves, the Effective Fitted Radius (ERF) associated with each trajectory of maneuvering users on all nine horizontal curves was computed. The extracted data were then divided based on user type and direction of travel for each curve site. Subsequently, homogeneity and normality tests were performed using JASP to partition the extracted datasets for two different types of analysis: parametric and non-parametric. For the four sites that met the assumptions, parametric post-hoc ANOVA was performed in JASP. These sites include NE3, SW2, SE4, and SE3 as shown in Table 7. Five remaining sites that did not pass the homogeneity test due to large outliers will be analyzed with a non-parameter method. They include NW1, SW1, SW3, NE9, and NE8.

The post-hoc ANOVA result (Table 7) indicate that regardless of user type, significant statistical differences exist between left-turn and right-turn movements in both sharp curves of NE3 and SW2. However, for flat curves, no statistically significant difference was found. Further details about this result can be seen in the developed raincloud plots

in Figure 20. The plots consist of three components: smoothed density plots (violin), box plots with median lines, and scattered points. A red dotted line is added to each plot to show the actual radius of each curve, enabling comparison with the median of the interquartile range of the EFR values. For the curve site with the smallest radii (6 m), the median for left-turn users is consistently around 1 meter smaller than the actual curve, whereas for right-turn users, who exhibit a wider distribution and are less scattered, the EFR median surpasses the actual radius. This indicates that they are less bound to the geometry of the horizontal curve. In other words, left-turn users are cutting the curve at some points and are vulnerable to head-on conflicts with opposing users. This can be further explained with speed analysis in section 4.3 to confirm users' speeding.

Table 7 ANOVA with post hoc tests for Effective Fitted Radius per user type per movement direction.

Movement Type	Compares With	Mean Difference			
		NE3 (R1 = 6 m) EFR (m)	SW2 (R2=10 m) EFR (m)	SE4 (R3=22 m) EFR (m)	SE3 (R4=78 m) EFR (m)
Bike LT	Bike RT	-2.492	0.48	-2.204	-5.272
	E-scooter LT	0.056	-0.184	-0.24	-0.780
	E-scooter RT	-1.776	0.312	-1.184	-4.432
Bike RT	E-scooter LT	2.548	-0.664	1.964	4.492
	E-scooter RT	0.716	-0.168	1.02	0.840
E-scooter LT	E-scooter RT	-1.832	0.496	-0.944	-3.652

Bold represents the significant differences at the 0.05 level.

In larger radii (22 and 78 m), the patterns observed in Figure 24 persist with right-turn users for smaller radii, while left-turn users tend to adhere to the curve geometry, avoiding lane violations. Additionally, the post-hoc ANOVA results confirm that for flat curves (R = 22 m and 78 m), there are no statistically significant differences between different users and directions of movement. Consequently, they are less prone to conflicts as the EFR of the movement is close to the actual radius. Given their larger radii, a mean difference of 2 to 5 meters can be neglected. However, for sharp curves, this difference can constitute a significant portion of the radii and lead to significant safety differences. For the sharpest curve in the group (R=6 m), the variance is much higher: 41% (bike LT and RT), 29% (bike LT vs E-scooter RT and vice versa), and 30% (e-scooter LT and RT). As the radius increases to 10 meters, the variance significantly reduces to as low as 3% to 6%, for significant cases. These variances can be easily seen through the raincloud plots in Figure 24a and 24b. The main difference between them is that in a smaller radius, right turn users tend to take a flatter trajectory (EFR > Actual Radius) and left users are cutting the curve and take a sharper maneuver. However, as the radius increases for 4 meters, most users, regardless of their turn direction tend to take the cutting maneuver. For the flat samples (Figure 24c and 24d), there are no significant variances and the dotted red line, representing the actual radius matches the center of median value of the box plot.

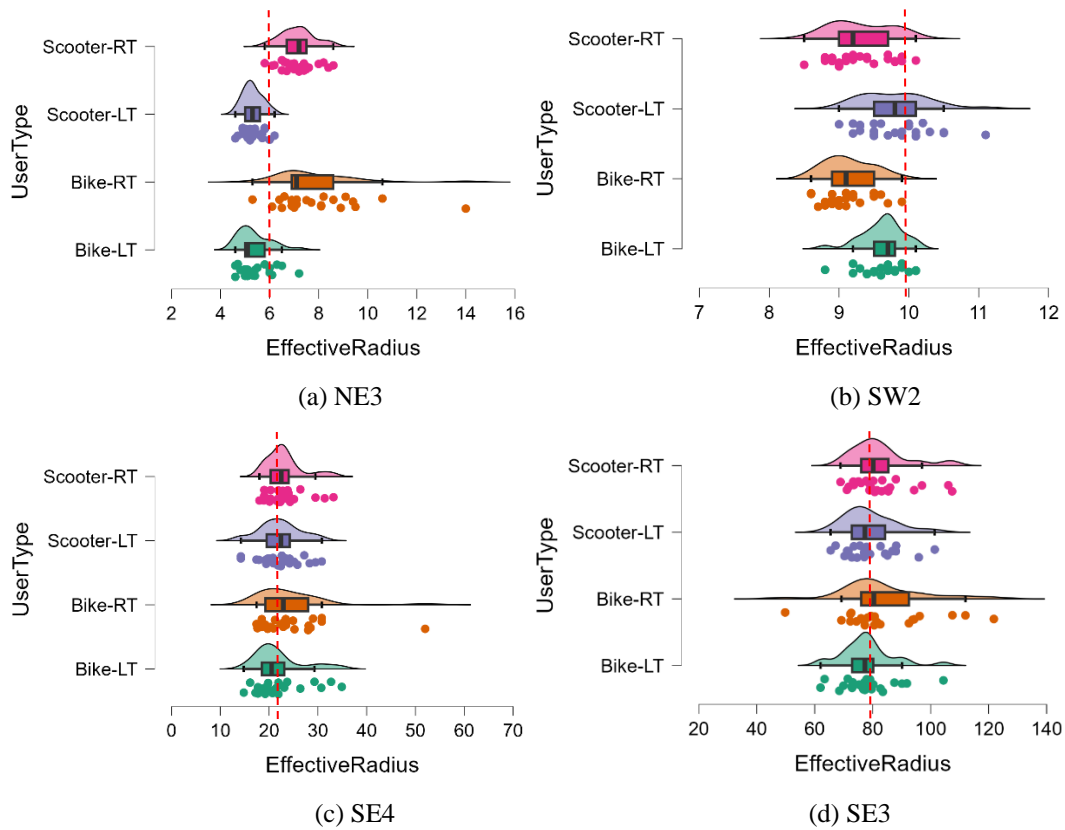


Figure 24 Raincloud plots of Effective Fitted Radius in four curve sites: NE3 (b) SW2 (c) SE4 (d) SE3.

For the remaining five curve sites showing high dispersion, unsuitable for ANOVA analysis, non-parametric tests like Kruskal-Wallis and Kolmogorov-Smirnov can be utilized to detect differences and compare distributions. In this study, Kruskal-Wallis test with Dunn post hoc analysis was conducted to pinpoint curve sites where users were less likely to adhere to the designed curvature, resulting in significant dispersion of EFR based on user type and movement direction. Results are summarized in Tables 8 and 9.

Table 8 Non-parametric Kruskal-Wallis test results for five curve sites with dispersed Effective Radius.

Curve Site	Kruskal-Wallis Results		Effect Size (Eta Square)	Median EFR			
	F	p		Bike-LT	Bike-RT	E-scooter-LT	E-scooter-RT
NW1 (R5=2m)	15.981	0.001	0.161	1.7	1.7	2	1.7
SW1 (R6=5m)	72.023	<0.001	0.728	3.4	8	3.5	16
SW3 (R7=5m)	24.888	<0.001	0.251	2.5	5.2	2.1	5.5
NE9 (R8=7m)	0.835	0.841	0.008	6.7	6.9	6.8	6.9
NE8 (R9=9m)	5.438	0.142	0.055	8.8	7.7	8.3	7.8

Bold represents the significant differences at the 0.05 level.

Table 9 ANOVA with dunn post hoc tests for Effective Fitted Radius per user type per movement direction.

Movement Type	Compares With	Mean Difference		
		NW1 (R5 = 2 m) EFR (m)	SW1 (R6=5 m) EFR (m)	SW3 (R7=5 m) EFR (m)
Bike LT	Bike RT	1.483	-4.856	-3.088
	E-scooter LT	-1.805	-0.554	0.269
	E-scooter RT	1.743	-7.204	-3.644
Bike RT	E-scooter LT	-3.288	4.302	3.356
	E-scooter RT	0.26	-2.349	-0.557
E-scooter LT	E-scooter RT	3.548	-6.651	-3.913

Bold represents the significant differences at the 0.05 level.

In Table 9, it is apparent that users at curve sites with minimum allowed radii (R=5m) and lower (R=2m) tended to deviate from the curvature, showing significantly lower EFR during left-turn movements and higher EFR during right-turn movements. This pattern occurred regardless of whether the curve site was located in a protected (SW1, SW3) or sidewalk (NW1) bike lane. In contrast, at sidewalk curves with radii of 7 m and 9 m, no significant differences in EFRs were observed. This highlights how users may disregard even a protected bike lane design if it does not align with their perception. Median EFR results suggest that users at these sites were more likely to follow the curvature, regardless of type or direction of movement.

7.2 Displacement Analysis

To gain deeper insights into areas within horizontal curves prone to conflict risks, a micro-level examination of wheel positions during navigation is essential. In this study, such insight is achieved by regionalizing areas within and outside the bike lane. As explained in Chapter 3, four main regions, Lane (LN), Center Line (CL), Opposite Lane (OPL), and Out of Lane (OTL), have been defined. These regions are further segmented into three parts, representing Point of Curvature (PC), Midpoint (MP), and Point of Tangency (PT) sections. They are utilized to create spatioregional heatmaps corresponding to the path footprints of moving users. Figure 23 illustrates two series of these heatmaps, facilitating a more detailed comparative study of user behavior on a sharp curve (R=6 m) and a flat curve (R=22 m). Each series comprises four heatmaps, delineating different user types, bike (B) and e-scooter (S), and directions of movement, left-turn (LT) and right-turn (RT). The heatmaps that do not contain the OTL are those in which no user has entered the outside bike lane area.

The heatmaps (Figure 25 and Appendix B) provide clear confirmation of the statistical results discussed in section 7.1. They illustrate that the flatter the curve, the more likely users adhere to the geometry, resulting in fewer violations. However, the heatmaps offer additional insights. Notably, they reveal that left-turn users tend to ride in the CL region, near the central marking, increasing their vulnerability to crossing-body conflicts with opposing users. This is attributed to the operational width of micromobility users, consisting of their body and potential motions during their path, causing lateral deviation. This trend is observed across both sharp and flat curves. Another significant observation is that the PC section is where most users ride within safe margins within LN, whereas

PT is not. A substantial portion of users (48% to 56%) are observed in the opposite lane (OPL) in the middle of the curve (MP). This further elucidates the results discussed in the previous section.

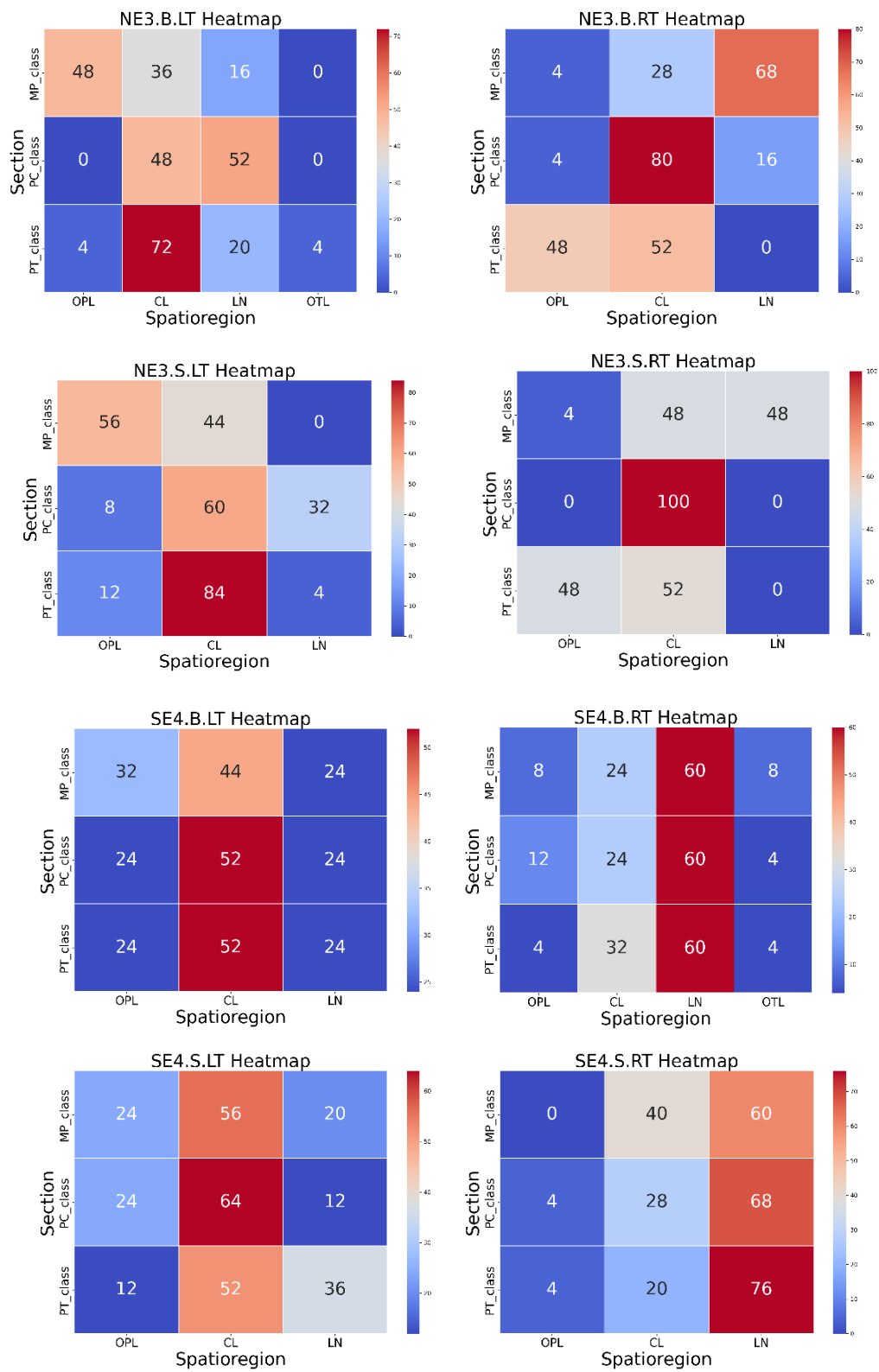


Figure 25 Heatmaps illustrating the percentage of user presence at each spatioregions and sections of curve. Example series for two curve sites of NE3 (R=6m) and SE4 (R=22m) divided by user type and movement direction.

7.3 Speed Effect

In this section, the impact of speed on risky behavior is examined, with a specific focus on cases identified in previous subsections with higher risks of conflicts. A descriptive analysis was conducted using JASP software, and the results are summarized in Table 10 to 13. Additionally, box whisker plots were created to visualize the distribution of speed ranges (see Fig. 26 to 29). Box whisker plots are more helpful to quickly observe the speed variation through the three segments. Looking at the median trend in Figure 26, it is apparent that on tangenets (PC and PT) speed is often reduced as the curve gets flatter. However, on the midpoint (MP) this trend is reversed, and two flat curve samples are showing higher speed comparing to the sharper curves. Ultimately, to identify segments with higher speed difference, a density bar chart divided by user type and direction of movement is developed for both segments of PC to MP and MP to PT, as demonstrated in Figure 29.

Table 10 Descriptive analysis of users speed for each four curve site at three sections (R1-R4).

	PC				MP				PT			
	R1=6m	R2=10m	R3=22m	R4=78m	R1=6m	R2=10m	R3=22m	R4=78m	R1=6m	R2=10m	R3=22m	R4=78m
Median	22	18	18	14	17	8	19	19	23	14	18	17
Mean	23.9	17.97	18	15.48	17.14	8.67	19.31	19.19	22.79	14.34	18.38	17.52
Std. Deviation	6.999	4.432	4.038	4.792	3.822	2.617	4.355	4.525	5.074	3.528	4.094	4.16
Minimum	11	7	10	7	9	4	8	9	10	6	10	8
Maximum	42	26	29	30	30	18	28	30	40	23	26	28
85th percentile	31.15	23	22	20	21	11	24	25	28	18	24	22

Table 11 Descriptive analysis of users speed for each four curve site at three sections (R5-R9).

	PC					MP					PT				
	R5=2m	R6=5m	R7=5m	R8=7m	R9=9m	R5=2m	R6=5m	R7=5m	R8=7m	R9=9m	R5=2m	R6=5m	R7=5m	R8=7m	R9=9m
Median	14	13	13	12	12	11	14	7	24	24	13.5	14	12	15	13
Mean	14.7	14.2	12.9	11.6	11.8	14.9	16.2	7.6	21.8	23	13.4	16.4	11.2	15.8	13.8
Std. Deviation	3.7	4.6	3.3	3.2	3	7.5	6.5	2.7	4.3	3	4	6.5	3.1	4.9	3.6
Minimum	7	6	5	5	6	4	5	2	12	14	3	7	4	6	5
Maximum	26	28	24	19	20	29	40	17	29	29	26	35	24	24	22
85th percentile	19	20	16	15	15	24	22	10	25	25	17	23.1	14	22	18

Table 12 Descriptive analysis of users speed for each user type and direction at three sections (R1-R4).

	PC				MP				PT			
	Bike-LT	Bike-RT	E-scooter-LT	E-scooter-RT	Bike-LT	Bike-RT	E-scooter-LT	E-scooter-RT	Bike-LT	Bike-RT	E-scooter-LT	E-scooter-RT
Median	16	17	20	20	16	16	18	17	16	16	19.5	20
Mean	17	17.3	20.7	20.3	15.16	14.85	17.48	16.82	16.66	17.1	19.86	19.41
Std. Deviation	5.51	4.27	7.91	4.86	4.745	5.764	5.776	6.617	4.127	6.064	5.115	4.608
Minimum	7	7	8	11	5	4	6	4	9	6	8	8
Maximum	33	28	42	32	30	30	28	30	30	32	40	28
85th percentile	22	21.1	30	25	19	20	24	25	20	24	25	25

Table 13 Descriptive analysis of users speed for each user type and direction at three sections (R5-R9).

	PC				MP				PT			
	Bike-LT	Bike-RT	E-scooter-LT	E-scooter-RT	Bike-LT	Bike-RT	E-scooter-LT	E-scooter-RT	Bike-LT	Bike-RT	E-scooter-LT	E-scooter-RT
Median	11.0	12.0	12.0	14.0	21.0	14.0	20.0	14.0	14	12	14	13.0
Mean	12.3	12.5	12.9	14.4	18.4	15.7	17.4	15.4	16	12.4	14.5	13.7
Std. Deviation	4.8	2.6	3.8	3.4	7.9	6.9	7.6	7.5	6.1	4	4.3	4.4
Minimum	5.0	7.0	5.0	6.0	2.0	3.0	3.0	5.0	6	3	5	5.0
Maximum	28.0	26.0	24.0	24.0	36.0	29.0	30.0	40.0	35	26	24	29.0
85th percentile	17.4	15.0	18.0	18.0	25.0	24.4	25.0	25.0	22	16	19	18.4

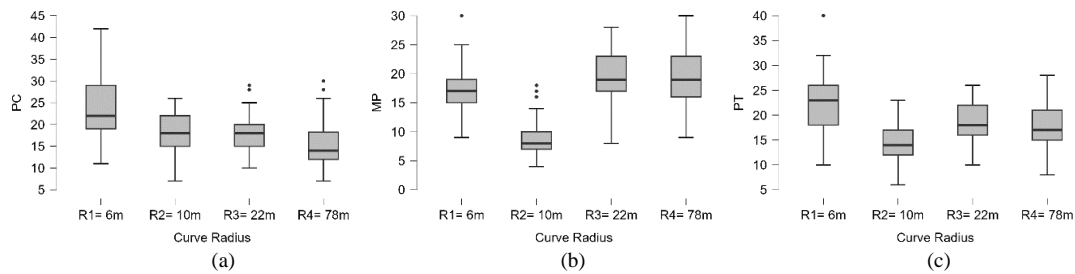


Figure 26 Box whisker plots of speed data for different radii for curve R1-R4: (a) PC, (b) MP, and (c) PT.

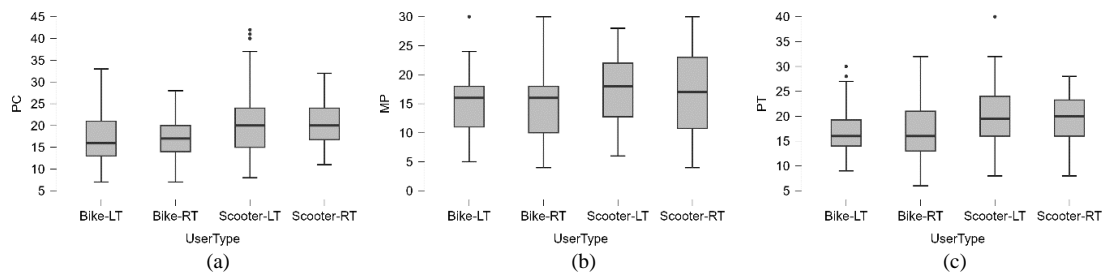


Figure 27 Box whisker plots of speed data for each user type and direction for curve R1-R4: (a) PC, (b) MP, and (c) PT.

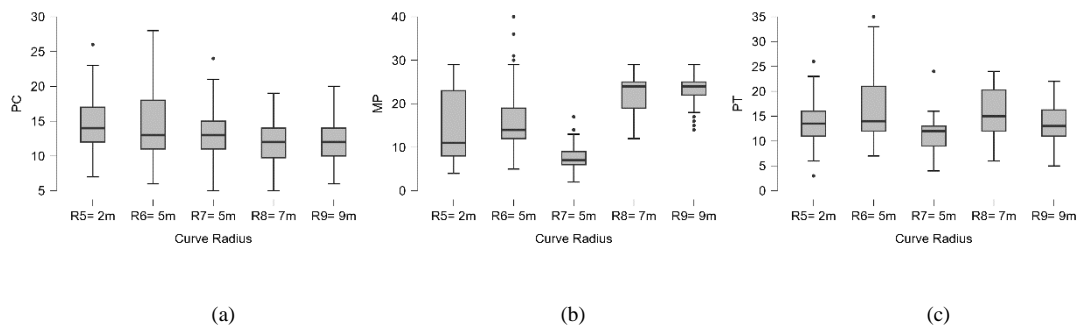


Figure 28 Box whisker plots of speed data for different radii for curve R5-R9: (a) PC, (b) MP, and (c) PT.

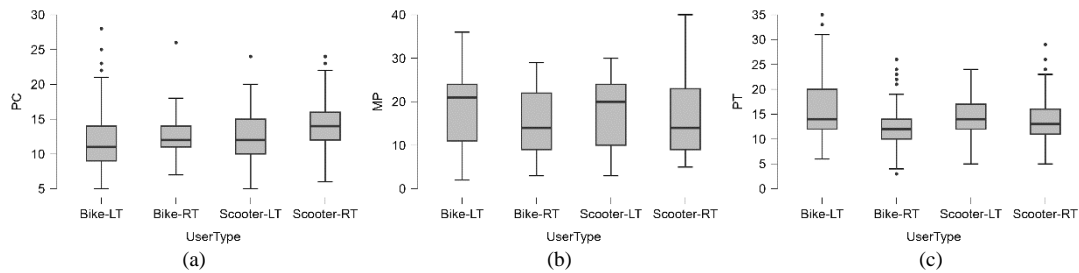


Figure 29 Box whisker plots of speed data for each user type and direction for curve R5-R9: (a) PC, (b) MP, and (c) PT.

Insight into the relationship between speed and risky behavior in the identified cases is provided by these analyses. Accordingly, the comparison of 85 percentile speed between four different curves shows that in fact the sharpest curve in this homogenized group (radius of 6 meters), experienced the highest speeding of the maximum of 31 km/h that is up to double the design speed of the curve (12 km/h). This record is observed on PC. Yet on PT as well the speed was as high as 28 km/h. The standard deviation analysis reveals that the sharpest curve in the PC, MP, and PT sections has the highest deviation. This, along with the risky trends identified in previous subsections, indicates that these curves are highly prone to potential conflicts on high-traffic bike lanes. When a large portion of users engage in risky maneuvers, the likelihood of such risks increases. Although near-miss scenarios are not included in this study, and the risk assessment is based solely on individual users' risky maneuvers, the results are still valuable for identifying risks caused by bad user behavior driven by poor geometry and for mitigating these risks. In terms of user type and direction, Table 24-27 suggest that users in general had lowered their speed at MP, to follow and navigate the curve. However, when looking into the user type for 85-percentile speed, it reveals that e-scooter riders have surpassed 20 km/h at all sections, with a maximum recorded value of 42 km/h on a left-turn movements.

Comparing the box whisker plots in Figure 16, interesting trends can be seen. Firstly, it shows when curve radius is increased by only 4 meters ($R_2 = 10m$), the speeding of users decrease significantly. Not only that but also the speed has less variance in R_2 (SW2) comparing to R_1 (NE3). However, for flatter curves the variance of speed is higher on MP comparing to sharp curves (R_1 and R_2). In Figure 28, the average speeds for different user types and turn directions are compared across three sections. The box whiskers combine data from all four sites to provide a comprehensive view of user speeding. The results indicate that e-scooters generally exhibit higher dispersion, with a median speed near 20 km/h at PC and PT, consistently higher than bike users who hover around 15 km/h. Specifically, when examining MP, it is evident that right-turn e-scooters' speeds are widely dispersed, with quartiles ranging from 10 km/h to 22 km/h, and whiskers extending up to 30 km/h.

To investigate speed differences across segments for user types and turn directions, density plots were generated, incorporating speed data from the four previously discussed curve sites (Figure 30). E-scooters consistently exhibited higher speed differences relative to bikes across both segments and turn directions, reaching differences of up to -25 km/h. This discrepancy suggests potential variations in caution levels or maneuverability between e-scooter and bike users. Additionally, left-turning users consistently displayed greater speed differences compared to their right-turning counterparts, particularly within

the same user type and segments, indicating potential challenges or the need for more substantial speed adjustments during left turns.

Furthermore, the MP to PT segment consistently demonstrated higher speed differences across all user types and turn directions, with left-turn bike users exhibiting the highest density at 0.14. This observation suggests that factors such as bike lane geometry, visibility, and lane conditions may contribute to these disparities along this segment. Moreover, speed differences for nearly 75% of users within the PC to MP segment ranged between 0 to 5 km/h. A comprehensive examination of these findings within the study's framework could uncover additional insights that inform strategies for addressing conflicts and enhancing road safety.

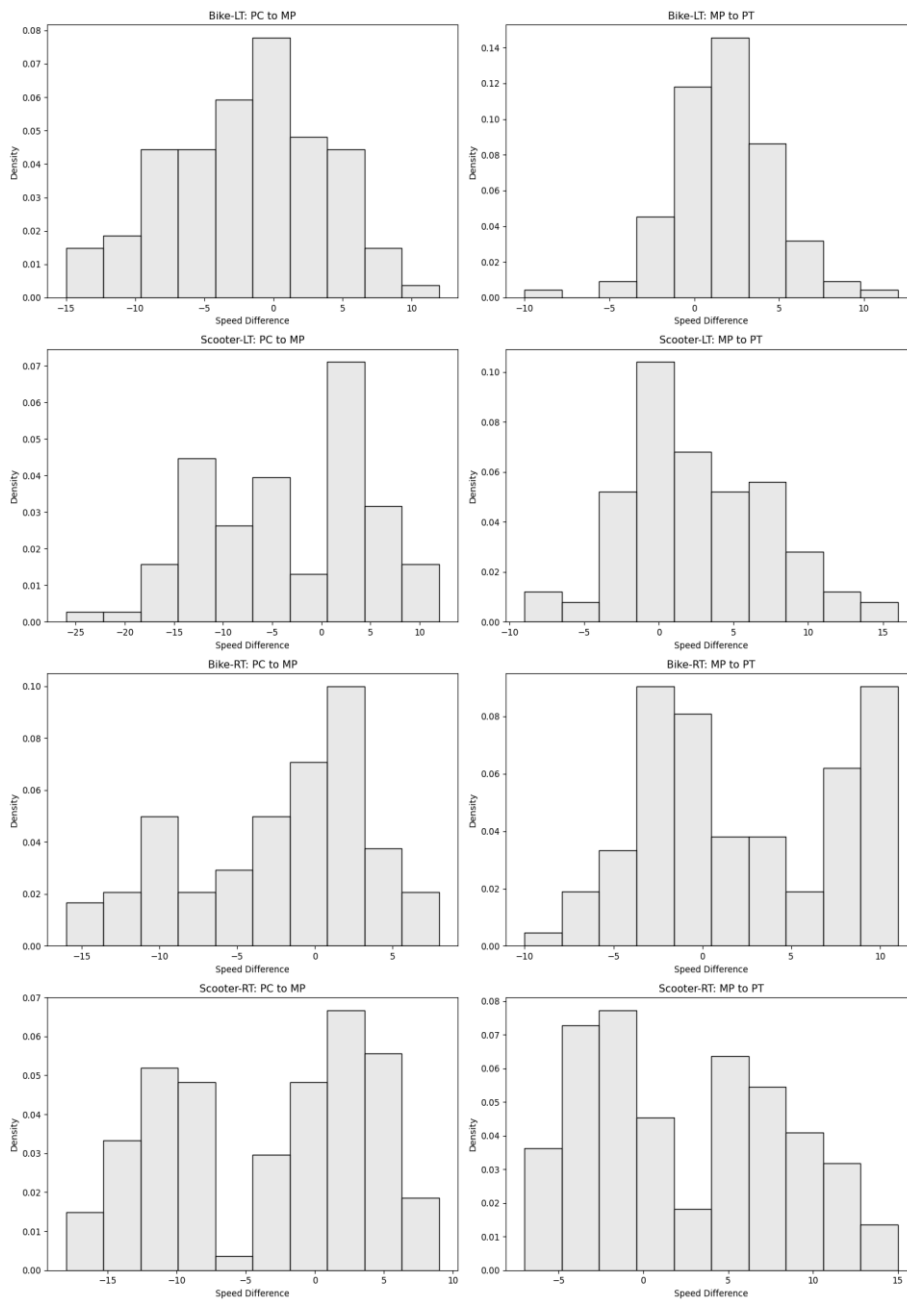


Figure 30 Speed difference bar charts between two segments of curve per user type per turn direction.

7.4 Track Analysis

To understand the diverse maneuvers of bike lane users, a detailed examination of track types previously outlined is undertaken. Six distinct track types were introduced in Section 5.4—Ideal behavior (ID), Normal behavior (NR), Correcting (CR), Cutting (CT), Swinging (SW), and Drifting (DR)—each representing different patterns of bike lane users' behavior and stability. In this section, these track types will be analyzed in the context of real-world cycling data, assessing how cyclists' paths align with the theoretical models. By examining the prevalence and characteristics of each track type, insights into cyclists' navigation strategies and the implications for bike lane design and safety will be gained.

7.4.1 Track Type Classification

Comparing Curve Sites R1 and R2 reveals notable differences in user behavior and conflict risk due to changes in curve geometry and the type of bike lane (sidewalk or protected). At R1, where the radius is 6 meters and the degree of curvature is 278 degrees, the majority of left-turn users cut the curve while most right-turn users correct their paths. Both types of users frequently pass through the opposite lane. This occurs in a condition where the bike lane is on the sidewalk, allowing users to take more aggressive maneuvers since there is no barrier to stop them, indicating a higher potential for conflict in this sharper curve. In contrast, at R2, where the radius increases to 10 meters and the degree of curvature decreases to 178 degrees, users are mostly passing through the central segments. Most right-turn users cut and swing the curve, which increases the risk of potential conflicts. Meanwhile, left-turn users in R2 tend to drift through the central segment.

Figure 31 illustrates an example of these trends for curves R1 and R2 (see Appendix B, Section 7.4 for additional examples). It shows how the reduction in curve sharpness at R2 affects track patterns and the associated risks of conflicts. For reference, 28 acronyms used in the pie chart, which were thoroughly explained in Chapter 5, are summarized in Table 14.

The pie charts reveal that left-turns exhibit more diversity in track-segment types, with up to 12 different types observed. In comparison, right-turns show a maximum of five different types, with the majority involving cutting, correcting, and swinging. This suggests that left-turn users have a wider range of track patterns, indicating that regardless of user type and geometry, users moving outside the curve are more likely to maneuver with large variance. This was also revealed previously in the comparative analysis of variances in section 7.1.

Regarding the impact of user type (e-scooter vs. bike), as mentioned earlier, the frequent track-segment does not show significant variance. However, it is apparent that in a sharper curve, e-scooters maneuver with less type-variance compared to bikes, whereas when the curve gets wider (R2), this trend reverses. This indicates that e-scooters tend to have more consistent behavior in tighter curves but become more variable in wider curves, while bikes exhibit the opposite pattern. The difference in maneuvering patterns between e-scooters and bikes, especially in varying curve geometries, underscores the need for tailored infrastructure designs to accommodate the distinct behaviors and ensure safety for all users.

Table 14 Acronyms for classifying maneuvers by track type and lateral segment.

#	Acronym	Track Type_Lateral Segment
1	ID_LN	Ideal_Lane
2	ID_CL	Ideal_Central Marking
3	ID_OPL	Ideal_Opposite Lane
4	ID_OTL	Ideal_Out of Lane
5	NR_LN	Normal_Lane
6	NR_CL	Normal_Central Marking
7	NR_OPL	Normal_Opposite Lane
8	NR_OTL	Normal_Out of Lane
9	CR_LN	Correcting_Lane
10	CR_CL	Correcting_Central Marking
11	CR_OPL	Correcting_Opposite Lane
12	CR_OTL	Correcting_Out of Lane
13	DR_LN	Drifting_Lane
14	DR_CL	Drifting_Central Marking
15	DR_OPL	Drifting_Opposite Lane
16	DR_OTL	Drifting_Out of Lane
17	SW_LN	Swinging_Lane
18	SW_CL	Swinging_Central Marking
19	SW_OPL	Swinging_Opposite Lane
20	SW_OTL	Swinging_Out of Lane
21	CT_LN	Cutting_Lane
22	CT_CL	Cutting_Central Marking
23	CT_OPL	Cutting_Opposite Lane
24	CT_OTL	Cutting_Out of Lane
25	UN_LN	Unclassified_Lane
26	UN_CL	Unclassified_Central Marking
27	UN_OPL	Unclassified_Opposite Lane
28	UN_OTL	Unclassified_Out of Lane

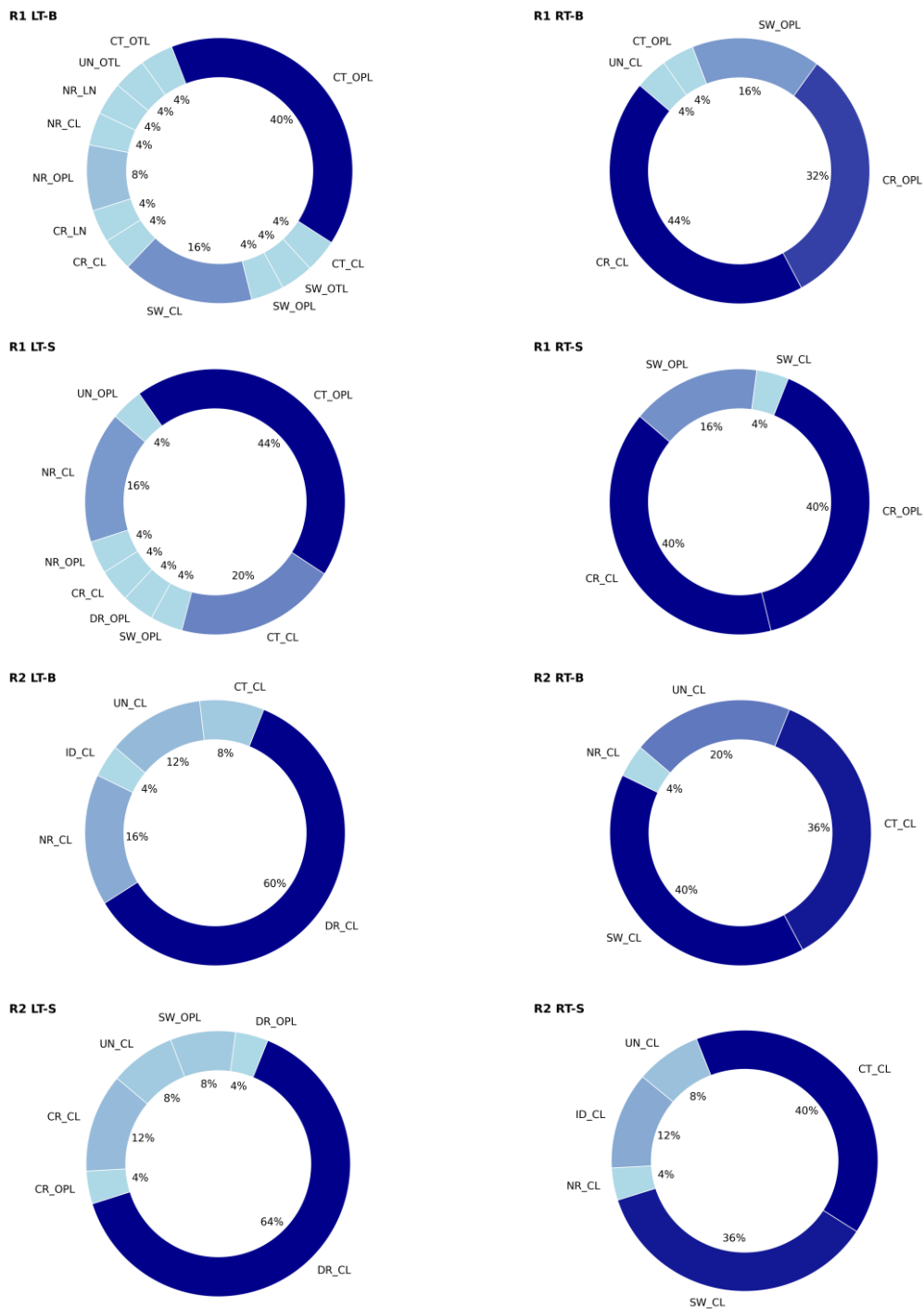


Figure 31 Track-segment occurrence on curve sites R1 and R2 by user type and direction.

The analysis of user behavior and conflict risk across the remaining curve sites R3 to R9 (see Appendix B) reveals similar patterns to those observed in earlier sections. At R3, characterized by a flat radius of 22 meters and low curvature (78 degrees), both left-turn and right-turn users frequently exhibit drifting maneuvers (DR), passing through all segments of OPL, CL, LN, and OTL. Moving to R4, which is the flattest curve site with a radius of 78 meters, users not only exhibit drifting but also frequent swinging maneuvers, with CL segments being the most frequently passed through. At R5 and R6, with the lowest radii of 2 and 5 meters respectively, patterns similar to those observed at

R1 and R2 are apparent. Track patterns become more consistent, particularly with left-turn users demonstrating a higher occurrence of cutting maneuvers while touching the opposite lane (CT_OPL). A major difference between R5 and R6 is observed among right-turn users. At the lower radius site (R5), users tend to cut the curve, whereas at R6, users frequently correct their maneuvers outside the bike lane, even though the bike lane is protected. In fact, these users often leave the bike lane at the curve. Sites R7 and R8 exhibit significantly similar patterns, with left-turn users frequently engaging in cutting maneuvers (CT_OPL). However, for right-turn users, a combination of various maneuvers is apparent, with drifting, correcting, and swinging being the most frequent. These findings emphasize the necessity for tailored infrastructure designs that accommodate varying user behaviors and ensure safety across different curve geometries.

To gain a comprehensive understanding of user behavior across all sites, an occurrence heatmap was developed (see Figure 32). A quick glance at the heatmap reveals that cutting maneuvers passing through the opposite lane (CT-OPL) are the most prevalent among the sharper curves (R5-R9 and R1). This indicates a higher propensity for users to cross into opposing lanes in these areas, suggesting a greater potential for conflicts. Additionally, drifting and correcting maneuvers are the most frequent among left-turn users at site R2 and right-turn users at site R6. This trend indicates that as the curve becomes sharper (with R6 having a radius of 5 meters), the direction of the turn significantly influences maneuvering patterns. Specifically, sharper curves appear to compel users to adjust their paths more aggressively, with distinct differences in behavior observed between left and right turns. These findings underscore the importance of considering turn direction and curve sharpness in the design of bike lane infrastructure to enhance user safety and reduce conflict risks.

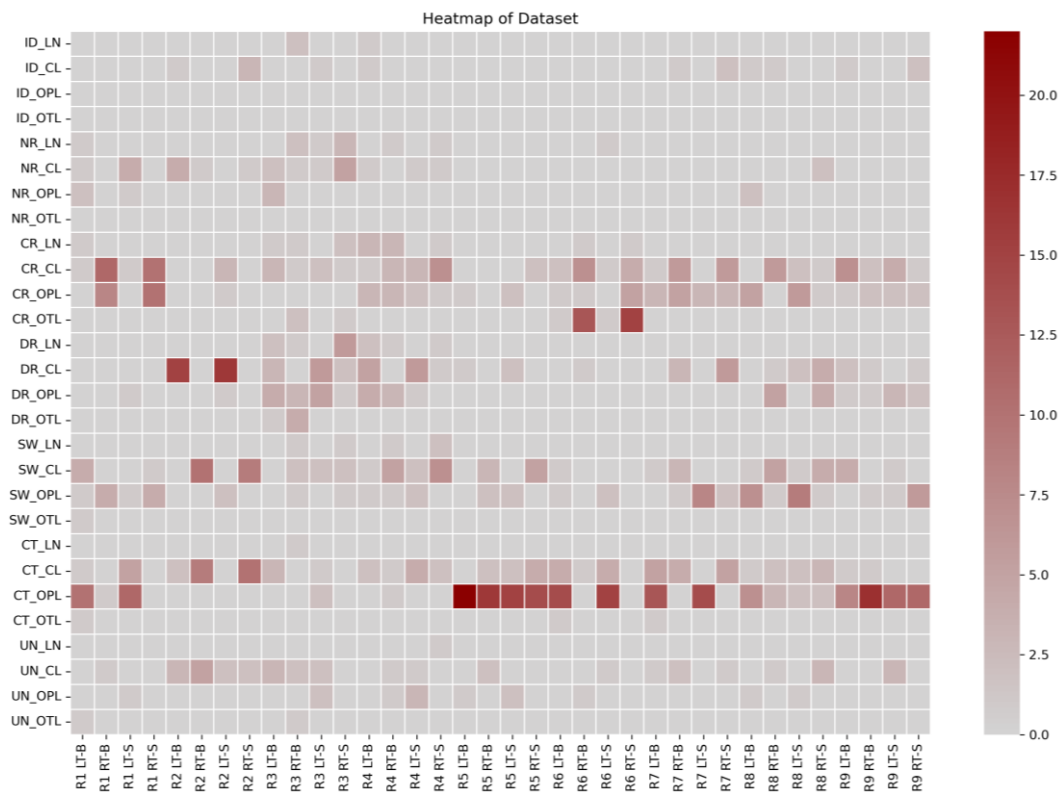


Figure 32 Track-segment occurrence on all nine-curve sites (R1-R9) by user type and direction.

7.4.2 Track Clustering

The clustering analysis resulted in five distinct clusters (0, 1, 2, 3, 4) with an additional group of outliers labeled as -1. Each cluster represents a unique pattern of lateral offsets (d) at each section of interests (pc, mp, pt) across the track sections (see Table 15).

- **Cluster 0 (Cutting):** This cluster is the largest, with 757 data points. It has a mean d-pc of 26.88, suggesting a slight offset to the right in section pc, and small mean values for d-mp (6.84) and d-pt (11.05). The standard deviations indicate a moderate spread in these values, especially for d-mp and d-pt, suggesting variability in the offsets in these sections.
- **Cluster 1 (Correcting):** This small cluster contains 8 data points and shows large negative mean values for d-pc (-150.25) and d-mp (-156.13), indicating significant offsets to the left in these sections. The mean d-pt is also negative (-114.63), reinforcing the leftward trend across all sections. The relatively low standard deviations suggest consistency in these offsets.
- **Cluster 2 (Correcting):** Comprising 7 data points, this cluster also shows large negative offsets for d-pc (-112.43) and d-mp (-167.57), but a positive mean d-pt (31.71), indicating a rightward offset in section pt. This cluster exhibits moderate spread, with standard deviations reflecting some variability.
- **Cluster 3 (Swinging):** With 22 data points, this cluster has negative mean values for d-pc (-82.82) and d-mp (-112.13), suggesting leftward offsets, and a negative mean d-pt (-114.32). The standard deviations show moderate variability, especially for d-mp.
- **Cluster 4 (Drifting):** The smallest cluster, with only 4 data points, shows significant negative mean values for d-pc (-153.5) and d-mp (-98.25), indicating strong leftward offsets. However, the mean d-pt is positive (12.5), suggesting a rightward offset in section pt. This cluster has low standard deviations, indicating very consistent offsets.
- **Outliers (-1):** This group contains 102 data points and is characterized by highly variable offsets, as indicated by the large standard deviations across all sections. These points do not fit well into any of the identified clusters and represent atypical track conditions or measurement anomalies.

Table 15 Summary of the clustering result.

Cluster	Count	d-pc_mean	d-pc_std	d-mp_mean	d-mp_std	d-pt_mean	d-pt_std
0	757	27	31	7	62	11	48
1	8	-150	10	-156	19	-115	30
2	7	-112	17	-168	16	32	11
3	22	-83	18	-112	30	-114	28
4	4	-154	12	-98	22	13	9
-1	102	-38	137	-110	205	-24	134

7.4.3 Track Type Prediction

Track Type Prediction analysis was performed using a decision tree due to its intuitive structure and ability to handle both numerical and categorical data effectively. Decision trees are highly interpretable, allowing for easy visualization of decision paths and

understanding of the model's logic. By mapping out the various factors influencing track type classifications, decision trees has revealed complex interactions between variables that may not be immediately apparent. The results of the analysis demonstrated that the degree of curvature is the most significant variable. The resulted decision tree regression plot is shown in Figure 33 and the improved version in Figure 34-35.

Decision Tree Regression

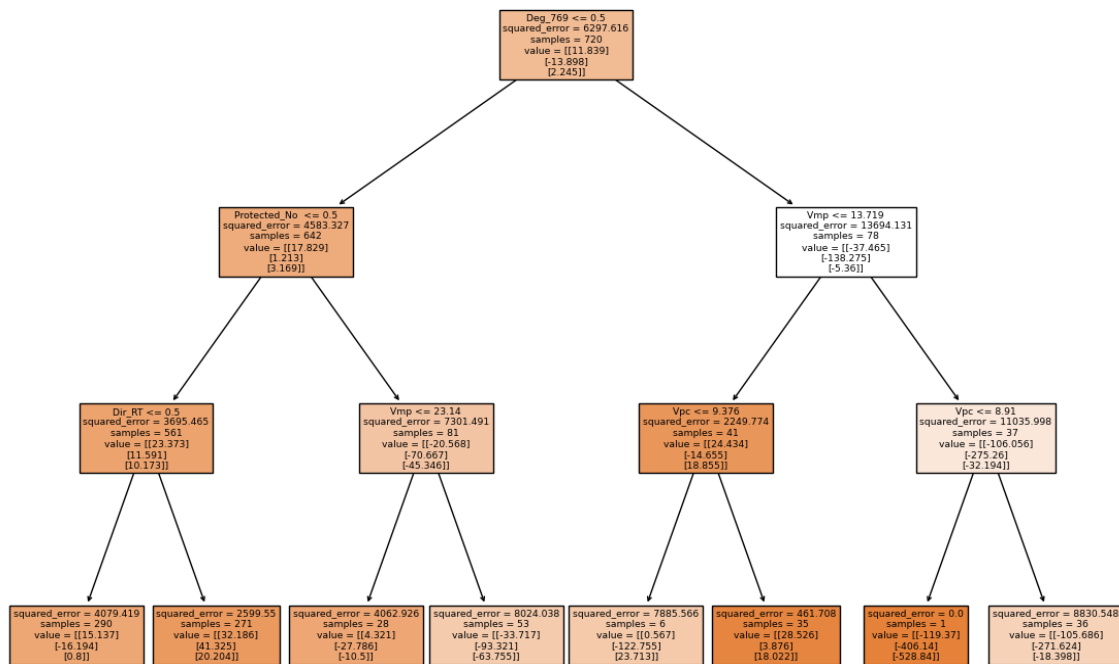


Figure 33 Decision Tree Regression model visualization showing feature splits for predicting variables d-pc, d-mp, and d-pt.

In the top leaf of the decision tree, each value provides specific insights into how the model makes decisions. The condition $\text{Deg}_{769} \leq 0.5$ (degree of curvature equal to 769 degree) determines the initial split at the root node, directing samples to either the left or right subtree based on whether Deg_{769} is 0 or 1. This binary column is derived from one-hot encoding of the original categorical feature Deg , where Deg_{769} equals 1 if the original Deg value is 769, and 0 otherwise. The $\text{squared_error} = 6297.616$ indicates the mean squared error (MSE) for the node, reflecting the variance of d-pc, d-mp, and d-pt within this group of samples. With a total sample of 720, 80% of training data points are included in this node, emphasizing its foundational role as the starting point in the decision-making process. The value = $[[11.839] [-13.898] [2.245]]$ signifies the average predicted values for d-pc, d-mp, and d-pt, serving as a baseline prediction for samples that fall under this splitting condition. This suggests that for the smallest radius ($R=2$ m) and highest degree of curvature (769 degrees) in the dataset, users tend to cut the curve more frequently. This behavior increases the likelihood of head-on conflicts at MP.

Furthermore, the decision tree's top node splitting on $\text{Deg}_{769} \leq 0.5$ initiates a division based on this feature, followed by subsequent splits on $\text{Protected_No} \leq 0.5$ and $\text{Vmp} \leq 13.719$. These splits facilitate the segmentation of data into more homogeneous groups, thereby reducing variance within nodes and minimizing prediction error. One-hot encoding transforms categorical features into binary columns, where numbers like 769 denote specific unique values from the

original Deg feature. This encoding process explains the presence of Deg_769 in the decision tree, highlighting its role in influencing predictions based on the dataset's categorical attributes.

Interpreting the results of the best decision tree involves comprehending both the model's performance metrics and its structural components. Through GridSearchCV, optimal parameters such as a maximum depth of 5, a minimum leaf sample size of 1, and a minimum split sample size of 2 were identified for the DecisionTreeRegressor. These parameters are crucial in mitigating overfitting by constraining tree complexity.

In total, 11 predictors existed in the initial dataset. These predictors were unmerged are grouped into distinct leaves based on their importance and value ranges. In the resulting tree, it is evident that the variables "user type" and "length of the curve" are not included, indicating they have no impact on the model's predictions. The top leaf identifies degree of curvature as the primary predictor. The second level is consisted of two leafs of bike lane type (protected or not) and mid-point speed (Vmp). In the third level four leafs are identified and predictors include direction, Vmp, and Vpc. The forth and fifth level categorizes predictors like chord, Vpt, Vmp, Vpc, and direction within specific ranges. These segments illustrate how the decision tree prioritizes and categorizes predictors, revealing their impact on predicting variables d-pc, d-mp, and d-pt with clarity and structure.

The best cross-validated score of 62.63 indicates the model's performance in predicting unseen data, with RMSE values of 56.31 for d-pc, 64.37 for d-mp, and 57.48 for d-pt, suggesting moderate prediction accuracy, with d-mp posing the greatest challenge among the target variables.

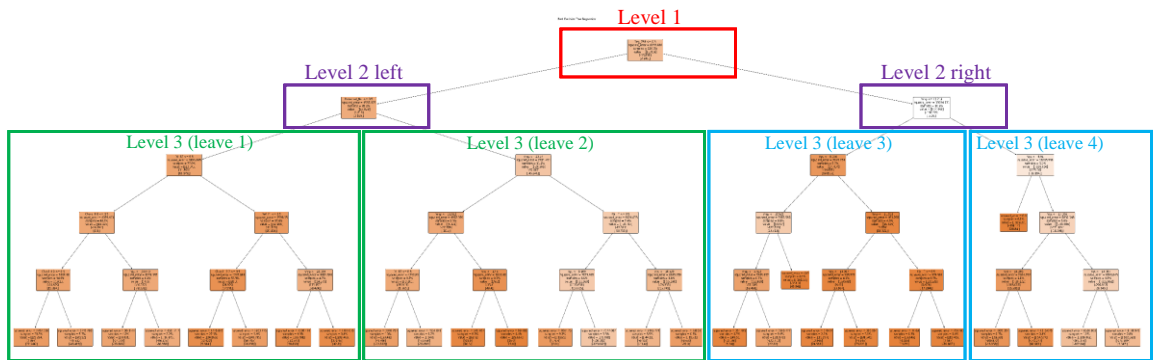
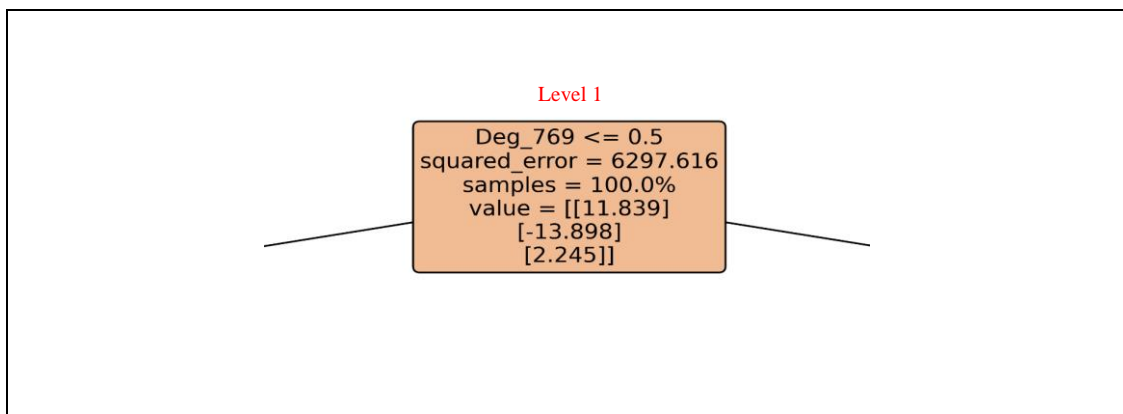
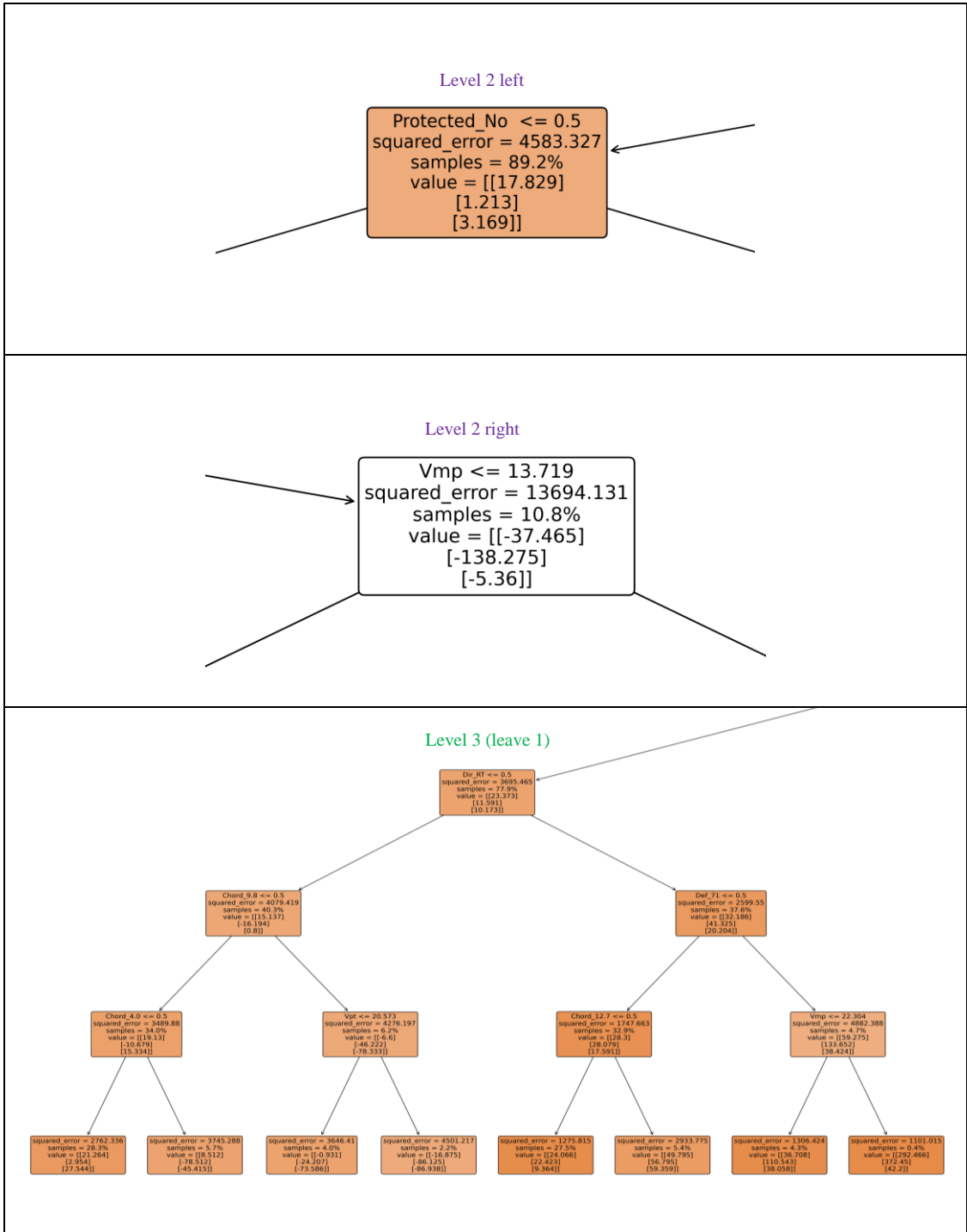
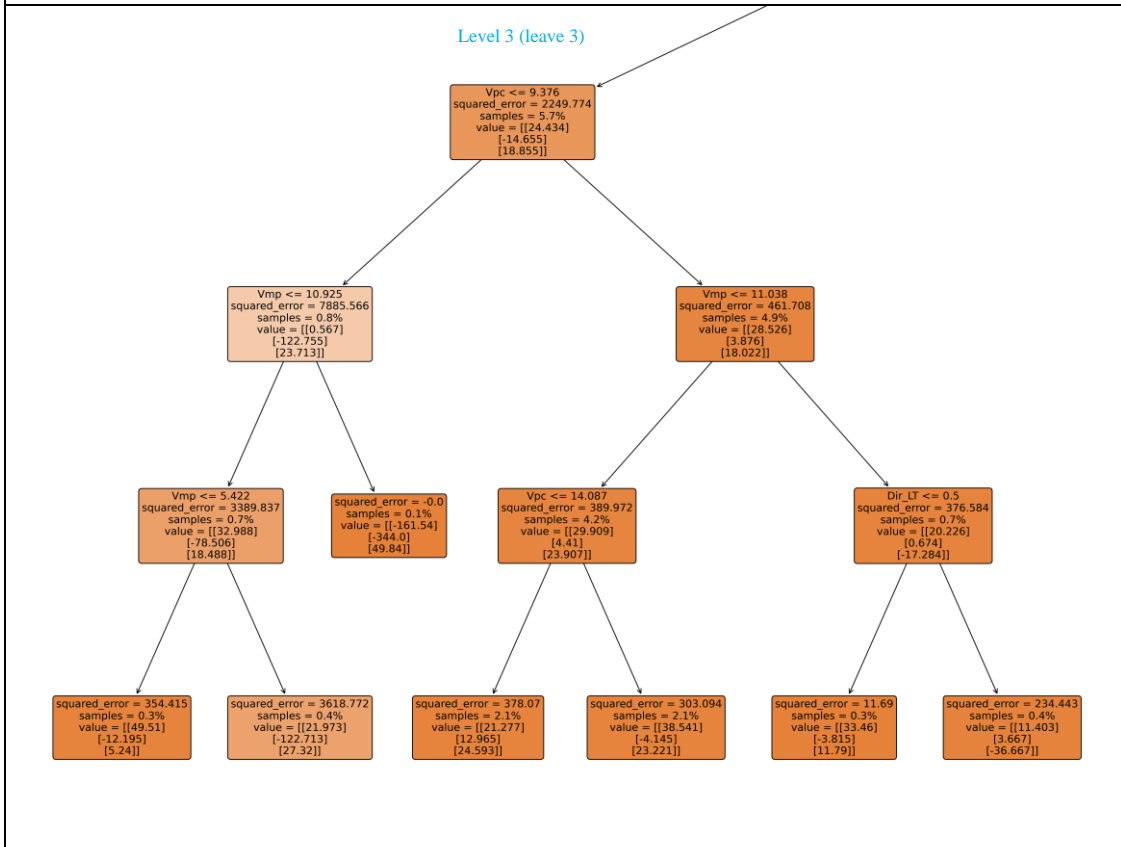
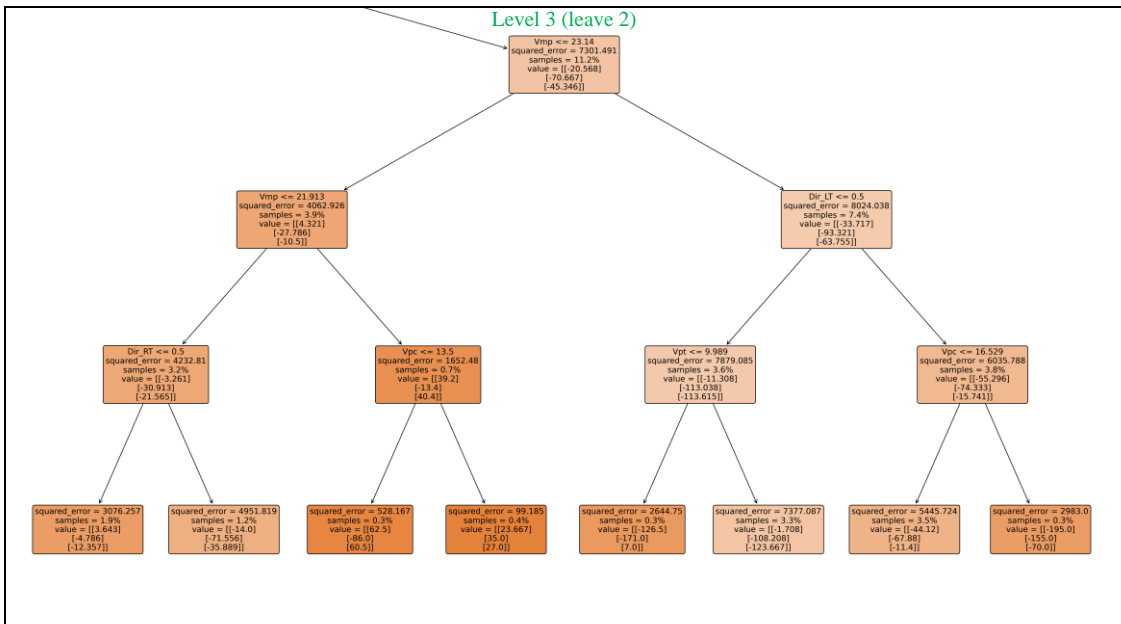


Figure 34 Improved Decision Tree Regression model visualization showing feature splits for predicting variables d-pc, d-mp, and d-pt (see Figure 35 for readability).







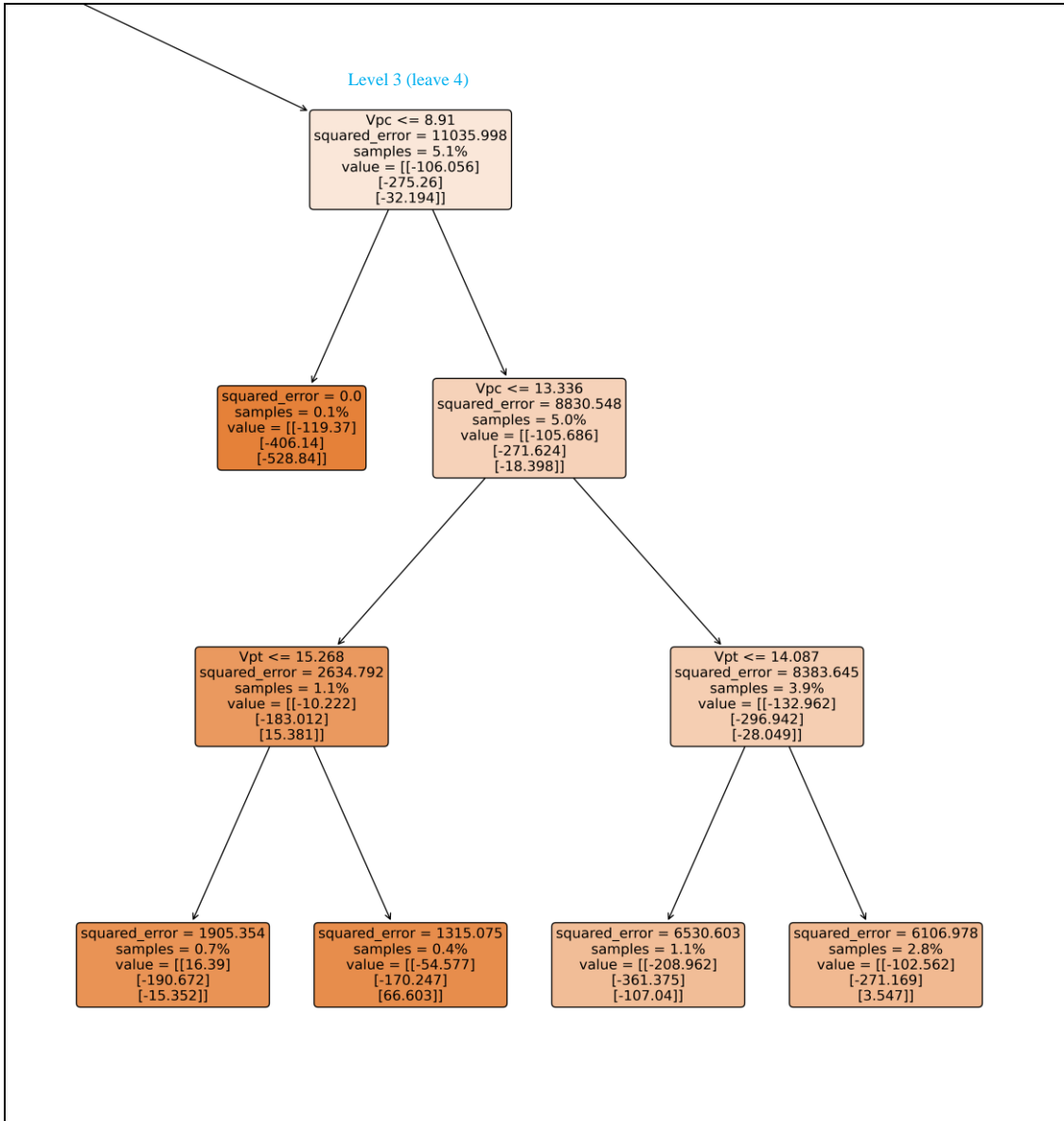


Figure 35 Magnified leaves of the improved Decision Tree Regression model in Figure 33.

7.5 Conclusion

The study investigated the maneuvering behavior of bike lane users across various curve geometries, focusing on the motion of the users, specifically their speed and trajectory during curve navigation. Effective Fitted Radius (EFR) was developed from three offset points to represent the variance of the trajectory in comparison to the actual radius of the curve, and for identification of the unsafe behavior. In order to have deeper understanding of unsafe maneuvers a lateral segmentation was conducted, based on which the users' position are mapped out. Key findings include:

- **Curve Geometry and User Behavior:** Sharp curves (with smaller radii) significantly influence user behavior, particularly left-turn users, who tend to cut curves, increasing the risk of head-on conflicts. In contrast, right-turn users generally follow a wider path, aligning more closely with the curve geometry.

- **Speed and Safety:** Speed analysis revealed that higher speeds, particularly in sharper curves, contribute to greater risk and variability in user behavior. E-scooters exhibit higher speeds and variability compared to bikes, highlighting the need for tailored safety measures.
- **Track Patterns and Conflict Risk:** Different user types and turning directions result in distinct track patterns, with sharper curves prompting more aggressive maneuvers. The study identified that left-turn users frequently engage in cutting maneuvers, while right-turn users often correct their paths.
- **Clustering Analysis:** DBSCAN clustering identified five distinct patterns of lateral offsets, with significant variability in user behavior. The largest cluster, accounting for 84% of the users (757), belongs to a cutting maneuver that passes through the CL region and though poses the risk of side conflict with the opposing users.
- **Predictive Modeling:** Decision tree regression analysis highlighted the degree of curvature as the most influential predictor of user behavior. The model's moderate prediction accuracy suggests room for further refinement to enhance its utility in infrastructure planning.

Chapter 8 Discussion

This chapter examines the challenges, objectives, and benefits of the proposed EFR concept and methodology. It does so by analyzing the results presented in the previous section, comparing them with previous research, and assessing their impact on infrastructure design. Additionally, the chapter addresses the study's limitations and offers recommendations for enhancing micromobility infrastructure and guiding future research.

8.1 The challenge of motion data extraction

In this study, efforts were made to simplify the computation process and reduce data requirements. Therefore, the minimum number of points necessary for generating an arc was used. The data collection method involved extracting offset values at three points on a curve, providing a practical solution to the complexity of generating accurate and effective trajectories from videos with angled views. Accessing drone or bird's-eye view footage is often impractical as they are not permitted to be used in urban areas. Consequently, the proposed data collection and extraction methods are scalable and practical for future applications.

Emerging computer vision algorithms like YOLO (You Only Look Once) could significantly enhance this research by improving the efficiency and speed of motion data extraction. However, two major issues were identified during data mining with tracking and obtaining accurate trajectories. First, generating accurate trajectories from angled view cameras is challenging due to the need for complex methods, such as applying Kalman filters, to convert and rotate 3D environments to a 2D (bird-eye) view. This means that a complex algorithm needed to be initially trained and calibrated for each of the recorded videos with varying angles, that was found to be impractical, time consuming, and often unreliable in terms of accuracy. Inaccuracy in the estimation of road users' sizes is a major limitation for automated detection, leading to overgrouping and oversegmentation (Saunier & Sayed, 2008). Second, e-scooters are frequently misclassified as pedestrians in most existing computer vision algorithms. Apurv et al. (2021) attempted to address this problem by training a model using a large sample of e-scooter images.

For overcoming the discussed challenges was that this study decided to use a video motion analysis tool called Kinovea. Kinovea is equipped with a simplified integrated calibration capability (calibration perspective grid), enhancing data extraction accuracy by allowing manual revisions of detections and trackings. Although this extraction method is time-consuming compared to automated detection and tracking methods, the results are more reliable and accurate due to the monitored process.

8.2 Effective Fitted Radius as Surrogate Measure of Safety

The findings from this study reveal several key insights into how micromobility users navigate curves and introduces Effective Fitted Radius (EFR) to effectively assess users' trajectories during navigation on horizontal curve. As thoroughly explained in the methodology, EFR refers to the radius of curvature of the trajectory at a given point. This radius describes how sharply the path curves and is inversely proportional to the curvature (κ) of the trajectory:

$$\text{Effective Fitted Radius (R)} = \frac{1}{\kappa} \quad (3)$$

Where the curvature κ is defined as:

$$\kappa = \frac{d\theta}{ds} \quad (4)$$

Here, θ is the angle of the tangent to the path, and s is the arc length along the trajectory. In practical applications, the curvature can be computed from the coordinates of the trajectory points.

For motor vehicles, besides trajectory, trajectory dispersion (DT) is used as a surrogate measure of safety since inconsistent lane positioning is a primary cause of single-vehicle run-off-the-road crashes and head-on collisions (Calvi, 2015). However, for micromobility devices, the effect of DT is assumed to be negligible due to their different dynamics, lighter weight, and greater steering capability and maneuverability.

To obtain the Effective Fitted Radius (EFR), the first step was to generate the best-fitted trajectory arcs from the X and Y coordinates of three sections/points (PC, MP, PT). For this purpose, Powell Optimization Method, a stochastic optimization algorithm was used (Hannah, 2015). This method does not require the gradient of the function and is designed to find its minimum. In this context, it is used to fit an arc through the three points, which are determined based on the wheel's displacement relative to the centerline marking on the curve.

To regenerate an arc from three points using Powell's optimization method, the objective is to minimize the error between the points and the arc. The parameters to be optimized typically include the center (x_c, y_c) and the radius \mathcal{R} of the arc. The objective function measures the sum of the squared distances from the three points to the arc. Given three points (x_1, y_1) , (x_2, y_2) , and (x_3, y_3) , the objective function f can be defined as:

$$f(x_c, y_c, \mathcal{R}) = \sum_{i=1}^3 (\sqrt{(x_i - x_c)^2 + (y_i - y_c)^2} - \mathcal{R})^2 \quad (5)$$

The computation and optimization of the Effective Fitted Radius (EFR) in the proposed methodology are automated in Python (see Figure 18). As the results in Section 7.1 proves, the primary advantage of EFR is its ability to quickly and accurately determine whether users are following the designed geometry of a curve. If users deviate, EFR can quantify the variance from the actual radius of the curve.

The displacement outputs can pinpoint the spatial locations of trajectories with high variance, which are considered risky, and to identify the types of conflict risks involved. This was enabled by “segmentation and regionalization” of a horizontal curve on bike lane, proposed in Section 5.3. This approach represents an initial attempt for spatial risk analysis of bike lanes at high-resolution. Additionally, the introduced curve segmentation methods offer benefits for microsimulation in micromobility applications in future research.

A major difference between EFR and previous SMOs like TTC and PET is that EFR is movement-based, while TTC and PET are time-based. Because EFR is movement-based, it can be used both with and without crash data (risk assessment). The occurrence of risky

maneuvers analyzed in this study can serve as a rapid and effective initial step in identifying aggressive maneuvers that are linked to a poor design. This is done by comparing the trajectories and their effective fitted radius (EFR) with the actual radius of the curve to identify the frequency of unsafe scenarios. For assessment of conflict scenarios, such as bike-bike or bike-pedestrian interactions, future research can link historical crash data (if available) with a combination of fitted trajectories, EFR, and the minimum distance or time between near-conflicting trajectories. This approach will enable a surrogate safety assessment at highest resolution. Studies have shown that movement-based approaches can identify near-misses more accurately than time-based measures, which often use a fixed time threshold (e.g., $TTC < 1.5$ seconds) to distinguish between safe and unsafe maneuver (Nabavi Niaki et al., 2019). Time-based measures may not always be accurate because they do not account for typical motion patterns and collision probability (Saunier & Sayed, 2008).

As shown in this thesis, EFR can assist in initial risk assessment for micromobility, especially when crash data for bike lanes is unavailable. This lack of data is a significant issue in micromobility safety. For incidents that do not involve motor vehicles, falls (SBC) and conflicts between users are the most common causes of serious injuries on bike lanes (SWOV, 2023b). These incidents often go unreported because the police are not involved, and if hospitals or emergency services do not record the causes of injuries, no data is available for effective surrogate safety assessment. Nevertheless, when crash data is available, EFR has the potentials to be combined with such data for a more impactful surrogate safety analysis.

8.3 Track classification, clustering and prediction

After the analysis of variance and spatial risk, a classification system for track types and spatioregions was defined. A six-class track classification, adopted from previous studies on motor vehicle tracks, was initially used and then extended to include an additional class for unclassified tracks and four lateral spatioregions, as detailed in Section 5.3. This resulted in a total of 28 possible combinations.

Additionally, the decision tree regression model was deemed suitable for this study because of its ability to handle complex, non-linear relationships and interactions among variables. This model effectively managed the multiple predictors influencing lateral offset, such as degree of curvature, bike lane type, and speed on MP, by splitting the data into branches based on the most significant predictors at each node. This approach provided clear, interpretable results and allowed for the identification of key factors affecting user behavior on curves, which was crucial for understanding and optimizing bike lane safety.

8.4 Comparison with Previous Studies

Although similar studies on safe riding behavior on bike lanes, particularly on horizontal curves, are lacking, various studies on road users have examined the geometric characteristics of curved road segments and their effects on driving performance with the aim of minimizing vehicle crashes. The findings of these studies align with this research on the effects of sharp curves on user behavior. For instance, Rondora et al. (2022) confirms that sharper curves increase the likelihood of risky maneuvers due to erroneous

perceptions that result in unsafe driving. The most common indicators for negotiating curves identified in these studies, such as speed profiles and lateral position, are similar to those considered in this research. Regarding data collection methods, most studies employed driving simulators, rather than naturalistic observation or experimental assessments (Rondora et al., 2022; Xia et al., 2024).

Similar to this research, ANOVA was the common quantitative method used for the comparative analysis of trajectories. A simulation-based study on curved roads have confirmed that the length of the tangent segment has no significant impact on driving behavior, while larger curve radii significantly improve safe driving behavior (Rondora et al., 2022). Research has also evaluated the effect of curve direction on a road segment under various lighting conditions, concluding that left-turning users tend to follow a less sharp path, allowing them to feel more comfortable and travel at higher speeds (Lemonakis et al., 2021; J. Xu et al., 2017). This finding aligns with the cutting maneuver observed on left-turn users on bike lanes. In bidirectional bike lanes, this tendency for left-turning users to cut the curve can increase the risk of potential conflicts with oncoming users.

A major contribution made in this study that completes previous research is the extension of track type classifications from six (Spacek, 2005) to twenty-eight by combining them with spatioregions. Additionally, this study integrates the effects of turn direction and micromobility user type, which have not been addressed together before. A similar study on road curves evaluated the impact of lateral friction on reverse curves and concluded that the length of the common tangent affects both lateral friction demand and driver trajectories (Aminfar et al., 2023). On bike lanes, particularly on curved segments, lateral friction is an important factor because micromobility users are lightweight, and even slight changes in surface conditions can impact their control. However, this aspect was not considered in this study, as all data were collected under dry conditions and with a uniform surface type on the bike lanes.

8.5 Limitations of the Study

Despite the valuable insights gained, this study has several limitations that must be acknowledged. Firstly, the data collection was limited to nine specific curve sites, which may not fully capture the variability of user behavior across the entire city of Valencia. Expanding the study to include a more diverse range of sites could provide a more comprehensive understanding of micromobility behavior and conflict risks.

Secondly, the study primarily focused on geometric parameters such as curve radius and degree of curvature, without considering other potentially influential factors like surface conditions, weather, and time of day. These factors were kept consistent across different sites. Additionally, due to the unavailability of crash data specific to incidents involving micromobility users, the proposed measure of Effective Fitted Radius (EFR) could not be further developed into a more robust Surrogate Measure of Safety (SMoS) incorporating historical crash data related to bike lanes (excluding incidents involving cars). Future research could benefit from including these additional variables to gain a more comprehensive understanding of the factors impacting user behavior and safety.

Moreover, while the decision tree analysis provided valuable insights into the predictive factors influencing user behavior, the model's moderate prediction accuracy suggests that there may be other unaccounted-for variables that play a significant role. Enhancing the model by integrating more comprehensive data and employing more sophisticated machine learning techniques could improve its predictive capability and robustness.

Finally, the study's reliance on observational data means that certain behavioral nuances and motivations underlying user maneuvers may not be fully captured. Complementing this approach with qualitative methods, such as user interviews or surveys, could provide deeper insights into the reasons behind specific behaviors, further informing the design of safer micromobility infrastructure.

In conclusion, this study enhances our understanding of micromobility behavior at various curve geometries and highlights the safety risks associated with sharpness of curves. The findings underscore the need for infrastructure designs that address user behavior patterns, such as incorporating wider curves and speed reduction measures. By addressing the study's limitations and exploring additional research avenues, urban planners and designers can develop more effective strategies to improve micromobility safety and reduce conflict risks.

Chapter 9 Conclusions

The primary goal of this study was twofold: (i) to introduce a novel surrogate measure (named as EFR) for accurately evaluating how well users follow the geometry of a horizontal curve and (ii) to examine how different types of users and their movement directions affect real riders' dynamic behavior, specifically in terms of trajectory and speed. Based on the results, it is evident that the geometry of horizontal curves significantly influences the maneuvering behavior of bike lane users. The Effective Fitted Radius (EFR) concept effectively identifies differences between the assumed parameters such as curve radius, user type, and direction of movement. Analysis using both parametric and non-parametric methods reveals significant variations in users' behavior across different curve sites. In particular, sharp curves exhibit distinct patterns where left-turn users tend to cut the curve, increasing the risk of head-on conflicts with opposing users. Conversely, right-turn users demonstrate less adherence to the curve geometry, posing challenges in maintaining lane integrity. Flatter curves, on the other hand, show minimal differences in behavior among different user types and directions of movement, suggesting lower conflict risks.

The initial hypotheses were confirmed through the analysis conducted in previous chapters. Hypothesis 1 demonstrated that users' motion on bike lanes encompasses various metrics including trajectory footprints, speed, acceleration, deceleration, lean, lane changing, and overtaking of micromobility devices. This was confirmed in the literature review and during data collection at site. Hypothesis 2 was validated through the Dutch guideline (CROW), revealing that bike lane infrastructure is effectively defined by its alignment, side lane, and pavement condition, all of which significantly impact user behavior. Hypothesis 3 was supported by the observation that assessing cyclists in free-flow conditions is crucial for understanding the effects of bike lane geometry on user behavior, as it removes the influence of user interactions. Furthermore, Hypothesis 4 was confirmed during video data collection and descriptive analysis of motion data. Accordingly, bike lane user motions are influenced by both human factors and infrastructure, with these elements contributing significantly to variations and risk levels in user behavior. Hypothesis 5 was corroborated by the finding that changes in the geometric design of a horizontal curve significantly influence riders' motion behavior. This is discussed in details in the result and discussion chapter. Lastly, Hypothesis 6 established that the motion of bike lane users can be detected, tracked, and measured through video motion analysis using computer vision tool that was used in this study.

The hypotheses tested in this research provided further insights into bike lane dynamics. Hypothesis 1 was confirmed in section 7.4, showing that bikes and e-scooters exhibit distinct motion patterns (track types) due to differences in size, steering angle, and handling characteristics. Hypothesis 2 was validated that the direction of turn on curves affects user trajectory and speed patterns (see section 7.1), emphasizing the need for bike lane designs that consider turn direction and lane widening measures. Additionally, Hypothesis 3 was confirmed as lateral segmentation of bike lanes was proved to be useful for identifying unsafe regions and potential causes, allowing for a detailed safety assessment. This can be seen in the displacement analysis in section 7.2. The analysis also supported the remaining tested hypotheses. Hypothesis 4 was supported by the result of post hoc ANOVA and track patterns analysis, showing that horizontal curves with radii below certain limits ($R < 10$ m) lead to increased violations, risky patterns, and higher speeds, highlighting the impact of curve sharpness on user behavior (see sections 7.1 and 7.3). Hypothesis 5 was verified in section 7.3, indicating that the highest frequency of

minimum speed occurs at specific points (MP), reinforcing predictions about speed patterns on bike lanes. Hypothesis 6 was tested in section 7.4, indicating that micromobility users navigating isolated curves generate specific trajectory patterns that can be clustered and classified. Finally, Hypothesis 7 was substantiated that curve geometry is a major predictor of user trajectory, underscoring the importance of geometric design in shaping bike lane usage and safety (see 7.4.3). These results collectively provide a robust understanding of how various factors influence bike lane behavior and safety.

The spatial analysis of wheel positions during navigation provides additional insights, highlighting specific regions within and outside the bike lane prone to conflict risks. Left-turn users are notably observed near the central marking, increasing vulnerability to crossing-body conflicts. Moreover, a significant proportion of users are observed in the opposite lane within the middle of the curve, emphasizing the importance of addressing potential conflicts in these areas. Speed analysis further elucidates the risks associated with high-traffic bike lanes, particularly on sharp curves where speeding behaviors are prevalent. The comparison of speeding trends across different curve radii reveals valuable insights for enhancing road safety. For instance, increasing curve radius leads to reduced speeding behaviors and variance in speed, indicating potential strategies for mitigating conflicts. The findings were visualized in box whisker plots for each site, segmented by user type and direction of turn (see Figure 28 and Appendix B). Hypotheses six and seven were addressed by these results. It was confirmed that users' trajectories on bike lanes could be clustered into distinct patterns, with a negligible maximum four percentage of unclassified track patterns observed across all samples

The DBSCAN algorithm (see section 7.4.2) successfully identified distinct patterns of lateral offsets in the dataset, with each cluster representing a unique trajectory type. Clusters 1, 2, 3, and 4 showed significant leftward or rightward biases in different sections, while Cluster 0 had a more moderate and variable offset pattern, that based on the mean could associate with the cutting maneuver. The outliers, marked as -1, highlight the presence of irregular data points that did not conform to the main patterns identified. This analysis provides valuable insights into the characteristics of different track sections and the potential impact on wheel alignment.

The classification and predictive analysis of different curve sites reveals that sharp curves, pose significant safety challenges. Here, left-turn users frequently cut the curve, while right-turn users correct their paths, with both types often crossing into the opposite lane and outside the bike lane. The absence of physical barriers in the sidewalk bike lane exacerbates these issues, increasing the potential for conflicts with pedestrians as well as users who are in the opposite direction. As curves gets flatter, users generally navigated through central segments with less aggressive maneuvers. Right-turn users still exhibited cutting and swinging behaviors, while left-turn users tended to drift, reflecting the curve's reduced sharpness.

The study further highlights that left-turn maneuvers exhibit greater diversity, with up to 12 different track-segment types, compared to a maximum of five for right turns. E-scooters, in particular, show more consistent behavior on sharper curves but become more variable on flatter (smoother) curves, whereas bikes display the opposite trend. Patterns observed at sites R3 to R9 reinforced these findings, with drifting being common at flatter curves and cutting maneuvers prevalent at sharper ones. The heatmap analysis also underscored that cutting maneuvers through the opposite lane are most frequent in sharper curves, indicating a higher risk of conflicts. These results emphasize the need for

tailored infrastructure designs that consider both curve geometry and bike lane type to better accommodate diverse user behaviors and enhance overall safety.

In conclusion, the findings underscore the importance of considering geometry and user behavior in designing and managing bike lanes, especially on horizontal curves. Strategies aimed at improving lane adherence, addressing conflict-prone areas, and regulating speeding behaviors can significantly enhance road safety for bike lane users. Further research using the framework introduced in this study may unveil additional patterns and trends to inform comprehensive safety interventions. As recommendation for future studies say that optimized radius of curvature can be computed not only for the users following the geometry but also for those who violate. Another idea is to use simulation methods to model the divided areas and study users perception through different scenarios. Moreover, this methodology has the potential to be applied to conflict-based events through more advanced statistical analyses, such as Extreme Value Theory (EVT), to better understand behavior in higher-risk situations.

Chapter 10 Future Research Direction

The development of this doctoral thesis has led to the creation of a geometric-based surrogate measure of safety utilizing Powell-optimized arc fitting. This advancement has enhanced our understanding of how micromobility users maneuver on horizontal curves with varying sharpness and radius. Additionally, the study has contributed to the classification and prediction of the most common track patterns observed during user curve navigation on bike lane. Consequently, this research has identified several promising areas for further investigation related to track types and speed patterns, highlighting their potential value.

10.1 Incorporation of crash data

One of the most significant improvements that can be made to the current study is the incorporation of crash data specific to bike lanes, as previously discussed. Currently, such data is scarce, and most existing data only includes incidents involving motor vehicles. However, if data on crashes specifically involving micromobility users on bike lanes becomes available, it could greatly enhance the effectiveness of the Effective Fitted Radius (EFR) as a Surrogate Measure of Safety (SMoS). By integrating historical crash data with EFR, the SMoS would be able to provide a more comprehensive assessment of safety risks and better identify areas where design improvements are needed. This combined approach would enable a more accurate evaluation of safety conditions on bike lanes and help in developing targeted interventions to improve user safety.

10.2 Automation of data filtering: image processing with AI

Future research should also focus on enhancing the automation of data filtering using advanced image processing techniques and artificial intelligence (AI). This approach will leverage AI-powered computer vision tools to automate the extraction and analysis of data from video recordings of cyclists and e-scooters on bike lanes. Machine learning algorithms will be employed to identify and track various micromobility users, segmenting their movements into essential metrics such as speed, trajectory, and lane position. AI models will enable differentiation between user types and detection of significant behaviors, including lane changes and overtaking.

To further improve the accuracy of trajectory path generation, a Kalman filter will be integrated into the process. The Kalman filter will be used to convert angled or perspective views into a 2D plane, enhancing the precision of path generation by minimizing distortions caused by the camera angle. This transformation will allow for more accurate tracking of user trajectories. The combined use of AI for automated tracking and the Kalman filter for perspective correction will significantly reduce manual data processing efforts and improve the overall reliability of the analysis. Future research should aim to refine these technologies to optimize data filtering and provide more precise, real-time insights into bike lane usage and safety.

10.3 Track type prediction

Another important step to complete this study is to build and test additional prediction models, such as neural networks, random forests, and other machine learning algorithms. These models could provide more accurate and robust predictions of track types by

leveraging complex patterns and interactions within the data. Neural networks, for instance, are particularly effective in capturing non-linear relationships and intricate data structures, while random forests can enhance prediction accuracy through ensemble learning and feature importance evaluation. Comparing the performance of these models with the existing approaches will help determine the most effective methods for predicting track types and understanding user behavior on bike lanes. This approach could lead to more precise and reliable safety assessments and better inform design improvements for bike lanes.

10.4 Using Extreme Value Theory to Model Extreme Conflict Events

In future studies, Extreme Value Theory (EVT) offers a robust framework for analyzing and predicting extreme conflict events between micromobility users, such as near-crashes, near-misses, sudden braking, and swerving to avoid collisions. EVT is particularly well-suited for this type of analysis because it focuses on rare, extreme occurrences that traditional statistical methods might overlook. By applying EVT to surrogate safety measures like time-to-collision (TTC) or post-encroachment time (PET), researchers can model the tail behavior of these extreme events and estimate the likelihood of even more severe near-crash events. This approach can address one of the limitations of this study, where data was collected under free-flow conditions using the Effective Fitted Radius (EFR) to evaluate lane violation events. While EFR has proven effective in identifying violations under free-flow conditions, it has great potential for being adapted to conflict event analysis in more complex traffic environments. By incorporating EVT and further exploring EFR's applicability in conflict scenarios, researchers could enhance the detection of high-risk situations and refine safety measures, ultimately improving the design and safety of bike lanes.

Acknowledgments

First and foremost, I would like to express my heartfelt gratitude to the Highway Engineering Research Group of the Polytechnic University of Valencia (HERG-UPV), particularly to my supportive supervisor, David Llopis Casetello, for his invaluable guidance and Alfredo Garcia for his insightful contributions.

I extend my sincere thanks to Professor Richard Balkin at the University of Mississippi for his advanced statistical course, which greatly enhanced my analytical skills. My heartfelt appreciation goes to the municipality of Valencia for granting permission to record video data essential for this research.

Lastly, I wish to thank my parents and my wife for their unwavering encouragement and support throughout this journey.

References

- AASHTO. (2011). *Policy on Geometric Design of Highways and Streets. E American Association of State Highway and Transportation Officials*. AASHTO Green Book, Washington DC., USA.
- AASHTO, N. R. C. (US) T. R. B. T. F. on D. of the H. S. (2010). *Highway safety manual* (Vol. 1). AASHTO.
[https://books.google.com/books?hl=en&lr=&id=M4fQiyfVRr8C&oi=fnd&pg=PP26&dq=American+Association+of+State+Highway+and+Transportation+Officials+\(AASHTO\),+2010.+Highway+Safety+Manual.+American+Association+of+State+Highway+and+Transportation+Officials,+Washington,+DC.&ots=ckqCizLGfr&sig=tb-9jPdI5QutXYvM7BkTI46NAme](https://books.google.com/books?hl=en&lr=&id=M4fQiyfVRr8C&oi=fnd&pg=PP26&dq=American+Association+of+State+Highway+and+Transportation+Officials+(AASHTO),+2010.+Highway+Safety+Manual.+American+Association+of+State+Highway+and+Transportation+Officials,+Washington,+DC.&ots=ckqCizLGfr&sig=tb-9jPdI5QutXYvM7BkTI46NAme)
- Abduljabbar, R. L., Liyanage, S., & Dia, H. (2021). The role of micro-mobility in shaping sustainable cities: A systematic literature review. *Transportation Research Part D: Transport and Environment*, 92, 102734.
- Afghari, A. P., Vos, J., Farah, H., & Papadimitriou, E. (2023). “I did not see that coming”: A latent variable structural equation model for understanding the effect of road predictability on crashes along horizontal curves. *Accident Analysis & Prevention*, 187, 107075. <https://doi.org/10.1016/j.aap.2023.107075>
- Ajuntament de València. (2019). Ordenanza de Movilidad. *Ajuntament de València, Regidoria de Mobilitat Sostenible: València, Spain*.
- Almallah, M., Alhajyaseen, W. K. M., & Dias, C. (2024). Safety assessment of on-road cycling lanes: A comparative study of different layouts using driving simulator. *Accident Analysis & Prevention*, 196, 107431.
<https://doi.org/10.1016/j.aap.2023.107431>
- Almannaa, M. H., Ashqar, H. I., Elhenawy, M., Masoud, M., Rakotonirainy, A., & Rakha, H. (2021). A comparative analysis of e-e-scooter and e-bike usage patterns: Findings from the City of Austin, TX. *International Journal of Sustainable Transportation*, 15(7), 571–579.
<https://doi.org/10.1080/15568318.2020.1833117>
- Aminfar, A., Boroujerdian, A. M., & Karimi, A. (2023). Evaluation of reverse curves focusing on the lateral friction demand on four-lane divided highways. *Transportation Engineering*, 13, 100188.
<https://doi.org/10.1016/j.treng.2023.100188>
- Amundsen, H. (1977). Traffic Conflicts. *Proceedings of the First Workshop on Traffic Conflicts, Institute of Transport Economics. Oslo*.
- Anke, J., Ringhand, M., Petzoldt, T., & Gehlert, T. (2023). Micro-mobility and road safety: Why do e-scooter riders use the sidewalk? Evidence from a German field study. *European Transport Research Review*, 15(1), 29.
<https://doi.org/10.1186/s12544-023-00607-z>
- Austin Public Health. (2019). *Dockless electric E-scooter-Related injuries study*. Austin, Texas.
- Bai, S., & Jiao, J. (2020). Dockless e-scooter usage patterns and urban built Environments: A comparison study of Austin, TX, and Minneapolis, MN. *Travel Behaviour and Society*, 20, 264–272.

- Blackman, R. A., & Haworth, N. L. (2013). Comparison of moped, e-scooter and motorcycle crash risk and crash severity. *Accident Analysis & Prevention*, *57*, 1–9.
- Bordagaray, M., Dell’Olio, L., Fonzone, A., & Ibeas, Á. (2016). Capturing the conditions that introduce systematic variation in bike-sharing travel behavior using data mining techniques. *Transportation Research Part C: Emerging Technologies*, *71*, 231–248.
- Bos, L., Slawinski, M. A., Slawinski, R. A., & Stanoev, T. (2024). Modelling of a cyclist’s power for time trials on a velodrome. *Sports Engineering*, *27*(1), 9. <https://doi.org/10.1007/s12283-024-00451-x>
- Bührmann, S., Wefering, F., & Rupprecht, S. (2011). *Guidelines: Developing and implementing a sustainable urban mobility plan*. Rupprecht Consult-Forschung und Beratung GmbH.
- Cabrera, F., & Sofía, A. (2021). *Caracterización de la maniobra de adelantamiento y el comportamiento frente al tráfico opuesto de los usuarios de vehículos de movilidad personal mediante el uso de un patinete eléctrico instrumentado con tecnología Raspberry Pi. Aplicación práctica en el distrito Algirós de la ciudad de Valencia*. <https://riunet.upv.es/handle/10251/175929>
- Cafiso, S., Di Graziano, A., Marchetta, V., & Pappalardo, G. (2022). Urban road pavements monitoring and assessment using bike and e-scooter as probe vehicles. *Case Studies in Construction Materials*, *16*, e00889.
- Calvi, A. (2015). A Study on Driving Performance Along Horizontal Curves of Rural Roads. *Journal of Transportation Safety & Security*, *7*(3), 243–267. <https://doi.org/10.1080/19439962.2014.952468>
- Carrignon, D. (2020). Connected and autonomous vehicles, electric e-scooter and their implications for road network design. *Transportation Research Procedia*, *49*, 160–169.
- Caspi, O., Smart, M. J., & Noland, R. B. (2020). Spatial associations of dockless shared e-scooter usage. *Transportation Research Part D: Transport and Environment*, *86*, 102396.
- Chang, A. Y., Miranda-Moreno, L., Clewlow, R., & Sun, L. (2019). Trend or fad. *Deciphering the Enablers of Micromobility in the US*. https://www.researchgate.net/profile/Annie-Chang-14/publication/335028238_Trend_or_Fad_Deciphering_the_Enablers_of_Micromobility_in_the_US/links/5d4b817692851cd046ab07be/Trend-or-Fad-Deciphering-the-Enablers-of-Micromobility-in-the-US.pdf
- Chang, F., Haque, M. M., Yasmin, S., & Huang, H. (2022). Crash injury severity analysis of E-Bike Riders: A random parameters generalized ordered probit model with heterogeneity in means. *Safety Science*, *146*, 105545.
- Chen, Z., Shen, H. T., & Zhou, X. (2011). Discovering popular routes from trajectories. *2011 IEEE 27th International Conference on Data Engineering*, 900–911.
- Cleveland, W. S. (1979). Robust Locally Weighted Regression and Smoothing Scatterplots. *Journal of the American Statistical Association*, *74*(368), 829–836. <https://doi.org/10.1080/01621459.1979.10481038>

- Clewlow, R. (2018). Urban Micromobility and Data for Planning and Policymaking. *Proceedings of the Fourth International Transport Energy Modeling Workshop, iTEM, Laxenburg, Austria*, 30–31.
<https://transportenergy.org/document/workshop-4/B3%20Clewlow%20-%20slides.pdf>
- Clewlow, R., Foti, F., Seki, S., & Mueting, E. (2022). *Developing Scalable Models for Safety Insights and Improvements Using E-scooter Exposure Data*.
<https://rosap.ntl.bts.gov/view/dot/63162>
- CNIG, O. A. C. N. de I. (2024). *Centro de Descargas del CNIG (IGN)*. Centro de Descargas Del CNIG. <http://centrodedescargas.cnig.es>
- Corcoran, J., Li, T., Rohde, D., Charles-Edwards, E., & Mateo-Babiano, D. (2014). Spatio-temporal patterns of a Public Bicycle Sharing Program: The effect of weather and calendar events. *Journal of Transport Geography*, 41, 292–305.
- Cortes, C., & Vapnik, V. (1995). Support-vector networks. *Machine Learning*, 20, 273–297.
- Deveci, M., Gokasar, I., Pamucar, D., Chen, Y., & Coffman, D. (2023). Sustainable e-scooter parking operation in urban areas using fuzzy Dombi based RAFSI model. *Sustainable Cities and Society*, 91, 104426.
- Dondi, G., Simone, A., Lantieri, C., & Vignali, V. (2011). Bike lane design: The context sensitive approach. *Procedia Engineering*, 21, 897–906.
- Dozza, M., Li, T., Billstein, L., Svernlöv, C., & Rasch, A. (2022). How do different micro-mobility vehicles affect longitudinal control? Results from a field experiment. *Journal of Safety Research*.
- Dozza, M., Li, T., Billstein, L., Svernlöv, C., & Rasch, A. (2023). How do different micro-mobility vehicles affect longitudinal control? Results from a field experiment. *Journal of Safety Research*, 84, 24–32.
- Du, Y., Deng, F., & Liao, F. (2019). A model framework for discovering the spatio-temporal usage patterns of public free-floating bike-sharing system. *Transportation Research Part C: Emerging Technologies*, 103, 39–55.
- Elmashhara, M. G., Silva, J., Sá, E., Carvalho, A., & Rezazadeh, A. (2022). Factors influencing user behaviour in micromobility sharing systems: A systematic literature review and research directions. *Travel Behaviour and Society*, 27, 1–25.
- Europeia, C. (2011). *Livro Branco: Roteiro do Espaço Único Europeu dos Transportes—Rumo a um Sistema de Transportes Competitivos e Económico em Recursos*. Bruxelas, CE.
- Farsiu, S., Robinson, D., Elad, M., & Milanfar, P. (2004). Advances and challenges in super-resolution. *International Journal of Imaging Systems and Technology*, 14(2), 47–57.
- Folco, P., Gauvin, L., Tizzoni, M., & Szell, M. (2023). Data-driven micromobility network planning for demand and safety. *Environment and Planning B: Urban Analytics and City Science*, 50(8), 2087–2102.
<https://doi.org/10.1177/23998083221135611>

- Fonseca Cabrera, A. S. (2021). *Caracterización de la maniobra de adelantamiento y el comportamiento frente al tráfico opuesto de los usuarios de vehículos de movilidad personal mediante el uso de un patinete eléctrico instrumentado con tecnología Raspberry Pi. Aplicación práctica en el distrito Algirós de la ciudad de Valencia*. <https://riunet.upv.es/handle/10251/175929>
- Fonseca-Cabrera, A. S., Llopis-Castelló, D., Pérez-Zuriaga, A. M., Alonso-Troyano, C., & García, A. (2021a). Micromobility Users' Behaviour and Perceived Risk during Meeting Manoeuvres. *International Journal of Environmental Research and Public Health*, 18(23), 12465.
- Fonseca-Cabrera, A. S., Llopis-Castelló, D., Pérez-Zuriaga, A. M., Alonso-Troyano, C., & García, A. (2021b). Micromobility Users' Behaviour and Perceived Risk during Meeting Manoeuvres. *International Journal of Environmental Research and Public Health*, 18(23), Article 23. <https://doi.org/10.3390/ijerph182312465>
- Foresee, F. D., & Hagan, M. T. (1997). Gauss-Newton approximation to Bayesian learning. *Proceedings of International Conference on Neural Networks (ICNN'97)*, 3, 1930–1935.
- Fraley, C., & Raftery, A. E. (2003). Enhanced Model-Based Clustering, Density Estimation, and Discriminant Analysis Software: MCLUST. *Journal of Classification*, 20(2), 263–286. <https://doi.org/10.1007/s00357-003-0015-3>
- Friedman, J. H. (1991). Multivariate adaptive regression splines. *The Annals of Statistics*, 19(1), 1–67.
- Gehrke, S. R., Russo, B. J., Sadeghinassr, B., Riffle, K. R., Smaglik, E. J., & Reardon, T. G. (2022). Spatial interactions of shared e-scooter trip generation and vulnerable road user crash frequency. *Journal of Transportation Safety & Security*, 14(10), 1798–1814. <https://doi.org/10.1080/19439962.2021.1971813>
- Geoportal València | Ajuntament de València. (n.d.). Retrieved June 4, 2024, from <https://geoportal.valencia.es/>
- Gomm, P., & Wengraf, I. (2013). *The car and the commute: The journey to work in England and Wales*. <https://trid.trb.org/View/1286258>
- Goodfellow, I., Pouget-Abadie, J., Mirza, M., Xu, B., Warde-Farley, D., Ozair, S., Courville, A., & Bengio, Y. (2014). Generative adversarial nets. *Advances in Neural Information Processing Systems*, 27.
- Google Maps. (2024a). *54 Hoskin Ave, Toronto, Ontario*. Retrieved from https://www.google.com/maps/@43.6641362,-79.398149,3a,75y,218.13h,61.33t/data=!3m6!1e1!3m4!1sQyz5SR3r_04M7RZHqWPvUQ!2e0!7i16384!8i8192!5m1!1e2
- Google Maps. (2024b). *Tarongers Street, Valencia*. Retrieved from https://www.google.com/maps/@39.4795167,-0.343174,3a,75y,251.81h,79.95t/data=!3m7!1e1!3m5!1spT1xwn_UDy_Khbx8jgwFWg!2e0!6shttps:%2F%2Fstreetviewpixels-pa.googleapis.com%2Fv1%2Fthumbnail%3Fpanoid%3DpT1xwn_UDy_Khbx8jgwFWg%26cb_client%3Dmaps_sv.share%26w%3D900%26h%3D600%26yaw%3D251.81%26pitch%3D10.049999999999997%26thumbfov%3D90!7i13312!8i6656?coh=205410&entry=ttu

- Gössling, S. (2020). Integrating e-scooters in urban transportation: Problems, policies, and the prospect of system change. *Transportation Research Part D: Transport and Environment*, 79, 102230.
- Greibe, P., & Buch, T. S. (2016). Capacity and behaviour on one-way cycle tracks of different widths. *Transportation Research Procedia*, 15, 122–136.
- Groot, R. de. (2007). *Design manual for bicycle traffic*.
<https://trid.trb.org/View/1153223>
- Guo, X., Tavakoli, A., Angulo, A., Robartes, E., Chen, T. D., & Heydarian, A. (2023). Psycho-physiological measures on a bicycle simulator in immersive virtual environments: How protected/curbside bike lanes may improve perceived safety. *Transportation Research Part F: Traffic Psychology and Behaviour*, 92, 317–336. <https://doi.org/10.1016/j.trf.2022.11.015>
- Guo, Y., Wu, Y., Lu, J., & Zhou, J. (2019). Modeling the unobserved heterogeneity in e-bike collision severity using full Bayesian random parameters multinomial logit regression. *Sustainability*, 11(7), 2071.
- Haasnoot, J., Happee, R., van der Wijk, V., & Schwab, A. L. (2023). Validation of a novel bicycle simulator with realistic lateral and roll motion. *Vehicle System Dynamics*, 0(0), 1–25. <https://doi.org/10.1080/00423114.2023.2264418>
- Hall, G. J., & Albers, C. A. (2023). Research study design. In R. J. Tierney, F. Rizvi, & K. Ercikan (Eds.), *International Encyclopedia of Education (Fourth Edition)* (pp. 695–702). Elsevier. <https://doi.org/10.1016/B978-0-12-818630-5.10079-X>
- Hannah, L. A. (2015). Stochastic Optimization. In J. D. Wright (Ed.), *International Encyclopedia of the Social & Behavioral Sciences (Second Edition)* (pp. 473–481). Elsevier. <https://doi.org/10.1016/B978-0-08-097086-8.42010-6>
- Hartigan, J. A., & Wong, M. A. (1979). Algorithm AS 136: A K-Means Clustering Algorithm. *Journal of the Royal Statistical Society. Series C (Applied Statistics)*, 28(1), 100–108. <https://doi.org/10.2307/2346830>
- Hawa, L., Cui, B., Sun, L., & El-Geneidy, A. (2021). Scoot over: Determinants of shared electric e-scooter presence in Washington DC. *Case Studies on Transport Policy*, 9(2), 418–430.
- He, S., & Shin, K. G. (2020). Dynamic Flow Distribution Prediction for Urban Dockless E-scooter Sharing Reconfiguration. *Proceedings of The Web Conference 2020*, 133–143. <https://doi.org/10.1145/3366423.3380101>
- He, Y., Song, Z., Liu, Z., & Sze, N. N. (2019). Factors Influencing Electric Bike Share Ridership: Analysis of Park City, Utah. *Transportation Research Record: Journal of the Transportation Research Board*, 2673(5), 12–22. <https://doi.org/10.1177/0361198119838981>
- Hossein Sabbaghian, M., Llopis-Castelló, D., & García, A. (2023a). A Safe Infrastructure for Micromobility: The Current State of Knowledge. *Sustainability*, 15(13), Article 13. <https://doi.org/10.3390/su151310140>
- Hossein Sabbaghian, M., Llopis-Castelló, D., & García, A. (2023b). A Safe Infrastructure for Micromobility: The Current State of Knowledge. *Sustainability*, 15(13), 10140. <https://www.mdpi.com/2071-1050/15/13/10140>

- Hosseinzadeh, A., Algomaiah, M., Kluger, R., & Li, Z. (2021). E-scooters and sustainability: Investigating the relationship between the density of E-scooter trips and characteristics of sustainable urban development. *Sustainable Cities and Society*, *66*, 102624.
- Hu, L., Hu, X., Wang, J., Kuang, A., Hao, W., & Lin, M. (2020). Casualty risk of e-bike rider struck by passenger vehicle using China in-depth accident data. *Traffic Injury Prevention*, *21*(4), 283–287. <https://doi.org/10.1080/15389588.2020.1747614>
- Jackson, S., Miranda-Moreno, L. F., St-Aubin, P., & Saunier, N. (2013). Flexible, Mobile Video Camera System and Open Source Video Analysis Software for Road Safety and Behavioral Analysis. *Transportation Research Record*, *2365*(1), 90–98. <https://doi.org/10.3141/2365-12>
- JASP 18.3. (2024). JASP - Free and User-Friendly Statistical Software. <https://jasp-stats.org/>
- Jiao, J., & Bai, S. (2020). Understanding the shared e-e-scooter travels in Austin, TX. *ISPRS International Journal of Geo-Information*, *9*(2), 135.
- Johansson, J. (2023). *Analysis of free-riding behaviour using instrumented bicycles*. <https://urn.kb.se/resolve?urn=urn:nbn:se:liu:diva-196596>
- Kamel, M. B., & Sayed, T. (2021). The impact of bike network indicators on bike kilometers traveled and bike safety: A network theory approach. *Environment and Planning B: Urban Analytics and City Science*, *48*(7), 2055–2072. <https://doi.org/10.1177/2399808320964469>
- Kaths, H. (2022). Cyclists' interactions with other road users from a safety perspective. *Cycling*, 187.
- Kathuria, A., & Vedagiri, P. (2020). Evaluating pedestrian vehicle interaction dynamics at un-signalized intersections: A proactive approach for safety analysis. *Accident Analysis & Prevention*, *134*, 105316. <https://doi.org/10.1016/j.aap.2019.105316>
- Kaufman, S. M., & Bütünwieser, L. (2018). The state of e-scooter sharing in United States cities. *Rudin Center for Transportation—New York University—Robert F. Wagner School for Public Service: New York, NY, USA*. https://wagner.nyu.edu/files/faculty/publications/Rudin_E-scooterShare_Aug2018.pdf
- Keogh, E., & Ratanamahatana, C. A. (2005). Exact indexing of dynamic time warping. *Knowledge and Information Systems*, *7*, 358–386.
- Kinovea. (n.d.). Retrieved March 24, 2024, from <https://www.kinovea.org/>
- Kononenko, I., & Kukar, M. (2007). Chapter 12—Cluster Analysis. In I. Kononenko & M. Kukar (Eds.), *Machine Learning and Data Mining* (pp. 321–358). Woodhead Publishing. <https://doi.org/10.1533/9780857099440.321>
- Laureshyn, A., Goede, M. de, Saunier, N., & Fyhri, A. (2017). Cross-comparison of three surrogate safety methods to diagnose cyclist safety problems at intersections in Norway. *Accident Analysis & Prevention*, *105*, 11–20. <https://doi.org/10.1016/j.aap.2016.04.035>
- Laureshyn, A., Jonsson, C., De Ceunynck, T., Svensson, Å., de Goede, M., Saunier, N., Włodarek, P., van der Horst, R., & Daniels, S. (2016). *Review of current study*

methods for VRU safety: Appendix 6-Scoping review: Surrogate measures of safety in site-based road traffic observations.

- Lazarus, J., Pourquier, J. C., Feng, F., Hammel, H., & Shaheen, S. (2020). Micromobility evolution and expansion: Understanding how docked and dockless bikesharing models complement and compete—A case study of San Francisco. *Journal of Transport Geography*, *84*, 102620.
- Lemonakis, P., Eliou, N., & Karakasidis, T. (2021). Investigation of speed and trajectory of motorcycle riders at curved road sections of two-lane rural roads under diverse lighting conditions. *Journal of Safety Research*, *78*, 138–145. <https://doi.org/10.1016/j.jsr.2021.05.009>
- Li, W., & Zhang, C. (2009). Markov Chain Analysis. In A. Kobayashi (Ed.), *International Encyclopedia of Human Geography (Second Edition)* (pp. 407–412). Elsevier. <https://doi.org/10.1016/B978-0-08-102295-5.10403-2>
- Liao, F., & Correia, G. (2022). Electric carsharing and micromobility: A literature review on their usage pattern, demand, and potential impacts. *International Journal of Sustainable Transportation*, *16*(3), Article 3.
- Llopis Castelló, D. (2018). *Desarrollo de una metodología para el diseño y mejora de carreteras convencionales a partir del análisis de la seguridad vial mediante modelos de consistencia* [Tesis doctoral, Universitat Politècnica de València]. <https://doi.org/10.4995/Thesis/10251/100271>
- López, G., Pérez-Zuriaga, A. M., Moll, S., & García, A. (2020). Analysis of Overtaking Maneuvers to Cycling Groups on Two-Lane Rural Roads using Objective and Subjective Risk. *Transportation Research Record*, *2674*(7), 148–160. <https://doi.org/10.1177/0361198120921169>
- López-Molina, M., Llopis-Castelló, D., Pérez-Zuriaga, A. M., Alonso-Troyano, C., & García, A. (2022). Skid Resistance Analysis of Urban Bike Lane Pavements for Safe Micromobility. *Sustainability*, *15*(1), 698.
- Lu, C., He, X., van Lint, H., Tu, H., Happee, R., & Wang, M. (2021). Performance evaluation of surrogate measures of safety with naturalistic driving data. *Accident Analysis & Prevention*, *162*, 106403. <https://doi.org/10.1016/j.aap.2021.106403>
- Lukes, R., Hart, J., & Haake, S. (2012). An analytical model for track cycling. *Proceedings of the Institution of Mechanical Engineers, Part P: Journal of Sports Engineering and Technology*, *226*(2), 143–151. <https://doi.org/10.1177/1754337111433242>
- Ma, Q., Yang, H., Mayhue, A., Sun, Y., Huang, Z., & Ma, Y. (2021). E-scooter safety: The riding risk analysis based on mobile sensing data. *Accident Analysis & Prevention*, *151*, 105954.
- Ma, X., & Luo, D. (2016). Modeling cyclist acceleration process for bicycle traffic simulation using naturalistic data. *Transportation Research Part F: Traffic Psychology and Behaviour*, *40*, 130–144. <https://doi.org/10.1016/j.trf.2016.04.009>

- MacQueen, J. (1967). Some methods for classification and analysis of multivariate observations. *Proceedings of the Fifth Berkeley Symposium on Mathematical Statistics and Probability*, 1(14), 281–297.
- Marshall, W. E., & Garrick, N. W. (2011). Does street network design affect traffic safety? *Accident Analysis & Prevention*, 43(3), Article 3.
- McKenzie, G. (2019). Spatiotemporal comparative analysis of e-scooter-share and bike-share usage patterns in Washington, DC. *Journal of Transport Geography*, 78, 19–28.
- Meuleners, L., Fraser, M., & Roberts, P. (2023). Improving cycling safety through infrastructure design: A bicycle simulator study. *Transportation Research Interdisciplinary Perspectives*, 18, 100768. <https://doi.org/10.1016/j.trip.2023.100768>
- Mishra, A., Agnihotri, A. K., Pipil, S., Gaur, S., & Ohri, A. (2024). Chapter 4— Surveying techniques for urban areas. In A. Kumar, P. K. Srivastava, P. Saikia, & R. K. Mall (Eds.), *Earth Observation in Urban Monitoring* (pp. 69–91). Elsevier. <https://doi.org/10.1016/B978-0-323-99164-3.00013-6>
- Mitchell, T., Buchanan, B., DeJong, G., Dietterich, T., Rosenbloom, P., & Waibel, A. (1990). Machine learning. *Annual Review of Computer Science*, 4(1), 417–433.
- Mohammed, H., Bigazzi, A. Y., & Sayed, T. (2019). Characterization of bicycle following and overtaking maneuvers on cycling paths. *Transportation Research Part C: Emerging Technologies*, 98, 139–151. <https://doi.org/10.1016/j.trc.2018.11.012>
- Møller, T. H., Simlett, J., & Mugnier, E. (2020). Micromobility: Moving cities into a sustainable future. *EY: London, UK*.
- Montella, A., Aria, M., D'Ambrosio, A., & Mauriello, F. (2012). Analysis of powered two-wheeler crashes in Italy by classification trees and rules discovery. *Accident Analysis & Prevention*, 49, 58–72.
- Mullakkal-Babu, F. A., Wang, M., He, X., van Arem, B., & Happee, R. (2020). Probabilistic field approach for motorway driving risk assessment. *Transportation Research Part C: Emerging Technologies*, 118, 102716.
- Nabavi Niaki, M. S., Saunier, N., & Miranda-Moreno, L. F. (2019). Is that move safe? Case study of cyclist movements at intersections with cycling discontinuities. *Accident Analysis & Prevention*, 131, 239–247. <https://doi.org/10.1016/j.aap.2019.07.006>
- NACTO. (2014). *Urban bikeway design guide*. Island Press. https://books.google.es/books?hl=es&lr=&id=VAzqAwAAQBAJ&oi=fnd&pg=PR2&dq=NACTO.+Urban+Bikeway+Design+Guide%3B+Island+Press:+Washington,+DC,+USA,+2014%3B&ots=61whjp4-3P&sig=7VzkSFA1vRpvoLfl5OtG_AzqrDA
- Nee, P. J., & Herterich, J. G. (2022). Modelling road cycling as motion on a curve. *Sports Engineering*, 25(1), 12. <https://doi.org/10.1007/s12283-022-00376-3>
- Nigro, M., Castiglione, M., Colasanti, F. M., De Vincentis, R., Valenti, G., Liberto, C., & Comi, A. (2022). Exploiting floating car data to derive the shifting potential

- to electric micromobility. *Transportation Research Part A: Policy and Practice*, 157, 78–93.
- NTSB. (2019). *Bicyclist Safety on US Roadways: Crash Risks and Countermeasures*.
- NYC DOT Web page. (2024). *Two-Way Bike Lane | NYC Street Design Manual*.
<https://www.nycstreetdesign.info/geometry/two-way-bike-lane>
- Oeschger, G., Carroll, P., & Caulfield, B. (2020). Micromobility and public transport integration: The current state of knowledge. *Transportation Research Part D: Transport and Environment*, 89, 102628.
- O’Hern, S., & Estgfaeller, N. (2020). A scientometric review of powered micromobility. *Sustainability*, 12(22), 9505.
- Ohri, V. (2013). *Developing test methods for the evaluation of e-scooter performance in winter conditions* [PhD Thesis]. <https://library-archives.canada.ca/eng/services/services-libraries/theses/Pages/item.aspx?idNumber=1032913841>
- Park, J., & Abdel-Aty, M. (2016). Evaluation of safety effectiveness of multiple cross sectional features on urban arterials. *Accident Analysis & Prevention*, 92, 245–255.
- Pérez-Zuriaga, A. M., Llopis-Castelló, D., Just-Martínez, V., Fonseca-Cabrera, A. S., Alonso-Troyano, C., & García, A. (2022). Implementation of a low-cost data acquisition system on an e-scooter for micromobility research. *Sensors*, 22(21), 8215.
- Politis, I., Papadopoulos, E., Fyrogenis, I., & Fytsili, Z. (2021). A Multi-criteria-Based Methodology for Assessing Alternative Bicycle Lane Implementation Solutions in Urban Networks. In E. G. Nathanail, G. Adamos, & I. Karakikes (Eds.), *Advances in Mobility-as-a-Service Systems* (Vol. 1278, pp. 435–444). Springer International Publishing. https://doi.org/10.1007/978-3-030-61075-3_43
- Prencipe, L. P., Colovic, A., De Bartolomeo, S., Caggiani, L., & Ottomanelli, M. (2022). An efficiency indicator for micromobility safety assessment. *2022 IEEE International Conference on Environment and Electrical Engineering and 2022 IEEE Industrial and Commercial Power Systems Europe (EEEIC/I&CPS Europe)*, 1–6. <https://ieeexplore.ieee.org/abstract/document/9854627/>
- Quinonero-Candela, J., & Rasmussen, C. E. (2005). A unifying view of sparse approximate Gaussian process regression. *The Journal of Machine Learning Research*, 6, 1939–1959.
- Rampf, F., Grigoropoulos, G., Malcolm, P., Keler, A., & Bogenberger, K. (2023). Modelling autonomous vehicle interactions with bicycles in traffic simulation. *Frontiers in Future Transportation*, 3. <https://doi.org/10.3389/ffutr.2022.894148>
- Reijne, M. M., Dehkordi, S. G., Glaser, S., Twisk, D., & Schwab, A. L. (2022). A Modelling Study to Examine Threat Assessment Algorithms Performance in Predicting Cyclist Fall Risk in Safety Critical Bicycle-Automatic Vehicle Interactions. *Contributions to the Th 10 International Cycling Safety Conference (ICSC2022)*, 28.
- Rondora, M. E. S., Pirdavani, A., & Larocca, A. P. C. (2022). Driver Behavioral Classification on Curves Based on the Relationship between Speed, Trajectories,

- and Eye Movements: A Driving Simulator Study. *Sustainability*, 14(10), Article 10. <https://doi.org/10.3390/su14106241>
- Rupprecht, S., Brand, L., Böhler-Baedeker, S., & Brunner, L. M. (2019). *Guidelines for developing and implementing a sustainable urban mobility plan, Rupprecht Consult(2nd ed.)*.
- Sadeghian, A., Kosaraju, V., Gupta, A., Savarese, S., & Alahi, A. (2018). Trajnet: Towards a benchmark for human trajectory prediction. *arXiv Preprint*.
- Sánchez, D. F. D. G. (2016). Real Decreto Legislativo 6/2015, de 30 de octubre, por el que se aprueba el texto refundido de la Ley sobre Tráfico, Circulación de Vehículos a Motor y Seguridad Vial [BOE n. ° 261, 31-X-2015]. *AIS: Ars Iuris Salmanticensis*, 4(1), 232–233.
- Sandt, L., West, A., Harmon, K. J., Bryson, M., Gelinne, D., Cherry, C. R., Sexton, E., Shah, N., Sanders, R., & Brown, C. T. (2022). *E-scooter Safety: Issues and Solutions*.
- Santacreu, A., Yannis, G., de Saint Leon, O., & Crist, P. (2020). *Safe micromobility*. <https://trid.trb.org/View/1696177>
- Saunier, N., & Lareshyn, A. (2021a). Surrogate Measures of Safety. In R. Vickerman (Ed.), *International Encyclopedia of Transportation* (pp. 662–667). Elsevier. <https://doi.org/10.1016/B978-0-08-102671-7.10197-6>
- Saunier, N., & Lareshyn, A. (2021b). Surrogate Measures of Safety. In R. Vickerman (Ed.), *International Encyclopedia of Transportation* (pp. 662–667). Elsevier. <https://doi.org/10.1016/B978-0-08-102671-7.10197-6>
- Saunier, N., & Sayed, T. (2008). Probabilistic framework for automated analysis of exposure to road collisions. *Transportation Research Record*, 2083(1), 96–104.
- Schultheiss, B., Goodman, D., Blackburn, L., Wood, A., Reed, D., & Elbech, M. (2019). *Bikeway selection guide*. United States. Federal Highway Administration. Office of Safety. <https://rosap.nhtl.bts.gov/view/dot/43669>
- Şengül, B., & Mostofi, H. (2021). Impacts of E-Micromobility on the sustainability of urban transportation—A systematic review. *Applied Sciences*, 11(13), Article 13.
- Shaheen, S., Cohen, A., Chan, N., & Bansal, A. (2020). Sharing strategies: Carsharing, shared micromobility (bikesharing and e-scooter sharing), transportation network companies, microtransit, and other innovative mobility modes. In *Transportation, land use, and environmental planning* (pp. 237–262). Elsevier. <https://www.sciencedirect.com/science/article/pii/B978012815167900013X>
- Shen, X., Huang, D., Li, P., & Xu, N. (2023). Chapter Eight—Trajectory super-resolution methods. In H. Zhang (Ed.), *Handbook of Mobility Data Mining* (pp. 139–156). Elsevier. <https://doi.org/10.1016/B978-0-443-18428-4.00010-4>
- Shoman, M. M., Imine, H., Acerra, E. M., & Lantieri, C. (2023). Evaluation of Cycling Safety and Comfort in Bad Weather and Surface Conditions Using an Instrumented Bicycle. *IEEE Access*, 11, 15096–15108. IEEE Access. <https://doi.org/10.1109/ACCESS.2023.3242583>

- Smith, C. S., & Schwieterman, J. P. (2018). *E-scooter scenarios: Evaluating the potential mobility benefits of shared dockless e-scooters in Chicago*. <https://trid.trb.org/View/1577726>
- Spacek, P. (2005). Track behavior in curve areas: Attempt at typology. *Journal of Transportation Engineering*, 131(9), 669–676.
- SWOV. (2023, November 15). *11th International Cycling Safety Conference 2023, 15–17 November 2023, The Hague, The Netherlands*, p.p 287-289. SWOV; SWOV Institute for Road Safety Research. <https://swov.nl/en/publicatie/11th-international-cycling-safety-conference-2023-15-17-november-2023-hague-netherlands>
- Tan, S., & Tamminga, K. (2021). A Vision for Urban Micromobility: From Current Streetscape to City of the Future. In E. G. Nathanail, G. Adamos, & I. Karakikes (Eds.), *Advances in Mobility-as-a-Service Systems* (Vol. 1278, pp. 158–167). Springer International Publishing. https://doi.org/10.1007/978-3-030-61075-3_16
- Teodorović, D., & Janić, M. (2017). Chapter 4—Traffic Flow Theory. In D. Teodorović & M. Janić (Eds.), *Transportation Engineering (Second Edition)* (pp. 163–196). Butterworth-Heinemann. <https://doi.org/10.1016/B978-0-323-90813-9.00004-7>
- Thomas, J., & Harden, A. (2008). Methods for the thematic synthesis of qualitative research in systematic reviews. *BMC Medical Research Methodology*, 8(1), Article 1.
- Tian, D., Ryan, A. D., Craig, C. M., Sievert, K., & Morris, N. L. (2022a). Characteristics and risk factors for electric e-scooter-related crashes and injury crashes among e-scooter riders: A two-phase survey study. *International Journal of Environmental Research and Public Health*, 19(16), 10129.
- Tian, D., Ryan, A. D., Craig, C. M., Sievert, K., & Morris, N. L. (2022b). Characteristics and Risk Factors for Electric E-scooter-Related Crashes and Injury Crashes among E-scooter Riders: A Two-Phase Survey Study. *International Journal of Environmental Research and Public Health*, 19(16), Article 16. <https://doi.org/10.3390/ijerph191610129>
- Tiwari, A. (2019). Micro-mobility: The next wave of urban transportation in India. *YS Journal*, January.
- Tomiyaama, K., & Moriishi, K. (2020). Pavement Surface Evaluation Interacting Vibration Characteristics of an Electric Mobility E-scooter. In C. Raab (Ed.), *Proceedings of the 9th International Conference on Maintenance and Rehabilitation of Pavements—Mairepav9* (Vol. 76, pp. 893–900). Springer International Publishing. https://doi.org/10.1007/978-3-030-48679-2_83
- Ul-Abdin, Z., Rajper, S. Z., Schotte, K., De Winne, P., & De Backer, H. (2020). Analytical geometric design of bicycle paths. *Proceedings of the Institution of Civil Engineers - Transport*, 173(6), 361–379. <https://doi.org/10.1680/jtran.17.00162>
- Voinov, A., Morales, J., & Hogenkamp, H. (2019). Analyzing the social impacts of e-scooters with geo-spatial methods. *Journal of Environmental Management*, 242, 529–538.

- Wang, C., Xie, Y., Huang, H., & Liu, P. (2021). A review of surrogate safety measures and their applications in connected and automated vehicles safety modeling. *Accident Analysis & Prevention, 157*, 106157. <https://doi.org/10.1016/j.aap.2021.106157>
- Wang, K., & Chen, Y.-J. (2020). Joint analysis of the impacts of built environment on bikeshare station capacity and trip attractions. *Journal of Transport Geography, 82*, 102603.
- Wang, T., Chen, J., Wang, C., & Ye, X. (2018). Understand e-bicyclist safety in China: Crash severity modeling using a generalized ordered logit model. *Advances in Mechanical Engineering, 10*(6), 168781401878162. <https://doi.org/10.1177/1687814018781625>
- Wyman, A. (2022). *A safety evaluation of turn lane-adjacent bike lane configurations in Portland, Oregon*. https://ir.library.oregonstate.edu/concern/graduate_thesis_or_dissertations/xw42ng954
- Xia, T., Chen, H., Yang, J., & Guo, Z. (2024). Geometric field model of driver's perceived risk for safe and human-like trajectory planning. *Transportation Research Part C: Emerging Technologies, 159*, 104470. <https://doi.org/10.1016/j.trc.2023.104470>
- Xing, Y., Wang, K., & Lu, J. J. (2020). Exploring travel patterns and trip purposes of dockless bike-sharing by analyzing massive bike-sharing data in Shanghai, China. *Journal of Transport Geography, 87*, 102787.
- Xu, C., & Yu, X. (2019). Modeling and Analysis of Crash Severity for Electric Bicycle. In G. De Pietro, L. Gallo, R. J. Howlett, L. C. Jain, & L. Vlacic (Eds.), *Intelligent Interactive Multimedia Systems and Services* (Vol. 98, pp. 367–375). Springer International Publishing. https://doi.org/10.1007/978-3-319-92231-7_38
- Xu, J., Lin, W., & Shao, Y. (2017). New design method for horizontal alignment of complex mountain highways based on “trajectory–speed” collaborative decision. *Advances in Mechanical Engineering, 9*(4), 1687814017695437. <https://doi.org/10.1177/1687814017695437>
- Xu, J., Shang, S., Qi, H., Yu, G., Wang, Y., & Chen, P. (2016). Simulative investigation on head injuries of electric self-balancing e-scooter riders subject to ground impact. *Accident Analysis & Prevention, 89*, 128–141.
- Xu, J., Shang, S., Yu, G., Qi, H., Wang, Y., & Xu, S. (2016a). Are electric self-balancing e-scooters safe in vehicle crash accidents? *Accident Analysis & Prevention, 87*, 102–116.
- Xu, J., Shang, S., Yu, G., Qi, H., Wang, Y., & Xu, S. (2016b). Are electric self-balancing e-scooters safe in vehicle crash accidents? *Accident Analysis & Prevention, 87*, 102–116.
- Yan, X., Yang, W., Zhang, X., Xu, Y., Bejleri, I., & Zhao, X. (2021). A spatiotemporal analysis of e-scooters' relationships with transit and station-based bikeshare. *Transportation Research Part D: Transport and Environment, 101*, 103088.

- Yang, H., Ma, Q., Wang, Z., Cai, Q., Xie, K., & Yang, D. (2020). Safety of micro-mobility: Analysis of E-scooter crashes by mining news reports. *Accident Analysis & Prevention, 143*, 105608.
- Yao, Y., Zhang, H., Chen, J., Li, W., Shibasaki, M., Shibasaki, R., & Song, X. (2021). Mobsimilarity: Vector graph optimization for mobility tableau comparison. *arXiv Preprint arXiv:2104.13139*.
- Yuan, Q., Yang, H., Huang, J., Kou, S., Li, Y., & Theofilatos, A. (2017). What factors impact injury severity of vehicle to electric bike crashes in China? *Advances in Mechanical Engineering, 9*(8), 168781401770054. <https://doi.org/10.1177/1687814017700546>
- Zhang, X., Yang, Y., Yang, J., Hu, J., Li, Y., Wu, M., Stallones, L., & Xiang, H. (2018). Road traffic injuries among riders of electric bike/electric moped in southern China. *Traffic Injury Prevention, 19*(4), 417–422. <https://doi.org/10.1080/15389588.2018.1423681>
- Zhang, Y., Brussel, M. J., Thomas, T., & van Maarseveen, M. F. (2018). Mining bike-sharing travel behavior data: An investigation into trip chains and transition activities. *Computers, Environment and Urban Systems, 69*, 39–50.
- Zhang, Y., Lin, D., & Liu, X. C. (2019). Biking islands in cities: An analysis combining bike trajectory and percolation theory. *Journal of Transport Geography, 80*, 102497.
- Zou, Z., Younes, H., Erdoğan, S., & Wu, J. (2020). Exploratory Analysis of Real-Time E-scooter Trip Data in Washington, D.C. *Transportation Research Record: Journal of the Transportation Research Board, 2674*(8), 285–299. <https://doi.org/10.1177/0361198120919760>
- Zuniga-Garcia, N., Juri, N. R., Perrine, K. A., & Machemehl, R. B. (2021). E-scooters in urban infrastructure: Understanding sidewalk, bike lane, and roadway usage from trajectory data. *Case Studies on Transport Policy, 9*(3), 983–994.

Appendix A

A.1 Publications in Indexed Journals

- 1) Hossein Sabbaghian, M., Llopis-Castelló, D., & García, A. (2023). A safe infrastructure for micromobility: the current state of knowledge. *Sustainability*, 15(13), 10140. <https://doi.org/10.3390/su151310140>
- 2) Hossein Sabbaghian, M., Llopis-Castelló, D., & García, A. (2024). Assessing Micromobility Safety on Horizontal Curves of Bike Lanes: A Video Motion Analysis Methodology. *Traffic Safety Research*. <https://doi.org/10.55329/mmw5208>
- 3) Hossein Sabbaghian, M., Llopis-Castelló, D., & García, A. (2024). Enhancing Micromobility Safety: Introducing Effective Radius for Safety Assessment on Horizontal Curves, *Accident Analysis and Prevention* (under review).
- 4) Hossein Sabbaghian, M., Llopis-Castelló, D., & García, A. (2024). Typology of Bike Lane Users Motion on Horizontal Curves: A Surrogate Safety Approach. *Transportation Research Record* (under review).

A.2 Participations in International Conferences

- 1) Hossein Sabbaghian, M., Llopis-Castelló, D., & García, A. (2023). Assessing Micromobility Safety on Horizontal Curves of Bike Lanes: A Video Motion Analysis Methodology. *International Cycling Safety Conference 2023*, Hague, the Netherlands, November 15th - 17th, 2023.
- 2) Hossein Sabbaghian, M., Llopis-Castelló, D., & García, A. (2024). Enhancing Micromobility Safety: Introducing Effective Radius for Safety Assessment on Horizontal Curves. *International Cycling Safety Conference 2024*, Imabari, JAPAN, November 5th - 7th, 2024. (accepted as oral presentation).
- 3) Hossein Sabbaghian, M., Llopis-Castelló, D., & García, A. (2024). Typology of Bike Lane Users Motion on Horizontal Curves: A Surrogate Safety Approach. *TRB 2025*, Washington, USA, January 5th - 9th, 2024. (accepted for presentation)

A.3 Participations in National Conferences

- 1) Hossein Sabbaghian, M., Llopis-Castelló, D., & García, A. (2024). Enhancing Micromobility Safety: Introducing Effective Radius for Safety Assessment on Horizontal Curves. *V CAMPUS CIENTÍFICO DEL FORO DE INGENIERÍA DEL TRANSPORTE (FIT)*, Cercedilla Madrid, 23 y 24 de abril de 2024.

Appendix B

Section 6.3

```
1 import cv2
2 import numpy as np
3 import argparse
4 import os
5 import sys
6 import json
7
8 # Create the parser
9 my_parser = argparse.ArgumentParser(description='Undistort video using camera calibration
parameters')
10
11 # Add the arguments
12 my_parser.add_argument('Video',
13                       metavar='video',
14                       type=str,
15                       help='path to video file')
16 my_parser.add_argument('Calib',
17                       metavar='calib',
18                       type=str,
19                       help='path to calibration file')
20
21 # Execute the parse_args() method
22 args = my_parser.parse_args()
23
24 input_path = args.Video
25 calib_path = args.Calib
26
27 if not os.path.isfile(input_path):
28     print('The path specified does not exist')
29     sys.exit()
30
31 if not os.path.isfile(calib_path):
32     print('The path specified does not exist')
33     sys.exit()
34
35 video_in = cv2.VideoCapture(input_path)
36 success, frame = video_in.read()
37
38 with open(calib_path, "r") as f:
39     data = json.load(f)
40
41 mtx = np.array(data['camera_matrix'])
42 dist = np.array(data['dist_coeff'])
43
44 h, w = frame.shape[:2]
45 newcameramtx, roi = cv2.getOptimalNewCameraMatrix(mtx, dist, (w, h), 0, (w, h))
46
47 fps = video_in.get(cv2.CAP_PROP_FPS)
48 video_out = cv2.VideoWriter('undistorted.avi', cv2.VideoWriter_fourcc(*"MJPG"), fps,
(np.size(frame, 1), np.size(frame, 0)), True)
49
50 count = 0
51 while success:
52     uframe = cv2.undistort(frame, mtx, dist, None, newcameramtx)
53     video_out.write(uframe)
54     success, frame = video_in.read()
55     count += 1
56
57 video_out.release()
```

Section 6.4

Table 16 Lateral Offset Distances from Center Line for Site R2-R9 by User Type and Direction.

#	Bike Left-Turn			Bike Right-Turn			E-scooter Left-Turn			E-scooter Right-Turn		
	PC	MP	PT	PC	MP	PT	PC	MP	PT	PC	MP	PT
R2 (R=10 m)												
1	18	17	44	42	0	17	12	-12	-37	62	18	21
2	16	25	47	49	10	17	6	15	30	18	15	16
3	10	6	17	88	22	16	8	8	30	50	26	12
4	12	13	10	65	14	18	5	22	37	42	13	13
5	11	14	17	45	18	13	6	17	25	47	7	8
6	7	11	17	35	12	7	0	12	35	67	37	14
7	8	10	38	57	0	19	5	7	45	68	37	14
8	6	8	28	87	23	12	7	19	33	38	3	8
9	0	7	25	50	17	21	7	16	17	39	0	4
10	9	10	17	107	27	10	7	17	7	38	7	11
11	8	8	28	60	32	17	0	19	17	45	7	0
12	8	23	73	87	18	7	5	8	52	57	7	15
13	11	8	30	33	12	13	11	8	47	70	7	10
14	5	7	7	60	0	17	2	12	8	52	0	10
15	6	11	30	52	7	8	12	9	30	85	0	0
16	10	12	27	40	13	10	7	17	45	62	12	14
17	8	3	58	53	5	7	8	13	68	70	9	5
18	5	12	27	23	12	5	8	12	38	18	8	10
19	6	5	17	37	6	12	5	9	13	61	8	7
20	5	4	15	47	15	8	0	11	-20	72	15	11
21	7	16	47	72	0	0	7	-5	-22	37	14	7
22	12	11	47	58	3	4	7	9	20	35	10	8
23	11	12	38	38	14	27	11	21	67	8	6	7
24	6	15	33	47	5	7	-8	-7	17	7	8	6
25	11	16	60	73	22	5	6	14	53	58	7	17
R3 (R=22 m)												
1	0	40	35	182	194	100	0	-57	0	58	67	82
2	46	50	55	107	116	125	-40	0	0	18	0	28
3	-140	-91	-37	45	70	90	0	44	67	61	36	-10
4	31	18	20	61	40	74	0	13	0	48	37	47
5	102	20	40	-40	55	100	0	27	52	30	25	39
6	-30	-60	-40	62	36	35	0	19	30	50	59	66
7	0	0	20	58	72	77	0	10	42	75	100	70
8	20	0	30	46	70	55	68	58	73	53	66	65
9	43	104	114	0	41	41	28	73	72	30	73	54
10	10	30	43	70	48	69	45	0	10	59	44	0

11	-152	-151	-133	135	144	114	40	52	12	50	67	80
12	48	0	27	75	53	50	-84	-50	-20	21	29	40
13	-64	-29	33	42	26	43	30	45	45	62	58	88
14	15	0	16	-91	-54	26	62	28	24	22	40	46
15	0	30	0	38	45	0	-104	-84	-50	64	55	65
16	33	67	33	200	222	285	0	35	75	51	31	45
17	32	0	0	29	0	-50	-10	0	59	55	65	71
18	0	-23	-21	100	100	110	0	-30	55	80	71	65
19	55	64	76	40	30	0	33	40	44	-11	44	53
20	31	61	100	50	50	61	-42	-21	30	84	88	76
21	49	64	49	56	50	75	35	30	10	40	25	0
22	-73	-51	-40	100	145	184	0	0	-34	100	170	67
23	-270	-217	-100	50	50	40	27	24	34	55	35	50
24	0	-20	0	-95	-60	30	40	20	27	60	70	75
25	0	0	40	40	47	10	-70	-35	0	25	35	45

R4 (R=78 m)												
1	0	29	50	-18	68	-2	8	41	24	46	18	17
2	42	42	46	52	30	65	12	27	43	56	38	47
3	29	59	90	66	47	40	28	40	-49	71	41	50
4	32	22	43	69	88	92	27	34	84	92	46	43
5	-19	36	-20	49	57	-18	40	0	45	-88	14	0
6	23	-40	0	-90	68	94	20	44	68	63	80	90
7	-35	36	41	94	73	58	-30	0	-52	74	85	60
8	30	45	64	0	53	32	0	40	30	62	56	65
9	39	40	52	78	84	76	30	50	45	43	57	44
10	-46	-81	0	49	35	20	34	30	66	90	90	49
11	50	79	60	49	53	40	0	-36	-40	0	38	0
12	25	0	37	68	33	-26	52	10	40	25	0	34
13	53	53	59	72	25	0	10	-10	-10	49	57	37
14	48	59	64	61	-72	53	42	35	68	0	60	0
15	0	56	53	-53	-46	-35	0	23	52	10	30	0
16	54	60	96	81	47	0	29	10	-47	60	34	10
17	77	91	80	-66	57	60	-39	-39	10	50	52	39
18	62	68	45	74	75	57	62	32	29	86	52	14
19	66	55	43	0	33	-10	0	10	14	0	40	42
20	50	34	70	83	32	14	-33	0	0	45	44	31
21	12	50	83	0	57	45	-40	10	14	76	70	45
22	-20	0	36	58	61	58	24	30	40	0	48	10
23	20	30	70	22	30	30	39	37	40	40	21	14
24	40	55	58	70	60	85	24	10	10	57	53	43
25	0	-68	-94	-35	-35	0	57	46	38	59	55	46

R5 (R=2 m)												
-------------------	--	--	--	--	--	--	--	--	--	--	--	--

1	0	17	19	72	-9	0	0	24	61	27	21	0
2	-51	-152	63	36	-18	18	39	-186	36	27	-190	-92
3	-119	-406	-529	-127	-204	72	0	15	-22	16	23	13
4	15	-119	54	34	20	6	0	0	-20	11	-22	0
5	-44	-175	72	43	19	10	-2	-340	-1	11	15	0
6	-31	-165	38	20	-142	-52	-131	-184	36	25	-11	13
7	-70	-254	-203	-31	-280	-100	16	-13	-40	28	0	11
8	-98	-193	-66	58	0	0	-147	-320	87	13	10	37
9	-110	-252	-59	56	-44	0	42	24	46	49	-9	35
10	14	-154	65	-16	-163	68	-82	-340	-136	41	9	0
11	-162	-344	50	38	-8	13	-238	-330	-140	48	-6	15
12	-72	-330	-23	10	-135	-58	-130	-320	64	59	37	27
13	23	-244	-122	40	29	13	-300	-350	-101	45	-30	35
14	-336	-346	-191	26	-216	-39	0	26	63	34.1 5	- 20.8	40
15	-107	-266	39	39	9	54	43	-182	38	-21	-256	60
16	-318	-440	-188	18	-50	0	0	17	-24	27	-12	15
17	-280	-411	-159	-21	-240	28	0	0	-21	29	0	11
18	0	38	-27	-360	-365	71	-3	-345	-2	14	11	38
19	36	-250	45	36	15	35	-135	-186	38	50	-10	36
20	33	-230	31	-83	-227	-258	18	-14	-43	42	10	0
21	-217	-225	27	49	-16	28	-149	-322	88	48	-8	14
22	56	6	56	53	-15	14	43	25	48	57	34	24
23	-220	-335	91	0	-12	0	-83	-342	-137	42	-28	34
24	-120	-278	80	36	0	0	-239	-333	-144	32	-22	43
25	-194	-348	-120	55	-11	-110	-132	-322	65	-22	-250	63
R6 (R=5 m)												
1	45	-66	-16	0	158	67	25	-26	25	0	174	44
2	49	-61	30	0	0	-60	50	-60	80	60	66	58
3	63	7	90	50	20	63	40	-33	20	-30	104	0
4	62	-14	24	0	90	50	0	-60	-45	-50	0	-90
5	17	67	46	0	106	30	0	-30	80	60	260	50
6	54	70	20	50	115	25	60	20	65	45	108	45
7	-11	-94	25	57	99	33	25	-110	0	85	157	45
8	44	-67	29	49	102	34	307	344	321	62	122	62
9	62	-122	20	61	68	0	-48	-77	90	0	85	42
10	47	-95	53	50	150	45	60	-74	0	0	80	35
11	28	-56	-66	50	150	70	0	184	61	60	155	78
12	10	287	285	45	150	70	45	-118	-20	40	80	0
13	59	28	83	0	60	65	32	-30	60	35	83	-47
14	66	-21	0	55	103	50	51	-20	68	20	90	58
15	107	16	50	40	115	68	90	44	84	275	355	63

16	32	293	-213	60	87	68	30	-86	-10	63	87	40
17	56	37	0	48	123	35	30	0	0	337	375	58
18	16	-105	8	60	140	53	100	-100	-69	61	105	61
19	-34	-331	-218	50	100	73	66	53	53	25	116	36
20	54	-17	60	44	127	71	59	0	70	256	360	-20
21	0	-158	0	60	131	44	55	20	38	60	126	30
22	35	-43	52	66	121	45	78	-59	-19	55	105	10
23	75	21	94	-33	65	0	0	-42	107	62	146	31
24	58	18	89	0	114	69	36	6	-86	51	154	78
25	33	-104	0	58	112	36	36	6	-86	284	382	89

R7 (R=5 m)

1	30	22	36	0	9	-40	-58	-66	-81	23	0	15
2	0	32	28	0	5	38	-62	20	-153	0	20	0
3	28	-56	-54	0	20	-55	40	-135	-64	10	14	12
4	-60	-58	-71	0	20	16	0	-180	-100	15	12	21
5	30	38	-57	0	18	0	0	-170	-80	0	25	0
6	14	12	32	20	12	0	0	-150	0	0	20	0
7	0	0	35	0	0	35	50	-140	-75	20	12	-55
8	25	-150	45	0	12	38	65	-110	-65	15	25	35
9	29	-85	-70	12	8	33	-80	-130	-145	10	15	12
10	0	35	-72	25	13	42	15	-140	43	23	0	-60
11	0	-75	20	15	16	48	40	0	-55	14	16	30
12	0	-165	-125	12	14	12	-56	-61	-83	0	25	0
13	20	12	26	18	0	-54	-64	24	-150	12	17	-60
14	10	0	15	10	18	-60	44	-125	-65	12	20	44
15	0	-156	-125	40	15	14	0	-177	-108	0	10	0
16	35	-78	45	12	20	45	0	-173	-85	0	0	55
17	20	-105	40	12	12	53	0	-155	0	14	25	0
18	45	-82	0	24	21	53	57	-144	-77	0	16	42
19	0	-150	-85	15	24	45	64	-112	-64	0	19	30
20	15	-128	-93	0	20	0	-83	-127	-141	0	15	25
21	47	30	12	12	25	-55	17	-142	45	22	12	14
22	0	-215	-105	38	0	12	42	0	-57	37	22	52
23	20	-140	-98	35	29	16	-89	-117	-151	11	20	-55
24	42	28	10	0	18	0	19	-132	48	36	20	56
25	0	-202	-101	0	47	-55	38	0	-52	10	22	-54

R8 (R=7 m)

1	52	59	-120	28	35	32	0	27	0	15	22	25
2	20	-93	-150	18	15	0	33	-110	-130	-143	-82	0
3	42	-90	-134	12	0	0	30	24	43	-140	-138	-82
4	-88	-94	-93	15	17	20	20	15	32	105	-80	0
5	-73	-112	-107	48	45	23	-115	-135	-147	0	25	47

6	-85	-110	-110	45	18	0	-75	30	-87	25	0	0
7	45	-90	-92	35	17	-14	-95	-116	-137	-80	-110	-95
8	-100	-155	-145	-70	37	0	52	-110	-152	40	23	12
9	48	-96	-109	-78	-70	15	40	-70	-70	-70	-97	-98
10	32	58	-119	0	12	0	10	18	-152	18	15	0
11	24	17	14	14	0	14	-20	46	-98	40	10	20
12	-59	-104	133	-152	-140	-73	15	-90	-135	0	10	12
13	15	-92	-65	-145	-148	-102	17	-66	-127	39	15	10
14	-70	-96	-116	-146	-94	18	18	20	-80	-70	-65	20
15	-82	-93	-90	-90	-82	35	38	20	15	-66	18	10
16	18	38	-75	10	18	0	30	35	45	20	0	0
17	45	-79	-115	12	0	15	0	15	44	-70	84	44
18	18	15	47	16	18	0	-71	-92	112	56	35	14
19	17	19	-114	-64	-66	15	90	-180	-130	12	10	10
20	-72	-90	55	48	18	0	42	-70	-110	0	0	30
21	18	16	-110	39	12	0	-69	-110	-135	20	0	15
22	-72	-102	-100	0	12	0	0	32	-70	38	34	0
23	10	15	-140	0	0	0	40	-128	-156	28	43	30
24	14	18	22	20	70	0	14	34	-159	10	28	44
25	-146	-150	-161	-62	-70	18	15	45	17	13	11	11

R9 (R=9 m)												
1	18	15	12	35	-82	89	-85	61	22	0	13	-78
2	36	27	22	61	-127	-98	65	63	16	33	35	42
3	22	58	18	-120	-158	-155	-155	-130	12	-123	-170	-82
4	15	0	17	-100	-178	-110	40	71	48	35	-83	-98
5	0	-120	-90	45	64	37	-125	-180	-120	38	55	-67
6	0	15	0	-97	-92	24	0	57	50	24	-119	-95
7	12	14	10	69	58	25	30	47	10	15	22	12
8	0	22	58	32	-78	-74	100	-95	35	-157	-152	-134
9	-92	-176	15	-130	-172	96	-110	-150	34	-188	-183	-140
10	-85	-95	28	15	-192	-120	-130	32	20	35	-180	-184
11	55	25	24	-100	-200	-215	-170	-87	20	-84	-178	-87
12	17	42	11	-170	-190	-130	22	-102	-95	-85	-177	-230
13	0	13	0	47	-178	132	0	17	12	37	-78	41
14	-83	-90	40	30	-42	22	0	0	18	59	-177	-210
15	15	-147	-103	15	0	14	20	0	0	32	-138	-97
16	0	-140	21	16	-185	-138	-235	-180	-152	-83	-185	-207
17	-68	-115	-104	-120	-185	-139	22	-78	25	36	-155	-103
18	12	-87	-84	53	-160	-120	-88	-120	-72	28	-71	-69
19	-123	-90	34	16	58	35	0	0	17	17	21	25
20	55	43	18	158	-225	-220	-90	-170	48	58	-102	-75
21	-110	-160	20	44	50	-156	-140	-180	-102	15	-107	-110

22	0	35	14	54	145	-195	-150	-245	-148	35	-132	-130
23	0	18	38	30	-87	49	0	-110	-150	70	-180	-130
24	0	12	10	58	-102	-90	90	-90	32	20	-185	-153
25	20	48	13	31	-99	-98	-119	-147	31	18	22	26

Table 17 Operating Speed Data per Section for Site R2-R9 by User Type and Direction.

#	Bike Left-Turn			Bike Right-Turn			E-scooter Left-Turn			E-scooter Right-Turn		
	PC	MP	PT	PC	MP	PT	PC	MP	PT	PC	MP	PT
R2 (R=10 m)												
1	12	9	17	14	8	8	8	8	8	20	11	8
2	7	9	15	13	12	10	8	9	20	16	16	16
3	10	9	18	15	10	6	8	8	20	24	16	11
4	10	8	14	25	18	8	21	9	14	26	17	10
5	17	9	15	19	10	9	17	10	15	24	9	18
6	15	14	19	13	5	7	18	11	16	23	6	18
7	13	11	15	23	8	17	19	11	16	20	7	18
8	16	10	14	18	7	15	12	7	12	25	7	15
9	15	9	12	19	7	15	15	9	16	18	7	13
10	15	12	14	18	7	15	14	8	11	18	8	18
11	15	10	12	20	7	16	23	9	14	26	9	21
12	15	9	12	24	8	17	19	11	17	24	10	22
13	14	11	13	21	6	15	22	10	16	20	8	20
14	18	14	15	17	6	14	20	9	14	20	8	23
15	12	9	10	13	6	14	26	11	15	19	8	21
16	22	11	14	16	6	13	23	11	17	19	7	15
17	17	8	11	17	6	13	24	13	18	17	7	18
18	22	9	13	16	6	14	22	11	16	15	6	18
19	13	5	9	20	8	17	24	10	17	23	8	11
20	24	9	13	20	7	17	15	8	13	12	4	10
21	22	9	14	20	7	16	23	12	18	24	7	21
22	16	7	10	19	8	18	15	8	14	18	7	10
23	17	7	11	20	6	10	15	8	15	19	6	12
24	18	7	12	15	5	10	15	6	17	16	5	11
25	22	8	12	13	4	11	18	7	14	22	8	14
R3 (R=22 m)												
1	16	17	18	12	15	13	16	18	18	16	17	16
2	11	14	13	14	18	16	24	24	24	16	18	15
3	14	14	14	15	19	14	22	18	16	22	23	20
4	16	20	20	20	28	22	22	18	18	16	17	16
5	12	8	11	12	16	13	18	20	20	18	23	20

6	12	8	11	14	16	12	20	21	20	16	20	20
7	16	18	18	15	16	12	18	19	20	28	28	24
8	16	18	20	22	28	22	20	22	22	24	25	22
9	15	16	16	12	14	11	18	20	22	22	25	22
10	18	19	20	18	19	18	15	17	18	20	22	18
11	18	19	18	16	18	16	16	19	22	22	25	20
12	20	23	24	15	18	14	20	21	22	18	16	15
13	14	17	16	18	18	16	18	20	18	18	20	20
14	20	23	22	18	20	16	18	20	20	16	18	16
15	13	13	12	18	19	18	24	28	24	15	19	20
16	16	16	16	14	15	12	18	20	20	24	24	24
17	18	19	20	13	14	13	24	26	26	28	27	24
18	16	19	18	10	10	11	20	24	24	20	19	19
19	14	15	16	14	13	13	20	24	24	20	20	18
20	18	19	20	15	14	13	24	25	24	22	23	22
21	11	11	11	20	19	20	18	18	20	24	24	22
22	12	11	10	16	16	15	24	24	24	16	16	16
23	20	23	18	12	16	16	22	23	22	25	25	25
24	18	19	20	22	20	24	22	24	24	29	27	25
25	16	17	16	17	18	18	24	27	26	18	17	15

R4 (R=78 m)

1	13	18	17	23	24	21	11	19	17	26	27	22
2	10	16	14	19	13	11	11	18	14	25	24	22
3	17	21	19	17	22	20	30	25	21	18	15	12
4	18	22	19	12	14	11	13	18	10	19	26	22
5	17	19	18	19	24	24	12	24	24	24	25	18
6	11	18	17	23	21	23	20	22	17	16	25	21
7	10	19	17	20	26	23	9	15	16	13	19	17
8	9	16	15	13	16	18	14	17	16	20	21	14
9	9	15	16	7	9	12	12	22	19	23	30	26
10	9	15	17	17	23	21	12	19	19	17	21	19
11	17	13	12	24	30	28	10	16	16	16	23	24
12	16	18	18	28	21	20	23	25	21	11	17	19
13	11	15	13	16	21	18	22	26	23	19	19	24
14	16	17	16	13	16	10	18	24	21	25	14	16
15	12	17	15	14	16	10	19	22	21	19	25	24
16	11	15	16	10	12	16	12	19	10	14	16	14
17	10	16	14	16	15	14	10	21	19	18	23	20
18	13	15	14	14	17	15	11	16	16	21	26	20
19	12	15	15	14	17	16	11	16	16	13	16	15
20	9	21	16	14	18	16	12	23	23	16	20	18
21	10	15	16	12	15	15	13	25	23	16	21	16

22	17	16	20	12	14	9	15	20	19	24	24	21
23	16	16	20	14	12	14	15	23	18	19	25	21
24	15	15	17	12	10	8	14	18	15	18	25	24
25	13	13	16	12	10	9	13	22	15	20	25	25

R5 (R=2 m)

1	11	7	9	9	11	13	12	9	8	17	9	15
2	13	24	16	10	8	15	15	27	16	13	25	13
3	7	29	10	13	27	17	14	10	11	12	5	8
4	9	10	15	11	8	10	14	9	11	12	5	11
5	15	21	14	8	4	6	18	24	16	12	7	12
6	14	20	17	16	19	12	20	23	19	17	9	15
7	14	19	18	14	9	17	14	11	8	14	13	16
8	17	25	23	11	7	8	15	24	17	13	9	8
9	15	23	21	8	4	12	10	7	8	15	8	12
10	13	23	22	12	19	11	16	20	11	16	5	8
11	9	11	7	11	13	14	16	24	13	17	9	16
12	14	19	13	11	21	14	16	24	15	14	8	15
13	14	20	13	14	10	15	19	24	17	18	9	13
14	23	24	23	11	14	8	19	22	15	16	5	9
15	14	23	17	16	9	15	19	22	18	23	20	18
16	17	24	14	9	6	9	13	11	8	19	10	15
17	18	23	12	8	7	8	15	23	16	12	7	14
18	9	11	10	15	24	12	10	8	8	17	8	12
19	11	21	12	14	4	3	16	20	11	14	9	16
20	23	24	17	26	24	26	16	22	13	17	9	16
21	19	24	14	14	8	13	15	24	16	17	8	11
22	18	10	14	14	10	13	19	22	17	20	9	13
23	16	24	15	16	9	14	19	24	16	11	7	13
24	19	24	16	12	6	10	20	22	19	16	9	12
25	21	24	19	17	8	9	11	11	8	11	8	14

R6 (R=5 m)

1	20	21	30	10	12	13	15	15	15	9	9	13
2	20	23	21	11	12	12	17	12	10	15	10	14
3	28	18	19	12	10	12	18	12	12	14	14	13
4	13	17	22	10	11	10	19	18	19	13	11	13
5	10	13	12	9	14	13	15	8	8	13	12	13
6	11	19	16	12	14	10	8	5	7	12	12	14
7	28	22	35	10	16	13	16	18	16	13	12	14
8	18	36	25	13	17	13	11	27	18	15	19	16
9	9	20	15	12	12	13	15	11	16	11	13	11
10	13	15	22	11	19	10	11	14	14	10	9	13
11	19	11	12	11	12	10	14	13	14	10	9	13

12	16	19	26	12	9	10	24	30	23	16	20	16
13	14	17	23	11	13	9	18	17	17	22	21	19
14	8	7	15	10	11	11	12	10	15	13	9	12
15	6	14	27	11	14	14	12	10	8	12	30	15
16	10	13	31	12	19	12	19	22	17	12	8	13
17	22	29	30	14	19	16	10	12	14	15	28	19
18	25	31	33	12	18	15	10	14	9	9	14	15
19	22	29	33	9	11	8	18	9	11	16	17	13
20	12	16	31	10	14	12	9	9	9	20	40	26
21	11	26	22	10	16	12	18	11	11	11	22	17
22	15	19	22	10	13	10	14	18	21	20	22	18
23	17	22	27	11	10	8	20	24	13	24	15	21
24	13	21	27	12	12	11	19	18	21	21	14	24
25	20	17	15	10	13	12	19	18	21	21	23	29

R7 (R=5 m)												
1	8	4	6	14	17	13	13	11	15	14	8	9
2	13	7	10	14	14	12	9	5	14	15	10	11
3	12	5	7	14	12	9	8	4	13	17	12	11
4	11	4	7	13	9	14	10	6	13	21	13	12
5	11	7	10	14	9	12	11	6	13	12	8	10
6	11	7	11	13	8	24	11	3	5	13	6	8
7	5	5	9	14	9	5	7	5	12	18	14	12
8	13	5	11	14	9	12	7	6	13	15	10	13
9	10	2	7	17	10	6	5	5	7	12	6	10
10	10	6	13	17	9	7	10	6	14	18	7	11
11	9	7	12	15	9	7	15	9	15	16	7	11
12	14	7	15	17	8	10	14	12	16	15	7	11
13	20	7	13	12	7	7	10	7	14	13	5	6
14	12	6	11	14	12	11	10	7	13	16	7	10
15	15	6	12	13	8	10	11	6	13	13	8	11
16	9	3	10	15	11	11	12	8	13	13	5	8
17	14	6	13	13	9	12	11	5	7	13	6	9
18	13	6	13	13	9	11	8	5	12	14	7	9
19	11	6	12	12	6	8	7	6	13	10	6	7
20	10	6	13	11	4	8	7	5	8	17	11	15
21	18	11	14	15	10	9	10	7	14	12	5	6
22	11	6	14	10	3	4	14	10	16	24	13	15
23	14	7	13	16	9	12	16	14	16	18	9	16
24	12	7	12	15	8	13	11	9	14	19	9	12
25	11	8	14	14	8	11	10	8	13	15	8	11

R8 (R=7 m)												
1	11	19	15	12	12	10	12	25	19	6	12	9

2	11	28	24	11	19	16	12	25	23	15	24	15
3	7	19	15	12	18	11	11	25	17	19	24	22
4	10	28	21	15	25	22	11	24	18	18	20	23
5	12	24	15	14	25	21	11	21	13	17	24	12
6	13	25	24	17	25	17	10	25	20	9	14	6
7	8	25	17	14	19	17	11	25	12	12	25	16
8	6	17	9	13	19	14	14	25	22	16	25	22
9	10	25	17	9	17	10	13	25	24	11	20	15
10	8	25	21	16	25	14	15	25	23	12	16	15
11	6	24	11	13	22	15	11	25	18	12	18	10
12	6	24	15	12	16	13	9	25	23	10	22	11
13	8	25	16	18	29	22	7	24	15	10	15	9
14	9	22	14	12	28	16	9	23	13	14	24	14
15	9	25	22	17	27	19	11	16	13	16	25	19
16	10	25	20	12	19	17	10	25	23	8	19	10
17	9	26	22	12	24	13	19	25	20	12	20	11
18	6	12	10	12	19	10	10	25	23	13	20	11
19	5	17	12	10	25	15	14	25	23	13	19	9
20	13	29	22	15	26	14	11	25	23	12	15	8
21	7	19	10	17	23	23	14	25	23	16	16	11
22	10	29	20	10	15	9	10	21	11	16	19	12
23	8	14	14	13	19	14	11	25	16	15	15	9
24	7	21	13	14	18	18	8	17	12	13	12	9
25	7	25	21	12	21	15	9	17	12	14	17	10

R9 (R=9 m)

1	15	17	14	13	25	14	11	18	14	13	19	12
2	13	29	17	12	23	14	8	19	12	16	22	13
3	6	22	12	11	24	13	19	23	13	11	23	10
4	8	19	11	10	22	13	9	27	13	8	17	8
5	8	25	11	12	23	12	11	23	12	13	24	12
6	7	19	9	9	24	11	7	21	11	15	23	19
7	8	21	11	9	18	8	11	24	14	9	15	5
8	8	23	12	11	20	9	10	24	9	13	25	14
9	8	23	13	12	23	12	8	25	9	14	25	17
10	13	24	18	12	25	12	11	24	11	11	25	20
11	13	21	11	11	24	9	16	25	15	14	25	17
12	10	24	11	15	23	17	11	25	17	12	25	22
13	9	26	12	17	25	18	16	23	17	12	25	15
14	13	29	15	9	22	11	14	25	16	11	23	18
15	7	21	11	12	25	11	7	14	7	14	25	14
16	8	27	14	7	14	6	17	25	13	17	25	19
17	6	20	9	10	16	10	10	25	16	15	25	15

18	9	25	12	13	21	15	13	25	14	18	25	20
19	13	25	13	12	25	21	14	20	15	20	25	17
20	11	23	13	11	24	10	10	25	17	13	25	14
21	15	25	20	11	22	10	13	25	16	16	25	19
22	15	24	18	11	25	12	15	24	12	14	25	16
23	10	24	12	15	25	18	13	18	14	15	25	22
24	9	18	13	12	25	12	11	24	17	11	25	22
25	14	16	13	11	25	16	13	22	15	16	25	21

Table 18 Operating Speed Data per Section for Site R1-R9 by User Type and Direction.

#	Bike		E-scooter	
	LT	RT	LT	RT
R2 (R=10 m)				
1	9.4	8.9	10.1	9.1
2	9.7	9.1	9.9	9.9
3	9.7	8.9	9.5	9.8
4	10.1	8.9	10.0	9.4
5	10.0	9.5	10.1	9.2
6	9.9	9.6	9.7	9.9
7	9.4	8.6	9.3	9.8
8	9.6	9.0	10.0	9.2
9	9.7	9.2	10.2	9.1
10	9.9	8.9	10.5	9.3
11	9.6	9.7	10.5	9.4
12	9.3	8.9	9.2	8.9
13	9.5	9.5	9.2	8.8
14	10.1	8.6	10.3	8.8
15	9.7	9.1	9.5	8.5
16	9.7	9.5	9.6	9.0
17	8.8	9.0	9.0	8.9
18	9.8	9.9	9.5	9.7
19	9.7	9.2	10.0	9.0
20	9.7	9.5	11.1	9.0
21	9.5	8.7	10.1	9.7
22	9.3	8.9	9.8	9.5
23	9.5	9.2	9.3	9.9
24	9.8	9.1	9.5	10.1
25	9.2	9.3	9.3	8.8

R3 (R=22 m)				
1	29.3	52.0	14.2	21.6
2	22.2	22.3	28.3	18.0
3	21.9	22.9	25.1	25.2
4	20.7	17.4	25.8	20.1
5	14.8	30.8	22.6	20.3
6	17.7	19.7	23.3	22.5
7	20.2	23.4	20.0	31.4
8	17.7	28.1	19.7	24.0
9	30.7	28.5	29.5	33.2
10	23.1	18.3	17.4	26.4
11	20.5	28.1	30.8	22.8
12	16.2	20.3	22.8	21.9
13	19.8	19.0	24.2	19.0
14	19.2	18.5	19.3	23.8
15	32.7	30.8	20.8	20.3
16	34.9	18.5	21.8	19.0
17	19.1	25.2	17.9	22.8
18	19.7	21.2	14.2	21.9
19	21.9	24.9	22.6	29.5
20	21.4	20.9	19.4	24.3
21	26.5	19.2	24.2	23.5
22	23.7	23.1	27.2	154578.4
23	17.2	23.5	20.9	18.9
24	18.5	17.6	19.6	22.9
25	18.5	29.1	22.4	22.3
R4 (R=78 m)				
1	79.6	121.8	88.1	73.3
2	77.3	69.2	77.9	73.5
3	77.9	76.0	101.4	71.7
4	72.9	80.7	71.2	71.2
5	104.4	96.2	65.5	106.1
6	63.4	112.1	78.0	79.3
7	91.8	76.8	95.9	84.9
8	77.2	93.8	88.0	75.1
9	76.1	80.6	82.7	83.1
10	62.0	78.2	71.7	86.0
11	87.5	81.1	72.8	94.3
12	68.5	82.6	67.2	68.9

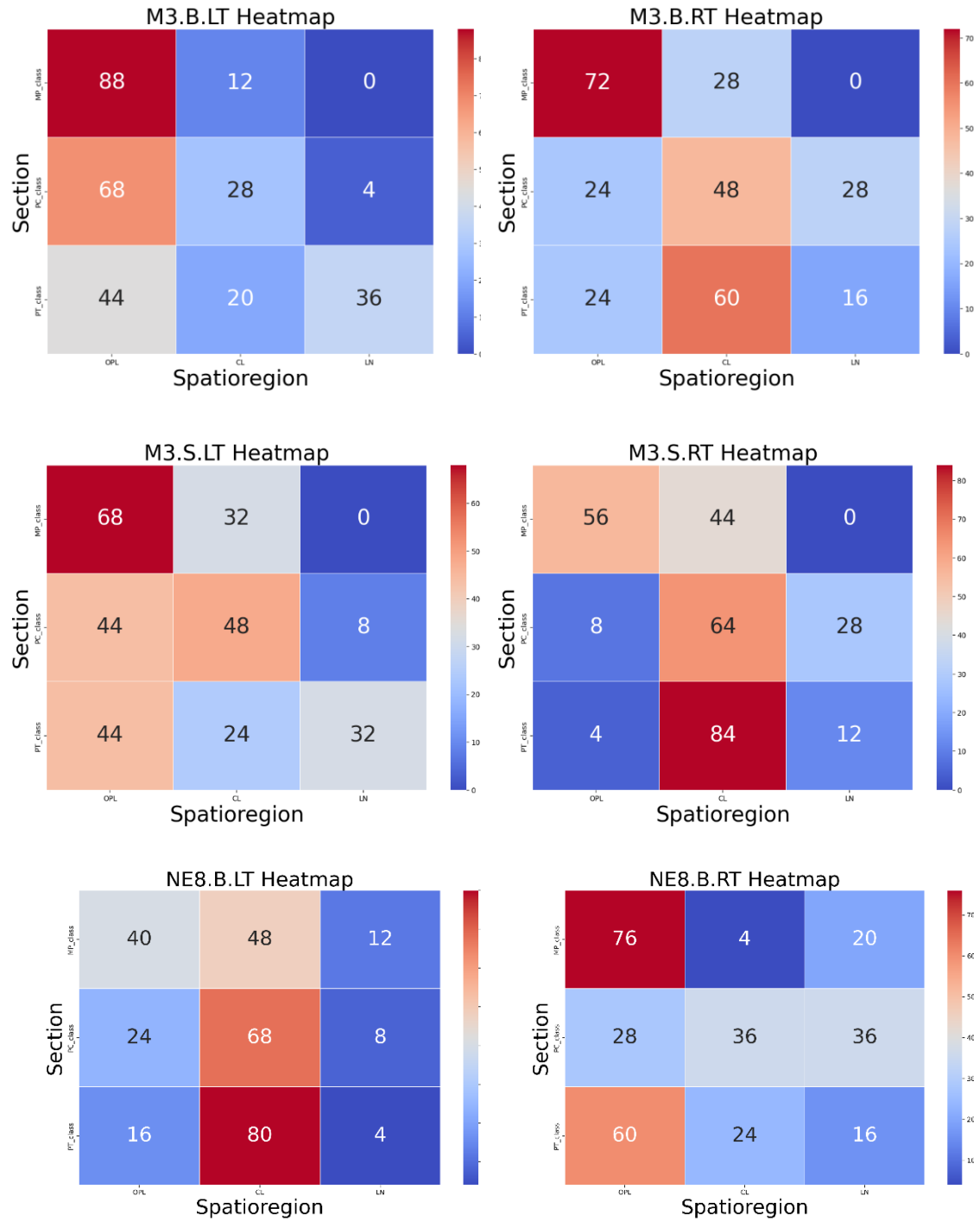
13	76.8	74.4	74.6	83.3
14	79.1	49.8	71.6	107.4
15	90.1	77.3	77.0	88.0
16	72.7	80.4	85.1	77.7
17	82.7	107.5	70.3	80.7
18	83.5	81.5	73.5	78.8
19	78.2	94.3	79.1	85.4
20	69.9	72.7	84.3	80.2
21	78.9	92.5	86.8	81.5
22	75.3	79.1	77.3	97.0
23	73.1	79.4	77.1	76.0
24	80.2	72.3	75.6	79.1
25	71.4	72.3	77.4	78.9
R5 (R=2 m)				
1	2.2	1.5	2.0	2.2
2	1.6	1.5	1.8	1.6
3	3.6	1.8	3.3	2.2
4	1.5	2.0	2.3	1.6
5	1.7	1.9	2.2	2.3
6	1.6	1.5	1.7	1.6
7	1.6	1.8	2.1	1.7
8	1.4	1.6	2.5	1.7
9	1.6	1.4	1.7	1.5
10	1.7	1.7	1.8	1.8
11	2.4	1.6	1.6	1.5
12	2.0	1.5	2.3	1.9
13	1.8	2.1	1.8	1.4
14	1.6	1.7	2.0	1.4
15	2.0	1.5	1.8	2.0
16	1.7	1.4	3.6	1.5
17	1.7	1.9	2.3	1.7
18	17.1	2.6	2.2	1.7
19	2.0	1.7	1.7	1.4
20	1.9	1.8	2.1	1.8
21	1.9	1.4	2.5	1.5
22	1.5	1.5	1.7	1.9
23	2.5	1.8	1.8	1.4
24	2.2	1.7	1.6	1.4
25	1.7	3.9	2.3	2.0

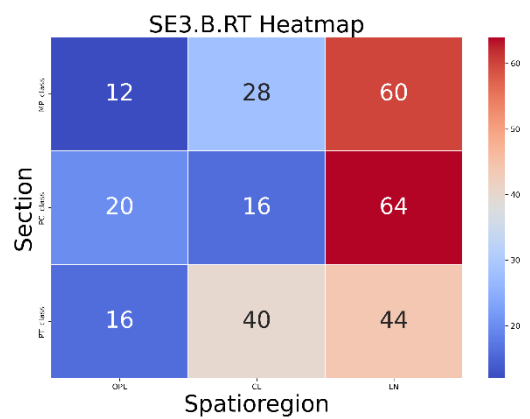
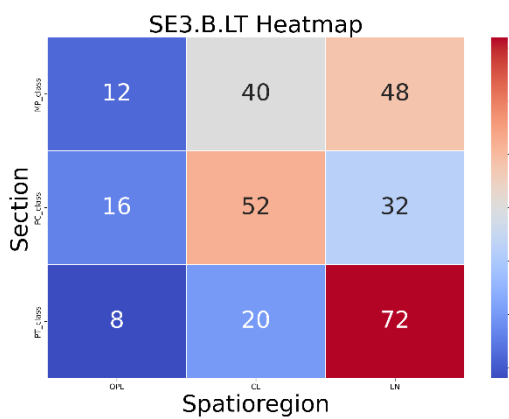
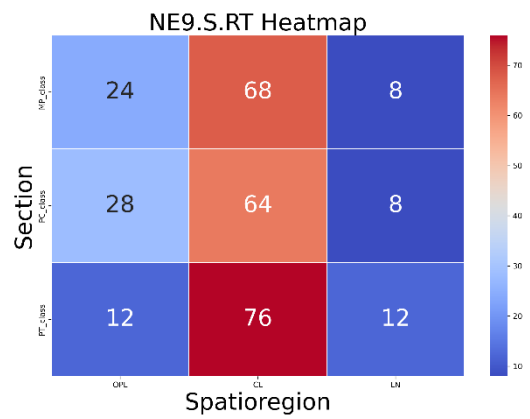
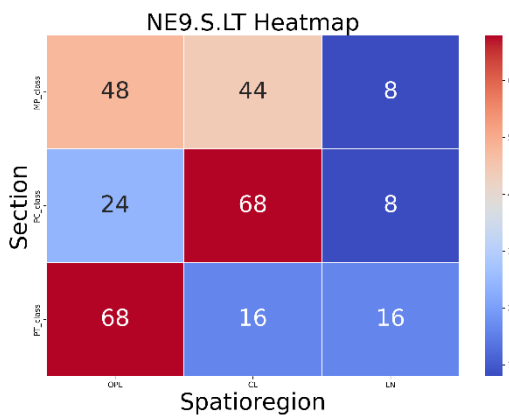
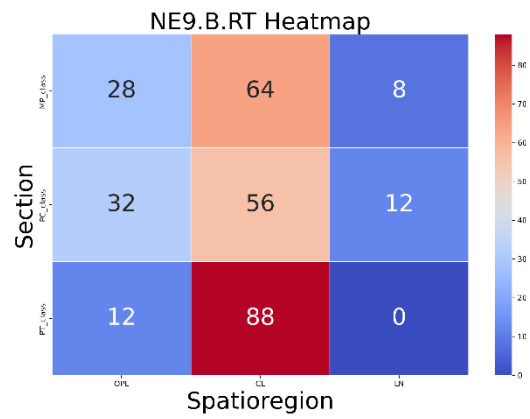
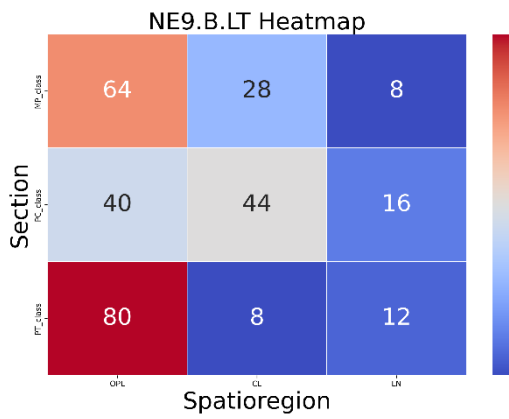
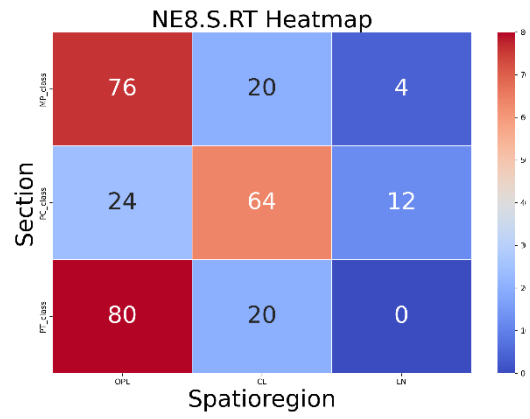
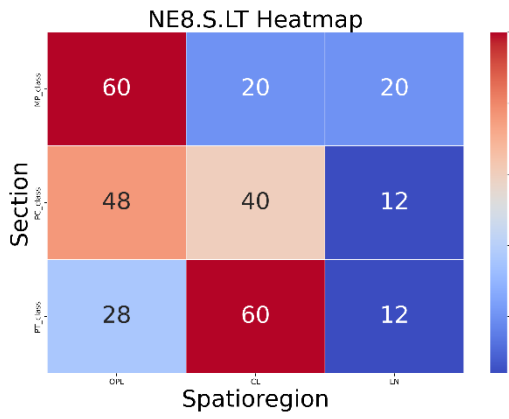
R6 (R=5 m)				
1	3.3	65192.2	3.6	58076.3
2	3.1	7.1	3.0	5.3
3	3.4	3.9	3.5	49250.5
4	3.6	15.4	3.9	18.6
5	7.7	217.9	3.5	16522.0
6	7.4	27.4	3.8	14.2
7	3.2	11.0	3.0	450.6
8	3.1	13.2	7.0	13.0
9	2.9	8.0	3.3	14.8
10	3.0	169050.1	3.2	14.1
11	4.0	143.5	54502.6	60.8
12	3330.3	955.8	3.0	13.1
13	3.8	6.9	3.3	13489.9
14	3.6	10.1	3.3	10.3
15	3.5	13.4	3.8	34850.4
16	3.2	6.4	3.2	7.6
17	5.5	36.9	4.5	29161.3
18	3.1	44.7	3.3	8.9
19	3.0	8.0	4.7	56.7
20	3.4	18.2	3.5	18133.7
21	2.9	30.3	4.1	35.5
22	3.2	15.5	3.3	20.9
23	3.5	62652.0	3.3	304470.6
24	3.6	32.1	7.6	114.7
25	3.1	15.3	7.6	21026.8
R7 (R=5 m)				
1	4.0	18.1	5.5	3.5
2	9.0	3.9	13003.6	9.8
3	2.9	129972.9	2.1	5.4
4	6.1	7.0	2.0	4.4
5	81579.3	8.9	2.0	13.0
6	4.0	5.3	2.0	9.8
7	3.7	3.7	2.1	19.7
8	2.0	4.4	2.2	5.0
9	2.5	3.8	3.7	5.5
10	41484.8	3.5	2.0	9.7
11	2.2	3.8	6.6	4.4
12	2.2	5.2	6.3	13.0

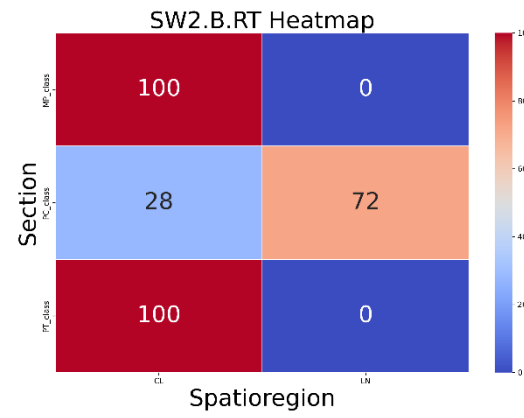
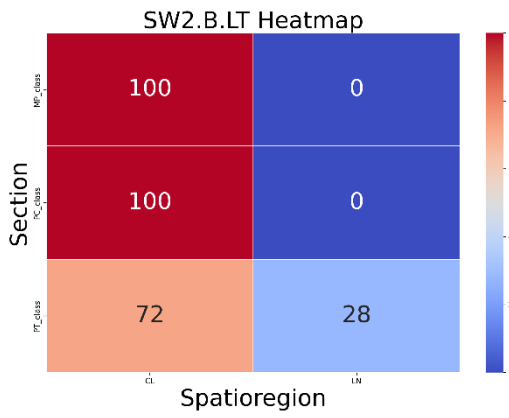
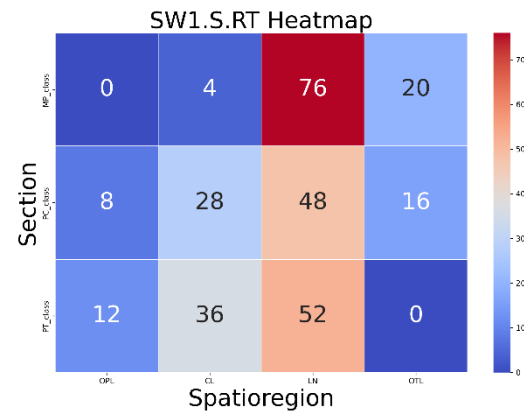
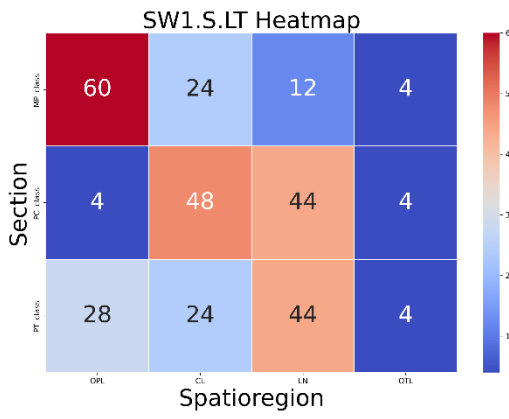
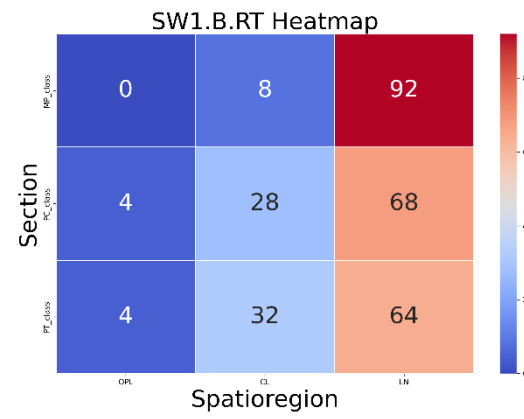
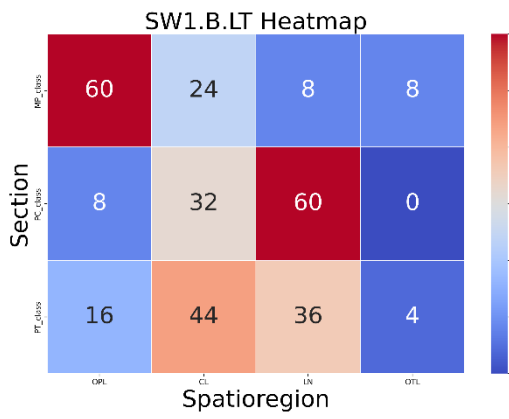
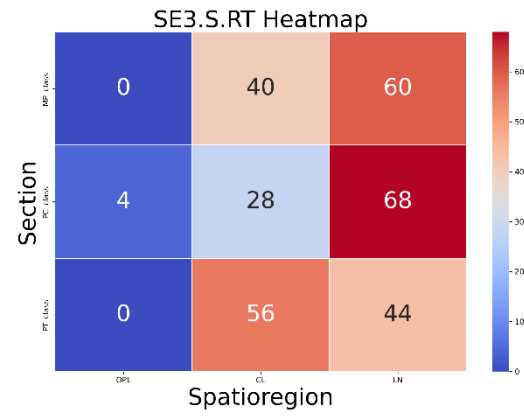
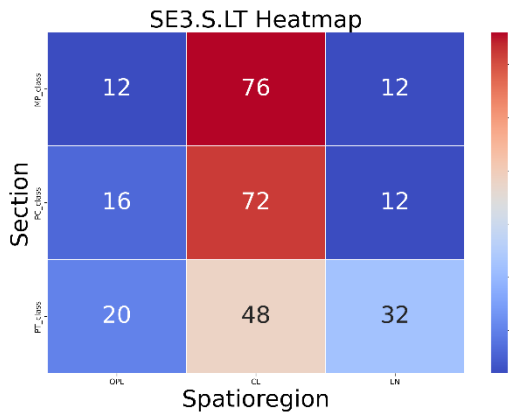
13	4.0	9.3	15342.7	936781.8
14	3.9	210684.3	2.1	4.3
15	2.3	4.0	2.1	6.6
16	2.0	4.2	2.0	3.3
17	2.0	3.5	2.0	8.9
18	2.1	3.6	2.1	4.6
19	2.1	4.4	2.2	5.6
20	2.3	9.8	3.9	5.3
21	5.1	152138.3	2.0	4.4
22	2.0	3.3	6.6	3.4
23	2.2	5.5	5.6	558953.7
24	5.3	8.9	2.0	3.2
25	2.0	35104.3	6.4	180185.9
R8 (R=7 m)				
1	13.7	7.1	7.9	7.1
2	6.5	7.2	5.9	6.9
3	6.2	6.8	6.7	6.4
4	6.9	7.0	6.7	5.1
5	6.5	7.3	6.9	7.1
6	6.7	6.9	16.3	6.7
7	5.8	7.2	7.0	6.4
8	6.2	10.8	6.0	6.9
9	5.9	6.2	5.9	6.7
10	14.9	7.4	13.1	7.2
11	6.9	6.6	15.2	6.5
12	5.2	6.4	6.4	7.1
13	5.7	6.4	6.9	6.7
14	6.9	6.5	9.3	6.1
15	6.8	6.0	6.8	8.9
16	10.4	7.4	6.9	6.7
17	6.2	6.6	6.8	13.9
18	6.6	7.3	5.4	7.0
19	10.6	6.1	5.1	7.0
20	5.6	6.8	6.3	6.6
21	10.1	6.8	6.8	6.5
22	6.6	7.4	10.4	7.5
23	11.9	7.0	5.9	7.4
24	7.0	9.8	16.1	7.0
25	7.1	6.0	8.0	7.0

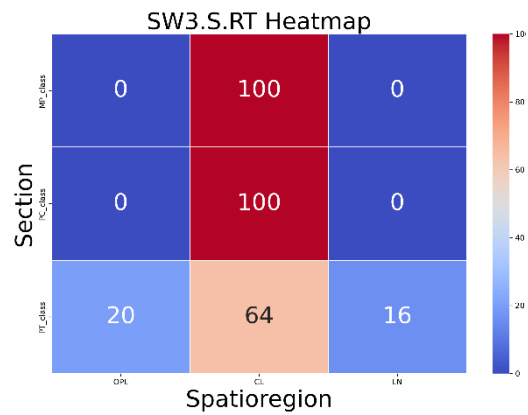
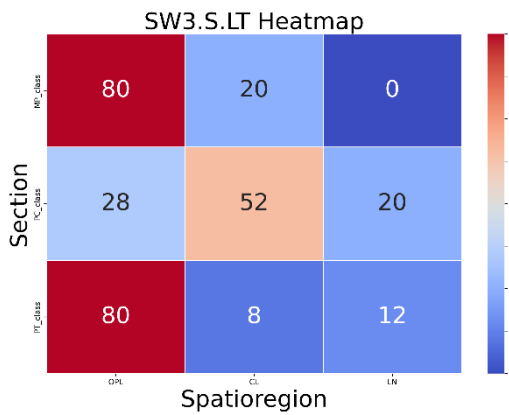
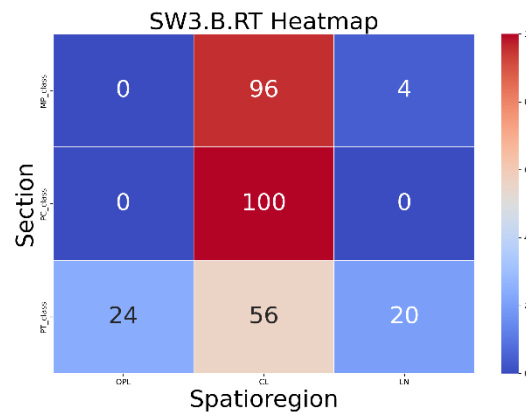
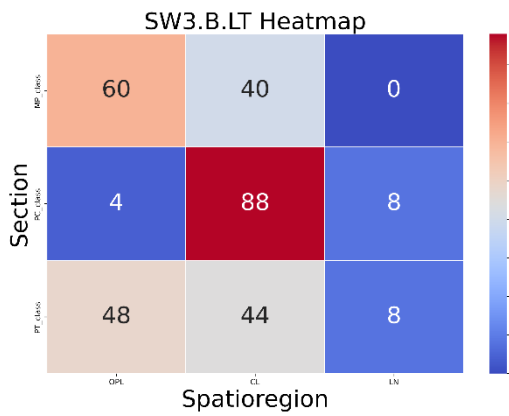
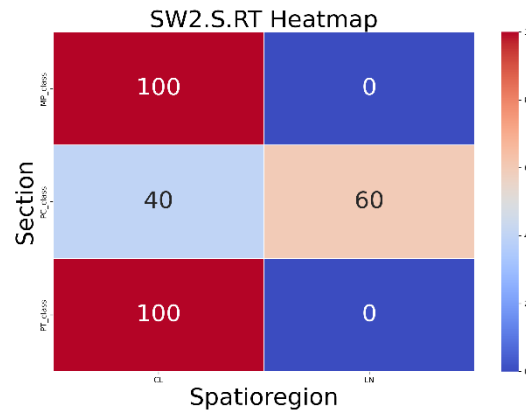
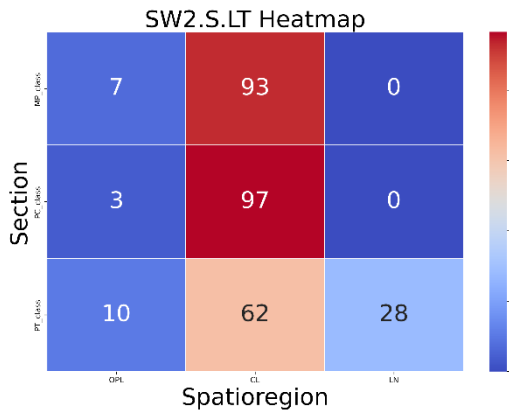
R9 (R=9 m)				
1	9.0	6.8	13.7	11.0
2	8.9	7.2	9.7	8.9
3	10.3	8.5	7.9	7.6
4	8.6	7.5	9.8	8.0
5	7.5	9.7	7.8	12.0
6	9.5	7.9	10.1	7.4
7	9.1	9.3	10.0	9.3
8	8.8	7.8	6.6	8.8
9	6.9	6.9	7.1	8.5
10	7.7	6.9	13.4	7.3
11	8.6	8.1	8.9	7.3
12	9.9	8.1	7.7	8.6
13	9.4	6.2	9.3	7.0
14	7.7	7.6	8.7	7.5
15	7.2	8.6	8.7	7.2
16	6.7	7.0	9.4	8.2
17	8.3	7.8	7.2	7.0
18	7.9	7.0	8.1	7.9
19	8.1	10.1	8.7	9.0
20	9.2	6.9	6.8	7.3
21	7.1	15.4	7.7	7.8
22	9.9	93.9	7.2	7.5
23	9.0	6.9	8.3	6.9
24	9.2	7.4	6.7	7.1
25	10.0	7.7	7.2	9.0

Section 7.2



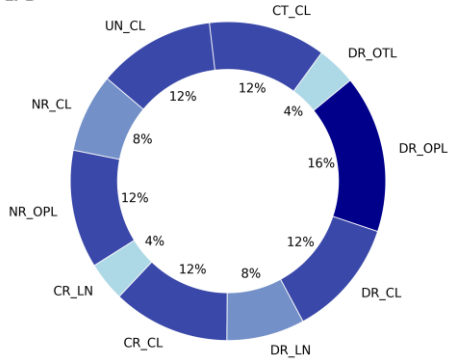




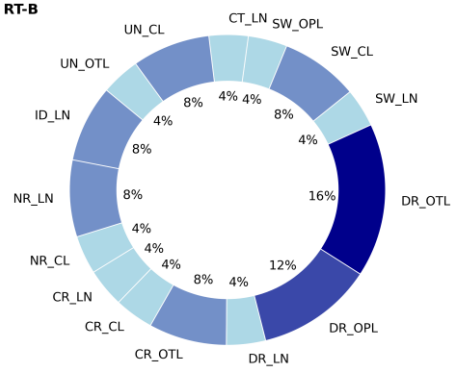


Section 7.4

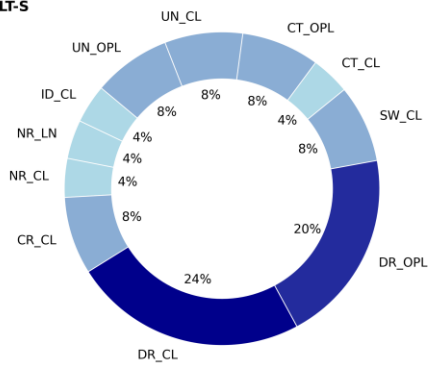
R3 LT-B



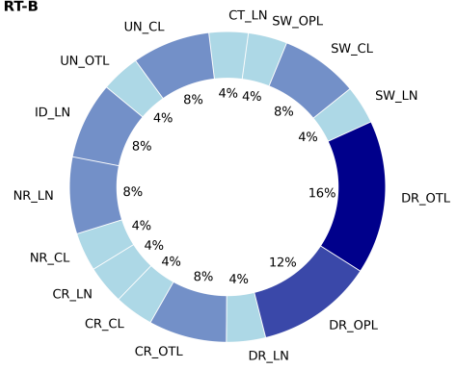
R3 RT-B



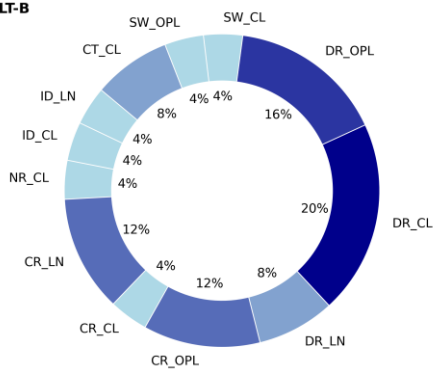
R3 LT-S



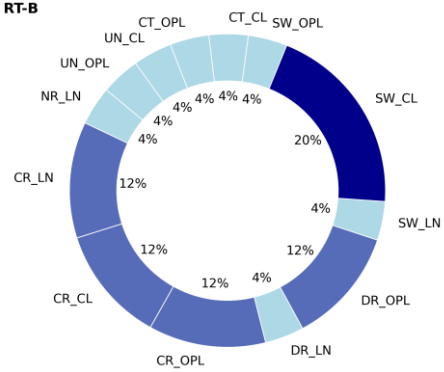
R3 RT-B



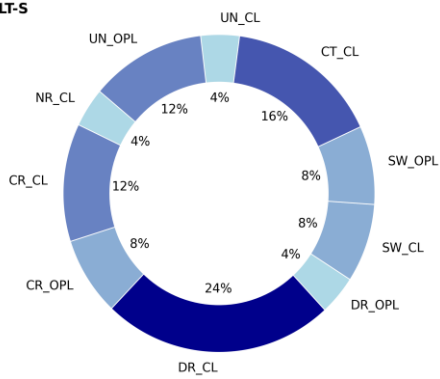
R4 LT-B



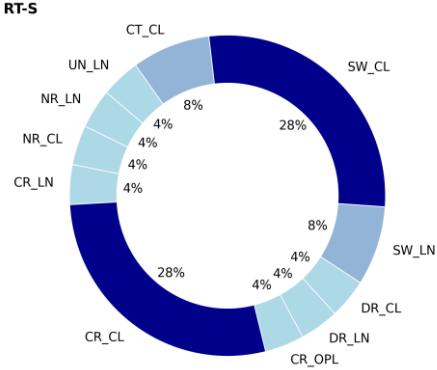
R4 RT-B



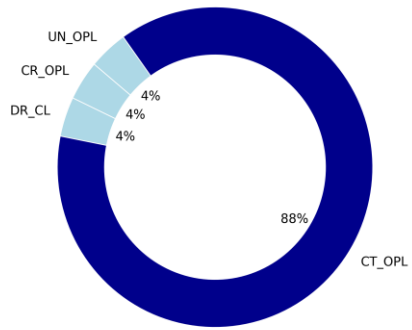
R4 LT-S



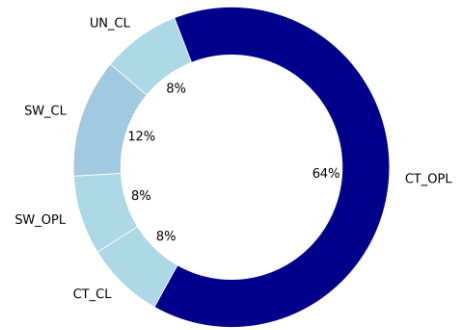
R4 RT-S



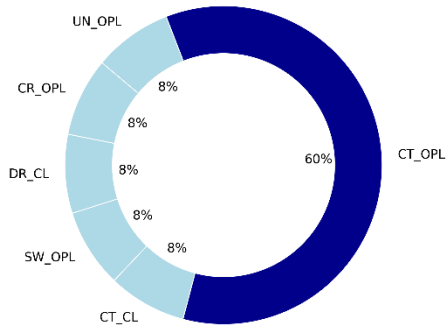
R5 LT-B



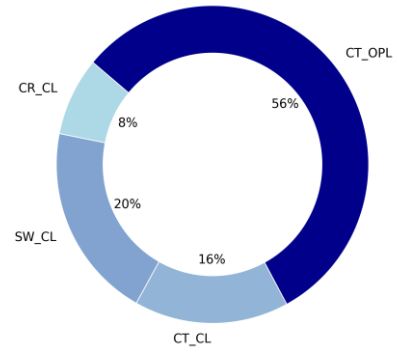
R5 RT-B



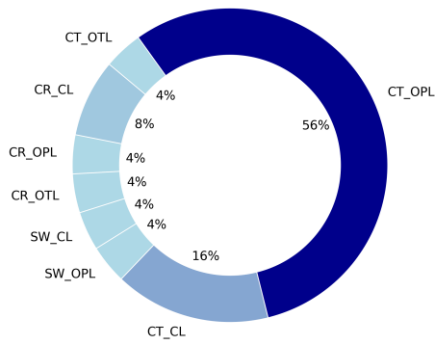
R5 LT-S



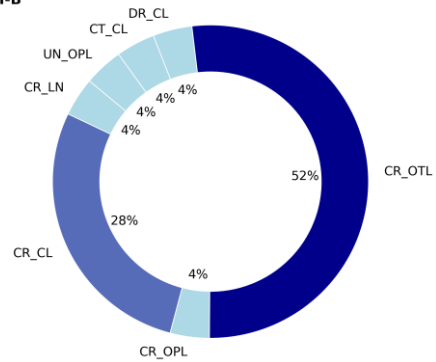
R5 RT-S



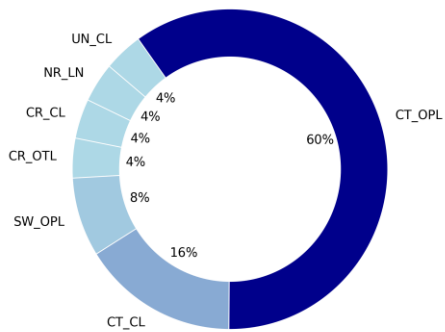
R6 LT-B



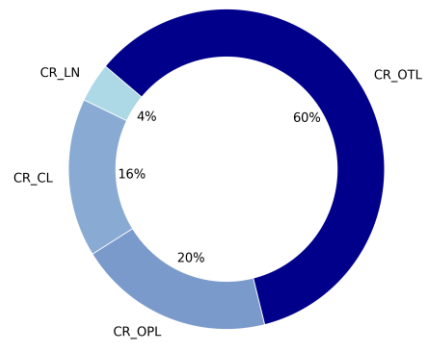
R6 RT-B



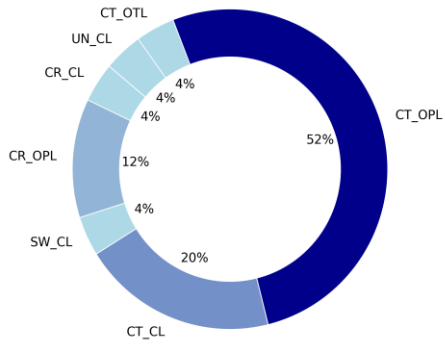
R6 LT-S



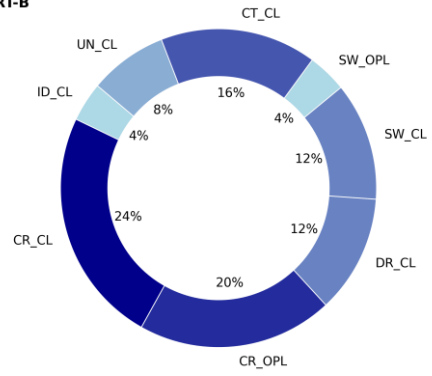
R6 RT-S



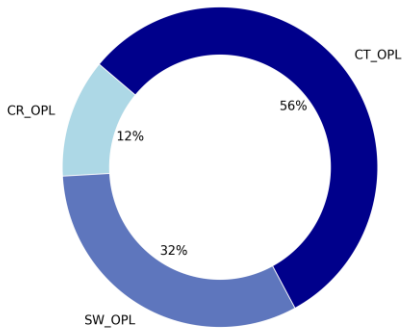
R7 LT-B



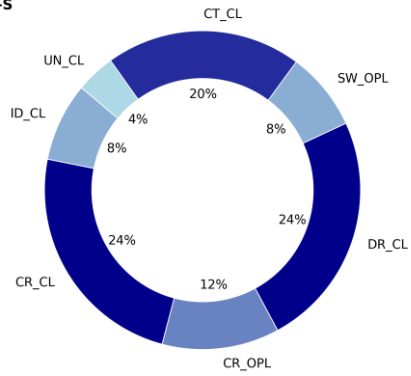
R7 RT-B



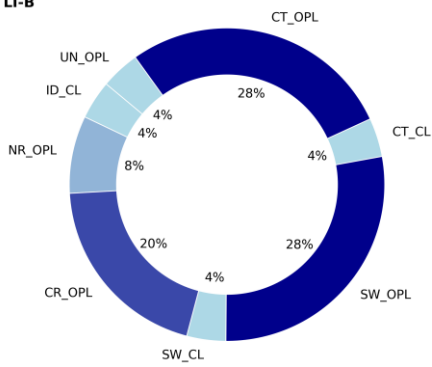
R7 LT-S



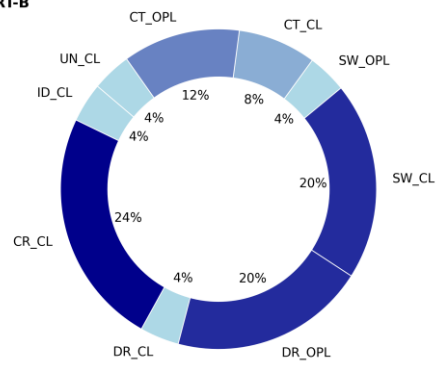
R7 RT-S



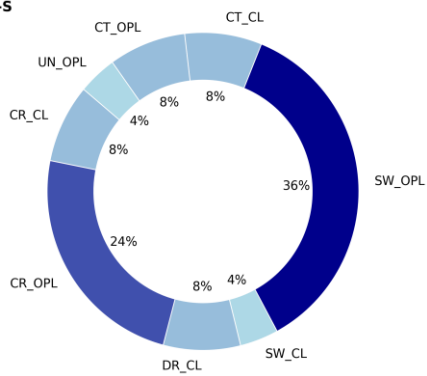
R8 LT-B



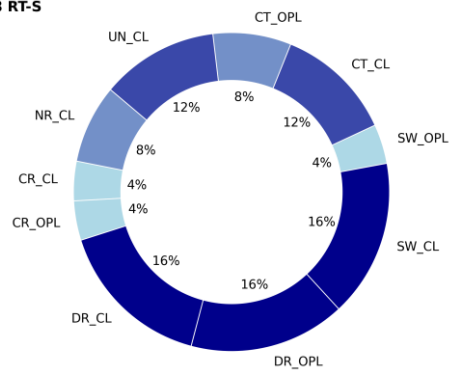
R8 RT-B



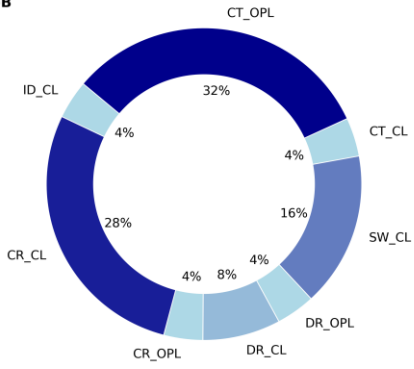
R8 LT-S



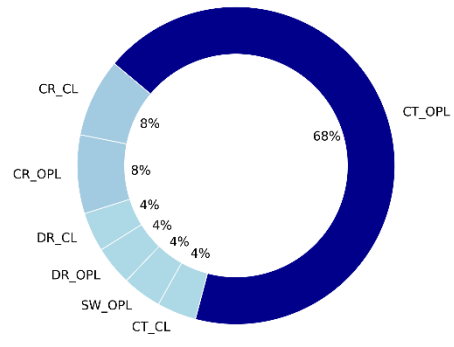
R8 RT-S



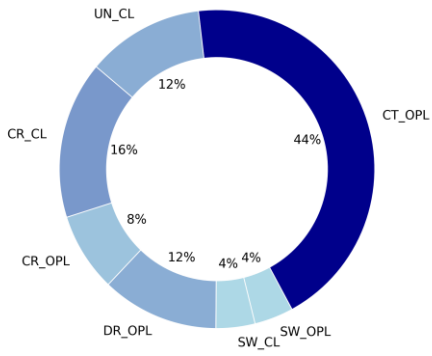
R9 LT-B



R9 RT-B



R9 LT-S



R9 RT-S

